1-1-2009

A Computer Science Approach to Identify and Classify Hyperactivated Spermatozoa

Norbert Kaula
University of Denver

A Computer Science Approach to Identify and Classify Hyperactivated Spermatozoa

---

A Disseration

Presented to

the Faculty of Engineering and Computer Science

University of Denver

In Partial Fulfillment

of the Requirements for the Degree

Doctor of Philosophy

---

by

Norbert Kaula

June 2009

Advisors: Anneliese Andrews, Ph.D. and Catherine Durso, Ph.D.

Co-advisors: Christopher Dixon, M.D. and Louise Dye, Ph.D.

Abstract

Author:	Norbert Kaula
Title:	Computer Science Approach to Identify and Classify Hyperactivated Spermatozoa
Advisors:	Anneliese Andrews (andrews@cs.du.edu)[1] Catherine Durso (cdurso@cs.du.edu)[1]
Committee Members:	Christopher Dixon (cdixon@svcmcny.org)[2] Louise Dye(l.dye@leeds.ac.uk)[3] James.K.Graham(James.K.Graham@colostate.edu)[4]

[1]University of Denver, Department of Computer Science, U.S.A.
[2]New York Medical College, Department of Urology, U.S.A.
[3]University of Leeds, Institute of Psychological Sciences, UK
[4]Colorado State University , Department of Biomedical Sciences, U.S.A

Degree Date: June 2009

Abstract

Effective Assisted Reproductive Technology (ART) relies in part upon accurate but easily conducted measurements of sperm motion parameters. Several established methods are widely used to assess possible reasons for male infertility, in human and veterinary Andrology clinics. Computer-assisted sperm analysis (CASA) devices quantitatively assess sperm motion parameters, which have been defined by the World Health Organization, and include the percentage of motile cells in a sample and the motion characteristics of individual cells, such as curvilinear velocity (VCL), average path velocity (VAP) and straight line

velocity (VSL). However, CASA analyses fail to define hyperactive sperm motility or determine the prevalence of hyperactively motile sperm in the sample. Hyperactively motile sperm swim in an erratic pattern, and this occurs only at the very end of sperm capacitation, a series of biochemical changes occurring in a sperm which enables it to fertilize an oocyte. The computational challenge for detecting hyperactivated sperm motility lies in precisely modeling sperm movement changes that accurately reflect the sperm's biomedical function, by developing an algorithm that detects and classifies these unique motility patterns. Currently, no such algorithms reliably classify hyperactivated spermatozoa. Therefore, several methods to automatically identify and classify hyperactivated spermatozoa trajectories are described and their performance compared to 'the gold standard' of visual classification, by experts.

The methods considered were: two existing methods, a mathematical modification to one of these, and three new methods, each examined independently and then two were combined to produce an integrated approach.

Evaluation of each method was performed by using each to analyze an initial data set containing tracks of hyperactivated and progressive sperm, which had been classified by experts in the field, and then to analyze data sets obtained from actual laboratory samples. Classifications as well as misclassifications were recorded in diffusion matrices. Two methods, the Minimum Bounding Square Ratio (MBSR) and the Rotated Rectangular Linearity (RRL) were more effective in accurately detecting hyperactivated sperm and were similar in correctly classifying hyperactivated sperm. However, RRL misclassified twice as many sperm as MBSR. MBSR also outperformed the other methods in correctly classifying progressively motile sperm and sperm exhibiting transitional motility. After develop-

ing this algorithm, it was applied to evaluate sperm from a large experiment to determine if sperm treated with different phosphodiesterase inhibitors, used in erectile dysfunction drugs, exhibit sperm motility. The experiment would not have been possible without these new computer algorithms. Taken together, this research demonstrates that newly developed algorithms can be used to identify critically important features of sperm, such as hyperactivity. One algorithm, MBSR may become an important tool improving Assisted Reproductive Technology's success.

Acknowledgement

A dissertation is not created in a vacuum. This is especially true for an interdisciplinary thesis which relies upon the input of many others. For this reason, I would like to acknowledge and show my appreciation and gratitude to those people who have contributed generously in various ways to the completion of this thesis.

Dr. Anneliese Andrews, Associate Dean, University of Denver, for believing in and supporting the idea of computer science methods of sperm motility analysis. Her analytical mind and challenging ideas have been a great stimulant which have propelled me forward throughout this research.

Dr. Catherine Durso, University of Denver, for her patience and tireless mathematical and bioinformatic explanations and models.

Dr. James Graham, Colorado State University, without whose generous support in granting access to his biomedical laboratory this dissertation would not exist. His continual support and scientific discussions helped to keep this computer science thesis in line with biomedicine. Thanks are also due to former lab support Masters student, Mindy Ann Marie Meyers for preparing and running an seemingly endless amount of sperm assays without hesitation.

Dr. Christopher Dixon, New York College of Medicine, for making sure the ideas and techniques presented in this thesis are applicable to humans.

Professor Louise Dye, University of Leeds, for posing the most challenging questions, and maintaining the highest level of academic integrity while trying to push me towards completion. Last but most definitely not least, my wife, Martina and my children, Claire and Lily, for supporting me through this and never losing confidence in me.

Table of Contents

List of Tables

List of Figures

List of Algorithms

Chapter 1

Introduction

Mammalian spermatozoa are special self-propelled reproductive cells. Contrary to the widely held belief, ejaculated mammalian spermatozoa do not have the immediate capacity for fertilization [8, 21, 33, 109, 118]. The spermatozoon must undergo several biochemical changes as a prerequisite to become competent to fertilize an oocyte. These processes lead to ”capacitation” [33] . Most visibly, the swimming pattern of the sperm (motility), changes from a more linear to an erratic star-spin pattern, called hyperactivation [78, 117]. These sperm movements (trajectories), can be observed under a regular microscope or digitized as 2-dimensional tracks using a computerized sperm scanner. Not only do the movement patterns of the sperm change, irreversible biochemical changes require the sperm to fertilize an ovum in the immediate future or it will die [21, 25, 33, 55, 109].

Current male fertility measurement parameters were standardized by the World Health Organization (WHO) as early as 1987 with some amendments in 1999. However, the WHO criteria do not provide computational algorithms for classifying hyperactivated sperms [30,

49, 57, 89, 103, 113]. Additionally, definitions and descriptions of sperm hyperactivity often vary from author to author, even on the same species [16, 55, 78, 111, 122].

Most hyperactivity classification approaches describe the track images of different stages. Rather than trying to repeat a similar method of describing the virtually endless number of possible track patterns, this thesis attempts to interpret the erratic sperm movement as a physiological ovum search pattern. Hence, robust computational algorithms to characterize these trajectories were derived. Using these and additional algorithms, we are able to automate sperm hyperactivation classification.

1.1 Problem and Scope

Capacitation with its visible effect, hyperactivation, is regarded as the terminal event of maturation of the spermatozoon, necessary for fertilizing an oocyte [42, 56, 117]. Assisted Reproductive Technology (ART) health care costs were reported in 2008 by Myers et al. to be an estimated $3 billion for the U.S [1, 62, 87]. Despite these high costs for infertile couples seeking medical help, computer assisted semen analysis (CASA) is often underutilized in favor of the most basic sperm analysis, which is on par with a manual microscopic sperm analysis. Although CASA has been shown to improve fertilization outcomes, surprisingly, many in-vitro fertilization (IVF) clinics do not use advanced sperm analysis methods [6, 24]. An often cited reason for the low utilization of CASA is the expense of acquiring a CASA device and skepticism about the clinically applicable value of currently used computer algorithms. In addition, human operator expertise is judged to be superior to a computer analysis [32]. Presently, no commercially available CASA device has specifically developed algorithms to classify hyperactive sperm. Users must

attempt to derive hyperactivity from existing measures. CASA devices, as they are today, are indeterministic, crude, idiosyncratic and calculate only convenient measures which are only tangentially relevant to hyperactivity. Sperm hyperactivation plays a critical role in the spermatozoa's life to fertilize an ovum. Therefore, a robust algorithm to classify hyperactivation could improve fertilization rates and could reduce examination costs.

In addition, reliable knowledge of hyperactivated sperm may be helpful in the cattle industry, where IVF is commonly preferred over the use of less successful intracytoplasmic sperm injection (ICSI) and could improve the breeding technique of live stock. [101]. It also may be beneficial for in vitro fertilization of equines, which is currently not possible without inducing sperm hyperactivation. The exact timing knowledge of capacitation and hyperactivation is crucial for equine reproduction.

Lastly, the development of more effective means by which to classify hyperactivity will assist scientists and practitioners to understand and develop better ART procedures and pharmaceuticals, which could have great ramifications for breeding and maintenance of endangered mammalian species.

1.2 Motivation

This thesis is focused on the physical phenomenon of hyperactive motility observed in the spermatozoa. Although capacitation and subsequent hyperactivation have been found to play an important role in fertility, little work has been done to develop adequate automatic robust computational tools for detection and classification of hyperactivated spermatozoa.

At the present time capacitation and hyperactivation is assessed by either flow cytometry assays, which are based on fluorescence staining procedures, completely loosing the important motility factor of the sperm, or using simple thresholding values provided by sperm scanners[77, 116]. Most hyperactivity research concentrated on capturing the sperm motility pattern pictorially, rather than algorithmically. After great interest in the mid 1990's by researchers in investigating computational and standardized sperm motility analysis methods, the interest waned in computer science approaches and even reversed in some areas back to manual techniques. Therefore, there is need to develop new measures based on bioinformatic algorithms to automatically capture and classify motility changes of sperm.

1.3 Research Questions

Since the discovery of the spermatozoa maturation cycle, termed "capacitation" in 1951 by Chang [20], Austin [8] and of hyperactivation in 1969 by Yanagimachi, many projects have been initiated to scientifically describe this phenomenon. Examples of such projects include mostly pictorial sperm hyperactivation pattern descriptions and a few mathematical analyses of sperm movement changes. Capacitation and subsequent hyperactivation are a result of biochemical changes of the sperm cell head, the acrosome, as well as intracellular changes. As such, to this day, only time consuming assays can be used to test for capacitated and hyperactivated sperm. In the last 10 years the interest diminished in finding a reliable and fast way to describe sperm movement changes. This thesis aims at investigating the automated identification and classification of hyperactivated spermatozoa.

R1: Can hyperactivated sperm be identified and classified from 2D trajectory data, obtained from industry standard semen scanners?

R2: Is it possible to develop computational algorithms to describe sperm hyperactivation?

R3: Can computer algorithms be used to accurately describe movement patterns?

R4: Can such algorithms match or surpass classifications by experts in the field?

R5: Can the existing sperm parameter measures be improved?

R6: Are those new measures and algorithms robust enough to be used in daily laboratory testing?

These research questions can be summarized as follows:

R7: Can we automatically detect types of sperm motility using existing laboratory technology with computer science algorithms?

Chapter 2

Existing Work

An extensive body of publications exists covering spermatozoa research. This is summarized and discussed in section 2.1. Further, this chapter is structured into a discussion on sperm morphology, sperm shape and anatomy, the internal components of the spermatoza cell (section 2.2); followed by a discussion of sperm motility properties (section 2.3) and sperm measurement parameters (section 2.4). Section 2.5 discusses sperm capacitation and section 2.6 describes sperm hyperactive motility (visible changes in the movement) of the sperm. Section 2.7 discusses established computer-aided sperm analysis CASA, followed by sperm hyperactivity classification (7.3.6). The chapter concludes with open problems in section 2.9. The term spermatoza means multiple sperm cells, while spermatozoon refers to a single sperm cell. Sperm is used as singular or plural. We apply these terms interchangeably throughout this dissertation.

2.1 Literature Search

A literature search was performed using the keywords: sperm, sperm morphology, motility, fertility, hyperactivation, capacitation, algorithms, sperm parameters, trajectories, CASA, human- animal study, reliability / standardization and identification/classification. We followed the paper reviewing technique as published by Engström et al.[36] in the broadest sense. The interdisciplinary topic of this thesis required deviation from their recommended search order, such as fulltext search first, since keywords have different meanings in different disciplines.

To ensure a broad search, no date restrictions were included. The subject of this dissertation is interdisciplinary, including computer science, human and veterinary medicine, engineering and biomedical sciences. 289 references were deduced from the databases below. Since papers directly dealing with the research area of this dissertation were not common, 79 final references were manually selected and categorized into a matrix containing five subject and seven approach sections (see table 2.3). Additional papers outside this matrix were included in this work to reference, for example, costs for IVF procedures. Most papers were retrieved from the electronic databases below. However, for completeness, a few references were also obtained from manuals and publicly available research reports. For example, reports from the U.S. Department of Health and Human Services were also examined for relevant data and information.

- PubMed US National Library of Medicine
  ($< www.ncbi.nlm.nih.gov/pubmed >$)
- IEEE eXplore

($< ieeexplore.ieee.org >$)

- SpringerLink

  ($< www.springerlink.com >$)

- ACM Digital Library

  ($< portal.acm.org >$)

Existing literature matrix on 'Subject':

Sperm Morphology: Is intended to provide biomedical background information about the shape of the cell. Often, detailed motility descriptions can be found in these papers.

Motility: Is a broad term, covering computer science and biomedical journals. It is intended to capture publications dealing with sperm motility in the widest sense.

Fertility: Is intended to uncover papers in the field of fertility, which uses sperm motility applications.

Hyperactivity/Capacitation: Is intended to retrieve biomedical background as well as specific publications, regarding uses of computer science within this subject.

Algorithms: Is intended to extract papers, dealing with algorithms and spermatoza.

Existing literature matrix on 'Approach':

Sperm parameters: Is limiting the search on parameters used in sperm research.

Trajectories: Is reducing the publication to the field of sperm track generation, usage and storage.

CASA: Discovers papers or sections of papers dealing with computer-aided sperm analysis.

Human study: Is intended to show how and what investigators published in human re-

search.

Animal study: Similar as above, however emphasis on animal studies.

Reliability/ standardization: Is intended to show sperm research, concerned about reliability/ standardization.

Identification/classification: Is intended to discover publications on identifying or classifying sperm in the widest sense.

The subjects of the literature search were intentionally kept broad, since specific computer science keywords of the paper title, abstract and fulltext did not yield enough 'hits" for this interdisciplinary topic. The approach categories allowed us to be more specific on the topic while still be general enough to not exclude potential papers of interest. The matrix of Table 2.3 shows the depth of coverage of each research area. It served well to provide an initial impression of the existing relevant published work. However, it can be improved, for example by dividing the matrix into 'basic background' and 'research relevant' papers.

An analysis by subject and approach revealed that 132 papers fit into the broad subject of motility, while only 27 papers published algorithms. Papers in the matrix are cited by subject and approach, therefore a citation can occur multiple times. There is a great interest in the areas of sperm capacitation and hyperactivation, seen by the 103 papers in Table 2.1. Judging by the number of papers in Table 2.2 a strong scientific interest exists for all seven approach categories.

Subject	Number of Papers
sperm morphology	52
motility	135
fertility	67
hyperactivation/capacitation	103
algorithms	27

Table 2.1: *Literature Search by Subject. There are many papers covering capacitation and hyperactivation, however little work has been done with algorithms. Note: papers may appear in multiple sections of the matrix. Number of papers are summed up by column, which include seven approach object categories*

Approach	Number of Papers
sperm parameters	67
trajectories	49
CASA	68
human study	55
animal study	36
reliability / standardization	60
identification/classification	49

Table 2.2: *Literature Search by Approach. Number of papers are summed up by row, including the five subject categories.*

Approach \ Subject	**Sperm Morphology**	**Motility**	**Fertility**	**Hyperactivity Capacitation**	**Algorithms**
Sperm Parameters	[3] [88] **[103]** [35] **[32]** [46] **[102]** **[117]** [92] [74] [114] **[109]**	[115] [88] **[75]** [35] [52] [47] [79] [94] **[32]** [12] **[80]** [46] **[31]** [60] [83] **[84]** **[105]** **[102]** [73] [68] [15] [114]**[55]**	[46] [92][74] [68] [15] [9] [107] **[55]****[19]** **[117]**	[115] **[75]** [79] **[80]** [60] [83] **[105]** **[102]** [73] [122]**[19]** [119] [114]**[55]** **[84]** **[117]** **[109]**	[3] [94] **[31]** [83] **[84]**
Trajectories	[88] **[103]** **[32]** **[33]**	[27] [88] **[75]** [52] [106] [79] [120] [94] **[32]** **[80]** **[31]** [60] [13] [83] [73] [15] [64]**[55]** **[84]**	[82][53] [15] [51] **[33]****[55]**	**[75]** [79] **[80]** [60] [13] [83] **[84]** **[82]** [73][53] **[33]** **[17]** [119]**[55]** **[117]**	[120] [94] **[31]** [83] **[84]**
CASA	[3] **[25]** [88] **[103]** [72] [43] [114]	[115] **[91]** [58] **[25]** [88] **[75]** [52] [38] [47] [120] [94] [108] **[31]** [83] **[105]** [122] [58] **[77]** [15] [93] [48] [43] [114] **[30]**	[23] [58] [58] [72] **[63]** [15] [93] [48] [65]**[19]** [15] [93] [48] [65] [122] [114] **[16]**	[23] [115] **[91]** **[75]** [83] **[105]** [122] **[77]** **[17]** [122]**[19]** [43] [114] **[16]**	[98] [3] [120] [94] **[31]** [83]
Human Study	[3] **[25]** [88] **[118]** [72] **[102]** **[33]** [113] [121] [43]	**[25]** [88] [52] [47] [79] **[80]** [83] **[84]** [122]**[55]** **[102]**[73] [68] [93] [66] **[113]** [43]	**[55]** [72][92] [68] **[33]** [93] [66] [9] [65] **[113]** **[19]**	[79] **[80]** [83] **[84]** [122] [55] **[118]** **[102]**[73] **[33]** **[113]** [121] **[19]** [43]	[3] [83] **[84]**
Animal Study	[46] [114]	[115] [58] [46] [60] [13] **[105]** [58] [15] [48] [114]	[23] [41] [58] [46] [58][53] [15] [51] [78] [48]	[23] [41] [115] [60] [13] **[105]** [53] [78] **[17]** [119] [114] **[100]**	[98] [78]
Reliablity/Standardization	[25] [88] **[103]**[35] [26] [112] **[32]** [72] [69] [74] [50] **[57]** [4] [114]	[94] **[91]** [27] **[25]** [88] **[75]** [35] [26] [38] [47] [106] [112] [108] **[32]** [12] [122] **[77]** [73] [50] [68] **[57]** [64] [48] [4] [114] **[30]** **[49]**	[23] [112] [72] [74] **[63]** [68] [48]	[23] **[91]** **[75]** [112] [122] **[77]** [73] [4] **[17]** [122] [114]	[94]
Identification/Classification	[3] **[21]** [102]	**[75]** **[80]** [13] [83] **[84]** **[105]** **[110]** [122] [55] **[91]** **[84]** [83] **[102]** [78] **[21]**	[23] **[55]** **[82]** **[19]** **[21]** **[16]**	[23] **[75]** **[21]** **[80]** [13] [83] **[84]** **[105]** **[110]** [122]**[55]** **[102]** **[82]** [78] **[17]** **[19]** **[21]** [119] **[100]** **[16]**	[98] [3] [83] **[84]** [78]

Table 2.3: *Matrix on Existing Literature of Spermatozoa Research*

2.2 Morphology and Anatomy

The mammalian spermatozoon belongs to the group of gamete cells that fuse with another gamete, the oocyte, during fertilization. The spermatozoon contains four segments: the head, middle piece, flagellum and end piece. In 1985, Cummins published linear sperm dimensions of 284 species, based on current literature. The length of mammalian sperm ranges from $33.5\mu m - 356.3\mu m$. A human sperm (homo sapiens) ranges from $54.5\ to\ 61.5\mu m$ in length. The species used in this study, the horse, produces spermatozoa that are approximately $60.6\mu m$ in length including a head that is $7.0\mu m$ long and $3.9\mu m$ in diameter [29, 42]. The head is flat and contains an acrosomal cap. This cap contains enzymes that when released, allow the sperm to penetrate the outer integuments of the oocyte. The middle piece consists of an axial bundle of microtubules surrounded by mitochondrial cells, that act as the cell's power plant and produce the ATP necessary for cell movement. ATP, Adenosine-5-triphosphate is a multifunctional nucleotide (organic compound), responsible for intracellular energy transfer. The principle part is the motile component of the spermatozoon and contains microtubuli, which slide past each other in the presence of ATP (Figure 2.1). This sliding motion causes the principal piece to bend back and forth causing the tail to beat and propelling the sperm forward. The head of the spermatozoon is approximately 20 times smaller than the oocyte.

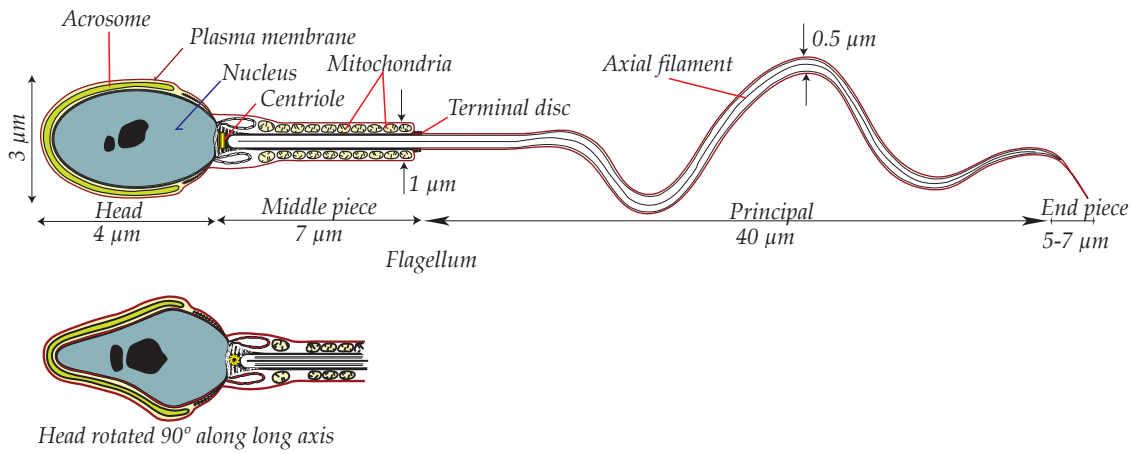

Figure 2.1: *Human Spermatozoa Diagram. Wikimedia Commons. Proofed for correctness by Graham [40, 104]*

2.3 Motility

The largest component of the sperm is the principal, which includes the flagellum. The cross section of the tail is oval with an approximate diameter of $0.5\mu m$ containing an inner and outer axial oriented set of fibers, responsible for a helical motion of the tail which propels the sperm. As soon as sperm are ejaculated the full motility pattern is displayed. A human gamete can travel at a progressive speed of $25-50\mu m/s$ [42]. Contrary to common belief, uterine and ovarian muscular contractions are mainly responsible for the transport of the spermatozoa through the female reproductive tract, rather than the propulsion of the sperm itself. In 1972 Baker performed an experiment in which both live and dead boar sperm were inseminated within the reproductive tract of a gilt and found that both, dead and live, sperm were transported up the reproductive tract [10], although dead sperm transport was less efficient than the live sperm. Another experiment by Kissler (2004) supported the

results of this passive transport mechanism by showing that isotope marked macroalbumin-aggregates [61] are transported through the female reproductive tract. However, spermatozoa motility traversing certain sections of the female tract including the utero-tubular junction and areas within the fallopian tubes, allow the sperm to come in contact with the oocyte. Sperm motility immediately post ejaculation is a linear, progressive motion. This pattern changes to an erratic star pattern at the end of sperm capacitation, when the sperm approaches the oocyte. This changing behavior pattern is further discussed in section 2.5 and 2.6.

2.4 Measures

The focus of this dissertation is sperm motility, thus mainly motility parameters are discussed here. We first describe in section 2.4.1 standardized measures as published by the World Health Organization (WHO), followed by non-motility measures relevant to this dissertation in section 2.4.2. For completeness, we include non-traditional motility measures in section 2.4.3. However, no standard parameter values or algorithms exist to classify hyperactivated sperm. Section 2.4.4 concludes with a discussion about these measures and their relevance to hyperactivity. The measures are summarized in Table 2.4.

2.4.1 Traditional and WHO Standardized Measures

The World Health Organization (WHO) published the laboratory manual for examination of human semen in 1987 and 1999[89]. It was followed in 2002 by the European Society of Human Reproduction and Embryology (ESHRE) and the Special Interest Group on Andrology (SIGA) [88]. These guidelines were an attempt to standardize spermatozoa

parameters for easier comparison between studies conducted at different sites. Figure 2.2 shows an example trajectory containing the definitions of the parameters. Both manuals provide guidelines for human studies. However, these guidelines have been used in animal studies as well. The guidelines cover many semen parameters including ejaculate volume and sperm concentration. The WHO motility parameters are defined as follows:

Curvilinear velocity VCL: This is the point-to-point velocity of the sperm head's center position in $\mu m/s$ divided by the recording time.

$$VCL = \frac{\sum_{i=0}^{m-1} \sqrt{(x_{i+1} - x_i)^2 + (y_{i+1} - y_i)^2}}{(m-1)\,\Delta t} \tag{2.1}$$

Here x_i, y_i are the data points of the trajectory and i and m are the indices of the first and last point, respectively. The sampling time is Δt.

Straight line velocity VSL: This is the length of the line between the first and last point of the trajectory, divided by the acquisition time in $\mu m/s$. VSL is an indicator for forward moving, progressive sperm. The shortcoming of this measure is that this formula only uses the first and the last point of the trajectory to calculate progressiveness, while ignoring the entire middle portion of the track:

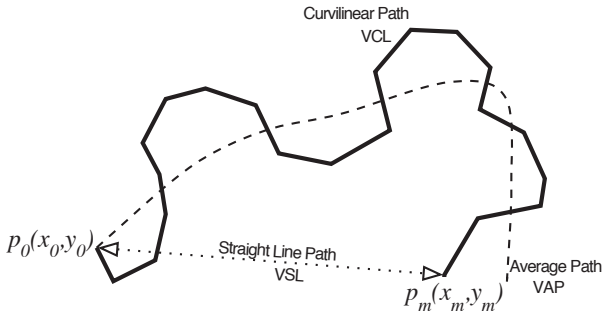

Figure 2.2: *WHO sperm motility parameters. The Curvilinear Path VCL represents the measured sperm track. The Average Path Velocity is calculated from a 5-point smoothed trajectory. The Straight Path Velocity is used in conjunction with VCL to represent "Straightness" of the spermatoza movement. All measures are distances μm, sampled at a fixed rate of 60 Hz and then represented as velocity $\mu m/s$.*

$$VSL \;=\; \frac{\sqrt{\left(x_m \;-\; x_0\right)^2 + \left(y_m \;-\; y_0\right)^2}}{\left(m-1\right)\Delta t} \tag{2.2}$$

Where x_0 and y_0 are the x, y coordinates of the first point of the trajectory and x_m and y_m are the coordinates of the last point of the trajectory.

The average path velocity VAP: This is a 5-point running average to produce a smoothed path of the trajectory.

$$VAP \;=\; \frac{\sum_{i=0}^{m-1} \sqrt{\left(\bar{x}_{i+1} \;-\; \bar{x}_i\right)^2 + \left(\bar{y}_{i+1} \;-\; \bar{y}_i\right)^2}}{\left(n-1\right)\Delta t} \tag{2.3}$$

Where x_i, y_i are the data points of the trajectory and i and m are the indices of the first

and last point, respectively. For the $\bar{x}$ component:

$$\bar{x}_k \;=\; \frac{1}{5}\sum_{k-2}^{k+2} x_i \tag{2.4}$$

and for the $\bar{y}$-component:

$$\bar{y}_k \;=\; \frac{1}{5}\sum_{k-2}^{k+2} y_i \tag{2.5}$$

Where x_k, y_k denote the new average trajectory points ($k = 3 \; ... \; m-2$). At the end of the trajectory the five-point average is reduced to a three-point average and finally to a one-point average to compensate for the missing last four points due to the five-point running average.

Linearity of a sperm LIN[1]*:* This is defined as the quotient of the straight linear velocity and the the curvilinear velocity of the selected track in percent :

$$LIN \;=\; \frac{VSL}{VCL} \tag{2.6}$$

[1]We adhere to WHO nomenclature, although the formula should correctly be written as $LIN = VSL * 100/VCL$.

Straightness STR[2]*:* Similar to the definition of LIN with the exception that it uses the average path instead of VCL:

$$STR = \frac{VSL}{VAP} \tag{2.7}$$

Beat cross frequency BCF: This is measured in Hertz for the selected track and is defined as the frequency with which the cell crosses the cell average path in either direction.

Amplitude of lateral head displacement ALH: Defined as twice of either the maximum or the average value of the distance of any point on the trajectory average path to the actual location of the sperm. In the literature [89], ALH is computed with different algorithms, so that values are not strictly comparable. ALH is dependent on the computation of an average path of the trajectory that can be difficult for extremely irregular tracks, such as are seen in hyperactivated trajectories and is therefore only defined for trajectories with $STR > 80\%$.

$$ALH = 2 \cdot MAX_{i=0}^{m-1} \left\{ \left[(\bar{x}_i - x_i)^2 + (\bar{y}_i - y_i)^2 \right]^{\frac{1}{2}} \right\} \tag{2.8}$$

Where x_i, y_i denote the x-coordinates of the trajectory point and $\bar{x}_i, \bar{y}_i$ are the average position y-coordinates calculated according to formula 2.4 and 2.5

Wobble WOB: Measure of oscillation of the actual path about the average path:

[2]As with LIN, the formula should be correctly written as $STR = VSL * 100/VAP$.

$$WOB = \frac{VAP}{VCL} \tag{2.9}$$

Mean angular displacement MAD: The time average of absolute values of the instantaneous turning angle of the sperm head along its curvilinear trajectory.

2.4.2 Non-Motility WHO Measures

The following measures relate only indirectly to motility classification. However, we include these for completeness, since they are typically part of a CASA data output.

ELONGATION: The longest axis of the ellipsoid shaped spermatozoa head. Used to differentiate between sperm cell and debris.

TOTAL COUNT: The total number of identified sperm cells by CASA, this includes live and dead cells.

MOTILE COUNT: The number of identified live cells by CASA.

MOTILE PERCENT[3]*:* The fraction of $(MOTILE\ COUNT)/(TOTAL\ COUNT)$.

2.4.3 Non-Traditional Motility Measures

The following motility measures are not standardized or endorsed by WHO. However, they are attempts by researchers to overcome the limitations of standardized measures to describe sperm hyperactivity [31]. Some are used frequently, others are more esoteric. The

[3] As previously stated with LIN and STR, we adhere to WHO nomenclature, although the formula should be correctly written as $(MOTILE\ COUNT * 100)/(TOTAL\ COUNT)$.

first two are based on the assumption that spermatozoa swimming patterns oscillate while moving forward and the oscillation increases in frequency during hyperactivation. An oscillation, or a derivative, is measured as a positive and negative lateral movement of the sperm head centroid in relation to the calculated average trajectory path [80, 84]. This certainly is valid for most progressive sperm and some hyperactivated spermatozoa with more regular paths (circle, linear with increased lateral movements). However, it becomes increasingly difficult to calculate for sperm trajectories that exhibit a zig-zag or trashing movement pattern because there is no clear distinction between the original sperm head position and its relation to the average path trajectory. [22].

The focus of the following measures is on motility or sperm hyperactivity:

Frequency of the fundamental harmonic HAR: The fundamental frequency of the oscillation of the curvilinear trajectory around its average path. HAR is computed using a Fourier transformation [32]. This measure is one of many similar to BCF (2.4.1), with the difference that a frequency spectrum is computed from the trajectory, based on the observation of increased lateral movements of a hyperactivated sperm [110].

Magnitude of the fundamental harmonic MAG: The amplitude squared height of the HAR spectral peak (MAG is a measure of the peak-to-peak dispersion of the curvilinear trajectory about its average path at the fundamental frequency. This is a derivative of HAR and dependent on an average path as defined in 2.4.1..

Head Angle Deviation Sum: This is an unusual measure proposed by Mazzilli et al. [73] and requires specialized equipment to visualize the spermatozoa head. The measure draws

a line along the long axis of the ellipsoid sperm head. Two consecutive lines are used to compute the 'Head Angle'. Adding all 'Head Angles' is the Head Angle Deviation Sum (Figure 2.3).

Flagellar Beat Angle FBA: Another unusual measure proposed by Schmidt et al. [105] to quantify the beating angle of the flagellum. FBA is defined by the authors as the largest angle during the left-right movement of the sperm tail. This measure requires specialized equipment the visualize the tail of the sperm.

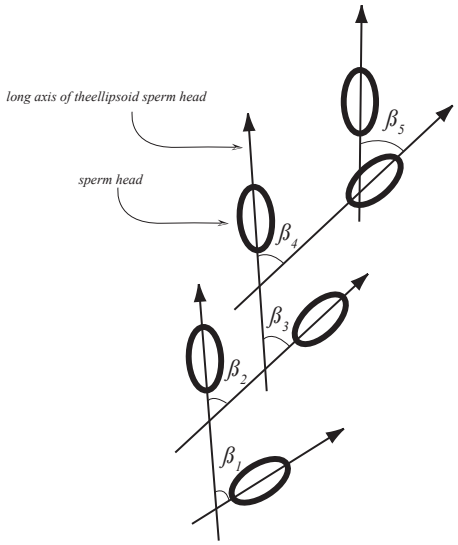

Figure 2.3: *Head Angle Deviation Sum. Chart adapted from Mazzilli et al. [73]*

2.4.4 Existing Measures and Relevance to Hyperactivity Classification

The aforementioned sperm measures describe physiological behaviors of the sperm. There are no direct or indirect measures for hyperactivity. In the past, researchers tried to link certain measures to sperm hyperactivity or non-hyperactivity, but with divergence on the measures in question. For example, Cancel et al. [17] investigated ALH, LIN, VCL, VSL, BCF and LIN and concluded that VCL and LIN are the best measures for hyperactivity. While Mortimer et al. [79] suggests including ALH, BCF, WOB and VSL in the hyperactivity evaluation. So does Baumber et al. [13] in a recent publication of 2006, recommending use of LIN, ALH and VCL for hyperactivity classification. Measures that require equipment (Table 2.6) beyond the one typically found in fertility laboratories restrict the use of a potentially new hyperactivity algorithm to a smaller circle of researchers and are considered unsuitable. We conclude that existing measures by themselves are not suitable to reliably classify sperm hyperactivity.

Acronym	Meaning	Description
VCL	Curvilinear Velocity	total speed of the trajectory
VSL	Straight Linear Velocity	linear speed from 1st to last point of the trajectory
VAP	Average Path Velocity	speed of 5-point running average
LIN	Linearity	straightness of trajectory using VCL and VSL
STR	Linearity	straightness of trajectory using VAP and VSL
BCF	Beat Cross Frequency	oscillation of sperm head around average path per second
WOB	Wobble	oscillation measure VAP/VCL
ALH	Lateral Head Displacement	maximum amplitude deviation off the average path

Table 2.4: *WHO Motility Measures.*

Description	Meaning
Total Count	total number of sperm cells including dead ones
Motile Count	total number of alive sperm cells
Motile Percent	number of alive sperm cells / total number of cells

Table 2.5: *WHO Non-Motility Measures.*

Acronym	Meaning	Description
HAR	Frequency of Fundamental Harmonic	oscillation around average path using Fourier Transformation
MAG	Magnitude of HAR	amplitude squared height of the HAR spectral peak
FBA	Flagellar Beat Angle	maximal left-right movement of the flagellum in 2D
-	Head Angle Deviation	ellipsoid long axis line angle between two consecutive sperm

Table 2.6: *Non-standard Sperm Motility Measures.*

2.5 Capacitation

Austin and Chang are credited for first describing in 1951 that ejaculate cannot immediately fertilize an oocyte, but must go through changes they called capacitation [8, 20]. After ejaculation, the mammalian spermatozoon must undergo the penultimate maturation step in its life cycle, known as capacitation (figure 2.4) before it can fertilize an oocyte. Lately, there is a controversy about the terminal effect of capacitation. Some investigators see capacitation as reversible, others do not [33]. However, there is agreement, that the acrosome reaction (sperm head lining, Figure 2.1) is exocytotic and cannot be stopped or reversed once induced [117]. Exocytotis is a process in which an intracellular sphere moves to the plasma membrane and subsequently fuses with it. Capacitation is a poorly understood series of events that result in a visible change in the motility pattern, from progressive to whiplash-like, thrashing movements and the ability of the sperm to undergo an

acrosome reaction. The main purpose of capacitation is enabling the sperm to penetrate the zona pellucida to bind to the egg's plasma membrane and to fertilize the egg. Although the mechanism of capacitation is not clear yet, during capacitation there is an influx of Ca^{2+}, predominantly coming from the female reproductive tract, that increases intracellular cAMP (cyclic Adenosine MonoPhosphate) a cell messenger, as well as an increase in the phosphorylation (the addition of a phosphate PO_4) of tyrosine, an amino acid, a component of proteins [96]. This in turn increases the sperm's motility [11, 21, 109, 117].

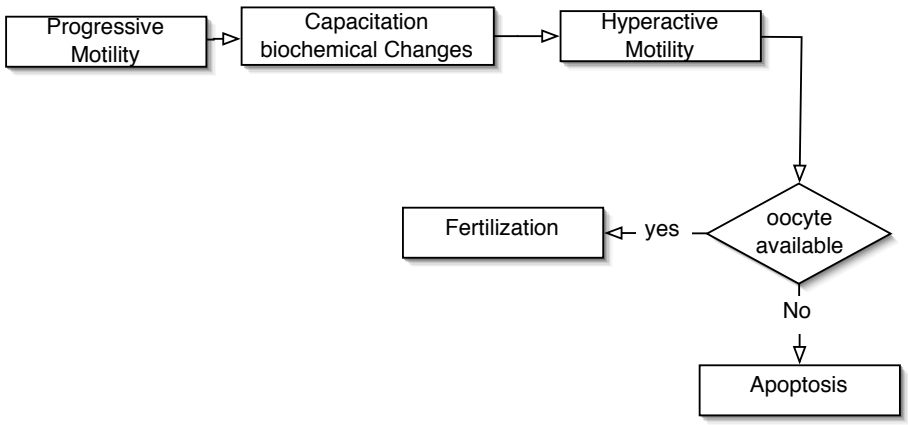

Figure 2.4: *Life Cycle of a Spermatozoa. Apoptosis is a irreversible programmed cell death due to biochemical events.*

2.6 Hyperactivity

Hyperactive motility of sperm, which was first reported by Yanagimachi in 1969 [117], is a capacitation-associated phenomenon. During hyperactivation a mammalian sperm develops a distinctive motility pattern, characterized by asymmetrical, vigorous, non-directional movements (Baumber, 2006[13]). Hyperactive motility may be critical for successful fer-

tilization, because it improves the ability of the sperm to penetrate through the zona pellucida of the oocyte. Hyperactivity appears as an essential event of capacitation associated with an increased velocity, a decreased linearity, an increased amplitude of lateral head displacement, ALH (2.4.1) and whiplash movements of the tail. The precise definition of hyperactivity is difficult and there is no consensus among researchers, especially since the movement pattern varies among species and the physical environment in which the sperm swims (Suarez 2003, Lamirande 1997 [33, 110]). Most investigators agree on subjective, although highly ambiguous, descriptions of hyperactivity (table 2.7) using language such as whiplash-like, jerky movement or changes in flagellar beat pattern (See figure 2.5). Objective definitions of hyperactivity vary as well, although most authors agree on an increased velocity (VCL, measure of section 2.1). However, ranges and thresholds differ between authors and investigated species (Table 2.8).

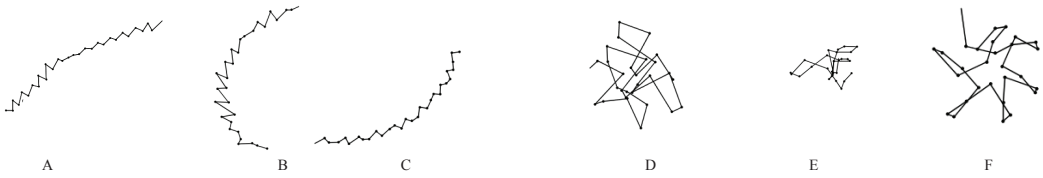

Figure 2.5: *Examples of Stallion Spermatoza Trajectories. Progressive: Trajectories A, B, C. Hyperactivated: Trajectories D, E, F.*

Subjective Hyperactivity Definitions in the Literature			
Author	Year	Hyperactivity Description	Species
[53, Katz et al]	1980	whiplash-like flagellar bending, waves of greater curvature, amplitude, and smaller wavelength	Hamster
[14, Boatman et al.]	1991	modification in flagellar pattern of the beat and sperm trajectory,	Human
[16, Burkman et al]	1991	trashing, circling high-curvature, helical, star-spin	Human
[122, Zhu et al]	1994	non-progressive, high curvature flagellar movements, large amplitude of lateral head displacement, transition phase, 'circling', 'thrashing', 'helical', 'star-spin', 'whiplash'.	Human
[119, Young et al]	1994	highly vigorous, non-progressive random motion, large lateral displacement of sperm head, wide-amplitude flagella movement, wobble parameter	Rabbit
[111, Sukcharoen et al]	1995	vigorous pattern, wide-amplitude, high-velocity, whiplash movements of flagellum, may be progressive, 'star-spin'.	Human
[75, Mortimer et al.]	1997	changes in the flagellar beat pattern, high amplitude whiplash, dancing, decreased flagellar beat frequency and increased flagellar curvature.	Several
[33, Lamirande et al]	1997	non-progressive, vigorous, whiplash type, frantic, high amplitude.	Several
[78, Mortimer et at.]	1999	'whiplash' style of flagellar movement, 'classic' star-spin pattern, 'transition' pattern of motility.	Ram
[73, Mazzilli et at.]	2001	vigorous pattern, high velocity, wide amplitude, whiplash movement, jerky movement, frequent changes in direction.	Human
[100, Rathi et al]	2001	biphasic motility pattern, vigorous, non-progressive movements, but then became static for a while before moving again.	Stallion
[110, Suarez et al]	2003	increase in flagellar bend amplitude, usually beat asymmetry, vigorously in circles	Several
[60, Kinukawa et al]	2003	vigorously, whiplash, figure-8, small circle, not swim in straight line, zig-zag.	Hamster
[105, Schmidt et al]	2004	vigorous, non-linear movement, whiplash.	Boar
[13, Baumber et al]	2006	asymmetrical, high-amplitude flagellar beats, causing vigorous, sometimes nondirectional movement.	Rhesus Macaque

Table 2.7: *Subjective Definitions of Hyperactivity in the Literature*

Objective Hyperactivity Definitions in the Literature

Author	Year	Hyperactive	Transitional	Species
[22, Chantler et al]	2004	$VCL \geq 180\mu m/s; LIN \leq 45\%; ALH \geq 6\mu m$	-	Human
[73, Mazzilli et al.]	2001	$angle\ sum \geq 760°$	$350° \leq angle\ sum < 760°$ @ $21 fr./sec$	Human
[122, Zhu et al]	1994	$VCL = 90\mu m/s$	-	Human
[111, Sukcharoen et al]	1995	$VCL = 90\mu m/s$	-	Human
[102, Robertson et al]	1988	$VCL > 80\mu m/s$	VCL¿ $80\ \mu m/s \wedge 19 < LIN \leq 34\%$	Human
[79, Mortimer et al]	1990	$VCL \geq 100\mu m/s \wedge LIN \leq 60\%$	VCL $\geq 30\mu m/s \wedge STR \geq 60\%$	Human
[16, Burkman]	1991	$ALH \geq 7.5\mu m$, $LIN \leq 65$, $VCL \geq 100\mu m/s$	-	Human
[100, Rathi et al]	2001	$VCL \geq 180\mu m/s \wedge ALH \geq 12\mu m$	-	Stallion
[13, Baumber]	2006	(1)$VCL \geq 150\ \mu m/s; LIN \leq 50\%; ALH \geq 7.0\mu m$ (2)$VCL = 303 \pm 50; ALH = 13.1 \pm 2; LIN = 34 \pm 15\%$	(1)$VCL \geq 130\ \mu m/s; LIN \leq 69\%; ALH \geq 7.5\mu m; STR \leq 97$ (2)$VCL = 295 \pm 40; ALH = 10.3 \pm 2; LIN = 56 \pm 10\%$	Rhesus macaque
[119, Young et al]	1994	$VCL \geq 137.6 \pm 52.0\ \mu m/s$	$VCL \geq 83.1 \pm 35.7\ \mu m/s$	Rabbit
[105, $Schmidt$]	2004	$VCL \geq 97\mu m/s; LIN > 32\%; ALH > 3.5\mu m/s$	$49° \leq FBA < 200°$	Boar
[17, $Cancel\ et\ al$]	2000	$VCL = 652.9\mu m/s; LIN = 9\%; ALH = 34.9\mu m$	$VCL = 496.0\mu m/s; LIN = 18\%; ALH = 23.5\mu m$	Rat

Table 2.8: *Objective Hyperactivity Definitions in the Literature. FBA: Flagellar Beat Angle. ALH:amplitude of lateral head displacement. LIN:* $Linearity = VSL/VCL; STR = VSL/VAP$. *The angle in* $angle\ sum$ *is defined between two consecutive longitudinal axis of a sperm's head, contrary to three consecutive points from a sperm trajectory.(1): 91% effective. (2): average of 50 measurements.*

2.7 Computer-Aided Sperm Analysis (CASA)

The term CASA usually refers to commercial and non-commercial sperm scanners with analysis capabilities conforming to WHO guidelines [89]. In general, the common components of CASA devices are a microscope attached to a camera, which in turn is connected to a video frame grabber and a CPU. The image of the microscope field is recorded by the camera and digitized by the frame grabber. These images are stored in the computer as dots, called pixels. A minimum number of pixels, with certain brightness and arrangement, such as a circle or ellipsoid are recognized as sperm heads, their position tracked over time and translated into 2-dimensional (x, y) data points. They are used to reconstruct the sperm trajectory in an cartesian coordinate system. The numerical values are analyzed, mostly by proprietary software. The typical sperm analysis report is a numerical printout of statistical semen parameters, such as the mean linearity of the sperm movement, percentage of pathological versus normal shapes of the sperm head, or dead versus live sperm in the sample. Widely used commercial CASA systems include the HTM-IVOS by Hamilton-Thorne Bioscience, Beverly, MA, and the Hobson Sperm Tracker by Hobson Sperm Tracking Ltd, Sheffield, United Kingdom. In addition, there are also noncommercial CASA systems used in laboratories. These often use tracking software designed for bacteria to track spermatoza [75].

This section covers how and to what extent computer-aided sperm analyses are being used by investigators for research and clinical diagnostics. The focus of this research is sperm motility and its hyperactivated mode. Hence, CASA's tools capabilities that are beyond those related to sperm motility are outside of the scope of this dissertation. More technical details of the CASA device used in this thesis are explained in detail in chapter 4.

With the advancement of computer hard- and software, first attempts appear in the literature to automate semen analysis with computer technology as early as 1973, Jecht and Russo [2, 5]. These authors reported that a motion-analysis system developed for the National Aeronautics and Space Administration at the Jet Propulsion Laboratory could track human sperm. At the time (1978), the tremendous hardware cost limited the installation to a single device at Woods Hole, MA. It was used to screen bull studs. With the advent of the personal computer and a drop in hardware prices, the first widespread use of computer-aided sperm analysis (CASA) devices was seen beginning in 1986. The use of CASA devices was supposed to bring a higher precision and a better provision of quantitive data than manual methods [30]. Interest waned after the initial hype about the capabilities of CASA devices. As in many other areas where computers were introduced, expectations were set too high. For example, there was the claim that CASA could replace laboratory andrologists [77]. Although much improved today, CASA initially had difficulties in distinguishing spermatozoa from debris, and therefore returned false sperm concentrations. A non-representative survey among andrologists and cryo sperm banks confirmed the less than favorable view of CASA [54]. There is a perception among professionals that a trained technician is superior to most computer-aided analysis. In addition, another often cited complaint about proposed new sperm measurements methods is the lack of proof of applicability in daily practice [5, 63].

2.7.1 CASA and Hyperactivation

The standard analysis reporting capabilities of CASA are frequently used by investigators to classify hyperactive sperm [17, 91, 105, 111]. For example, Mortimer et al.[77] in

2000, suggested using a warmed glass slide with a chamber depth of $30\mu m$ and a minimal frame acquisition setting of $50 - 60\ images/second$. The authors suggest tracking at least 200 motile spermatozoa for CASA analysis. It is not clear from the publication whether the author means 200 sperm tracked during one single scanning or from multiple spots from the same specimen slide. The author suggests using the following thresholds of WHO parameters to classify hyperactive sperm, $VCL \geq 150\mu m/s \wedge LIN \leq 50\% \wedge ALH_{max} \pm 7.0\mu m$. Then, hyperactive sperm are identified by using the 'SORT' function of the CASA device for measured WHO parameters. It should be noted that Mortimer stresses the boolean logic AND of these three sperm hyperactivity thresholds, an important detail often lacking in the work of other investigators. It is unlikely that simple thresholding of WHO measures can capture the complexity of hyperactive sperm movements correctly in multiple stages, (as even stated by the authors themselves) as the transition phase, or progressive hyperactivated motility, and the star-spin, or non-progressive hyperactivated motility. The author concludes that CASA provides a more effective and streamlined clinical management of sperm motility because, according to Mortimer, several hundred spermatozoa have to be studied for statistical significance, which is only practical with CASA.

Sperm hyperactivity in the boar was investigated by Schmidt et al.[105] in 2004. Their interest was to capture the fast beating flagellar motion up to 200 beats/s of single chosen sperm. This motion is usually not visible in commercial CASA devices. The researchers used a non-standard CASA experimental setup consisting of a custom frame grabber, a cell motion analyzer program and a spreadsheet for data analysis. The authors introduce a new motility parameter, the flagellar beat angle, FBA, which is, unfortunately, manually calculated and used in combination with WHO defined parameters. Their sperm hyperactivation

thresholds are listed as $ALHmean > 3.5\mu m$ as a single threshold or in combination with $VCL > 97\mu m/s, LIN < 32\%\ AND\ WOB < 71\%$. It is not clear, whether the authors apply a boolean AND among these thresholds.

Simple thresholds based on WHO measures are inadequate to reliably classify hyperactivity. Sperm hyperactivity is a change of the sperm movement pattern from progressive to an erratic pattern that cannot be captured by static thresholds alone. FBA captures the physical source of hyperactive flagellar beat increase, but requires specialized equipment and an increase in flagellar beat does not necessarily result in an erratic movement of the sperm. Hence, there is need for classification methods that more fully consider the physiology of the sperm trajectory. Figure 2.6 illustrates examples of different sperm hyperactivation approaches.

2.8 Sperm Hyperactivity Classification

Hyperactive sperm can be classified using the following types of approaches:

a: Manual

b: Computer assisted

c: Fully automated

Thus far, hyperactive sperm are often classified manually by trying to fit a sperm trajectory image into a set of images with known hyperactivity classification, clearly reaching the limitations of a human. The following section is divided into describing examples of sperm hyperactivation classification in a manual approach (2.8.1), by using the CASA results to-

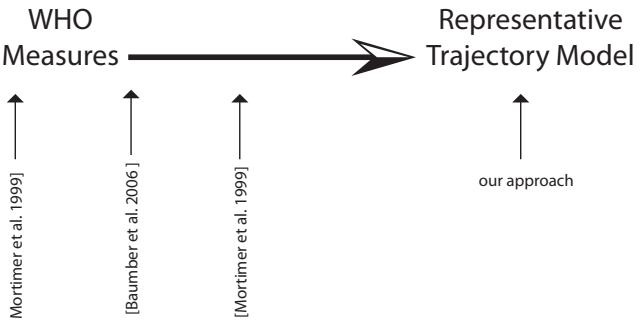

Figure 2.6: *Model-based Hyperactivity Classification*

gether with spreadsheet classification (2.8.2) and by using CASA with a model approach (2.8.3).

2.8.1 Manual Analysis

Mortimer et al. [79] in 1990 reported success in manually classifying capacitated human spermatozoa with the help of CASA into three visual categories: forward progressive, transitional and hyperactivated motility. Human hyperactive tracks were defined by these investigators as having the following thresholds: $VCL \geq 100\mu m/s$, $LIN < 60\%$ and $ALH \geq 5\mu m$, $STR < 60\%$, $VSL < 30\mu m/s$. Their approach was very pragmatic. Video recordings were magnified, replayed on a monitor, retraced on acetate sheets, and then classified by larger or less regular flagellar movement. WHO parameters were calculated manually (measured in millimeters) using a map measurer (opisometer) or curvimeter. Considering the limited technology, the results were nevertheless impressive.

2.8.2 Manual Analysis (CASA assisted)

Baumber [13] in 2006 reported a method of defining hyperactivity that could be routinely used in a laboratory. The method was applied to sperm of rhesus macaques. The authors artificially triggered hyperactivity in their sperm sample by pharmaceutical agents and examined it with CASA. The WHO motility parameters collected by the CASA device were then used as threshold for sperm hyperactivity classification. These thresholds were: $VCL \geq 130\mu m/s, LIN \leq 69\%, ALH \geq 7.5\mu m$. The authors reported a $> 91\%$ effectiveness in detecting hyperactive sperm trajectories. Transitional tracks were based on the 10th/90th percentile of the hyperactive thresholds. The investigators' results are surprising, because their thresholds for sperm hyperactivation include the amplitude of lateral head displacement, a measure based on the trajectory average path, which fails in classifying 'thrashing' in hyperactivated tracks.

2.8.3 CASA with Model Approach

In 1999 Mortimer et al [83] introduced another paper measuring capacitated and hyperactivated sperm tracks using three new parameters in addition to standard WHO measures. They stipulate that hyperactivated spermatozoa are consistently mis-classified within a laboratory because CASA measures, in particular the amplitude of lateral head displacement (ALH), rely on an average path calculation, which is ambiguous for irregular, hyperactivated trajectories. ALH assumes a sperm movement that increasingly oscillates around a calculated 5 point average path. This oscillation cannot be seen in a zig-zag hyperactive trajectory. The first new measure was the instantaneous velocity (VIN) as the velocity of the centroid between consecutive track points. The following formula notations from Mor-

timer's paper were adapted to conform with the labels and indices used in this dissertation.

$Distance_i \;=\; \sqrt{(x_i \,-x_{i+1}\,)^2 \,+\, (y_i \,-y_{i+1}\,)^2}$. Where $Distance_i$ is a segment between two consecutive point of the sperm trajectory and x_i, y_i are the data points of the trajectory ($i = 1, ..., n-1$).

Then $VIN_i \;=\; (distance_i \,\div\, mcf) \;*60\; Hz$, where mcf is a magnification factor to calibrate the measure. In the authors' case mcf was 3.54. The Velocity$-$angle measure VAM (Figure 2.7), defined by the investigators as the product of the change in direction of the centroid movement and the instantaneous velocity of the following segment is calculated from (x, y) data pairs using a spreadsheet. The angle definition is given as

$\cos\;\Theta_k \;=\; \frac{[distance(p_{k-1}\,,\,p_{k+1})]^2 \,+\, [distance(p_{k-1}\,,\,p_k)]^2 \,-\, [distance(p_k\,,\,p_{k+1})]^2}{2\,[distance(p_{k-1}\,,\,p_{k+1})\,\cdot\, distance(p_{k-1}\,,\,p_k)]}$.

VAM is then $VAM_k \;=\; \Theta_k \,\cdot\, distance\,(p_k\,,\,p_{k+1})$. The VAM product is taken for the entire trajectory, averaged and corrected for mcf.

The third new measure introduced by Mortimer is the three-point area (TPA) which gives the area bounded by three consecutive track points as

$TPA_{area} \;=\; \frac{1}{2}\;[distance\,(p_{k-1}\,,\,p_k)\cdot\; distance\,(p_k\,,\,p_{k+1})\;\sin\;\Theta_k]$.

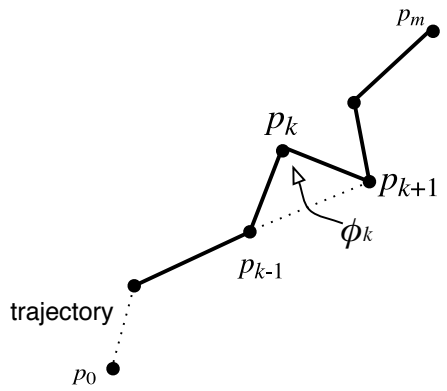

Figure 2.7: *CASA with Model Approach. Velocity-angle measure (VAM) and Three-point area (TPA) measure as proposed by Mortimer et al. in 1999.*

The investigators propose these thresholds for hyperactivated trajectories in the human: $VAM \geq 230\ rad\ \mu m/s$ AND $VIM_{max} \geq 250 \mu m/s$ AND $LIN \leq 50\%$ AND $fractal\ dimension > 1.19$ AND $TPA_{mean} \geq 1.05 \mu m^2$. The investigators do not cover the $fractal\ dimension$, but cite their paper of 1996 [84] covering this measure. There, the authors define $fractal\ dimension$ as $D = \frac{\log(n)}{\left[\log(n) + \log\left(\frac{d}{L}\right)\right]}$, where n is the number of intervals in the trajectory, d is the planar extent of the curve and L is the length of the trajectory. The $planar\ extent\ d$ is defined as the maximum distance between origin and any plotted point point in μm.

The authors found a $fractal\ dimension\ \geq 1.30$ to be a hyperactivated sperm trajectory. The authors concluded that TPA could not discriminate between hyperactivation and circling. Similarly, VAM had high values for circling and for hyperactivated trajectories and could not be used for sperm hyperactivation classification.

2.9 Open Problems

Little work has been done to identify and classify spermatozoa using bioinformatic algorithms that use more detailed trajectory analysis.

Some of the open research issues pertaining to computational approaches in spermatozoa hyperactivity include:

1: There is a lack of bioinformatic models of sperm trajectories that can form the basis for more sophisticated classification algorithms.

2: There is currently no clear and unambiguous definition of hyperactivity.

3: There is currently no automatic and robust classification algorithm to detect hyperactive sperm.

4: It is difficult to determine the true impact of sperm hyperactivity on fertilization because of the lack of a diagnostic hyperactivity detection tool.

5: In-vitro fertilization clinics and veterinary sciences lack information on the appropriate timeline for hyperactivation of a specimen. It is also unknown whether the fertilization rate is higher or lower, if the sperm in a specimen becomes hyperactive more quickly or more slowly.

The contributions in this dissertation concentrate on shedding light on items 1, 2 and 3.

Chapter 3

Comparative Example of Existing Measures

In this chapter, we apply selected often used existing WHO measures introduced in chapter 2 on two examples of a typical progressive, and a hyperactive stallion trajectory to allow a side-by-side comparison. In this chapter we present examples of the following WHO measures: VCL in section 3.1, VAP (3.2), ALH and BCF (3.3), VSL (3.4) and STR in section 3.5. We first plotted the original trajectory from their x, y data pairs, applied the respective WHO measure and overlaid the computed curves, if they exist. In addition to the graphics, we supply the numerical results for each applied measure. Labels used throughout this chapter are: p_0 denotes the first point of the sperm trajectory and p_m, the last point. A $25\mu m$ bar indicates the scale included in all the figures of this chapter.

3.1 Curvilinear Velocity VCL

VCL is the most basic measure of sperm motility (see 2.4.1). The measure simply adds the lengths of segments between data points in μ m and is divided by the data acquisition time receive the velocity in $\mu m/s$. Figure 3.1 shows the computed VCL values on a typical progressive and typical hyperactive sperm trajectory. Note the more than doubling (2.7 times) of the velocity in the hyperactivated sperm (II).

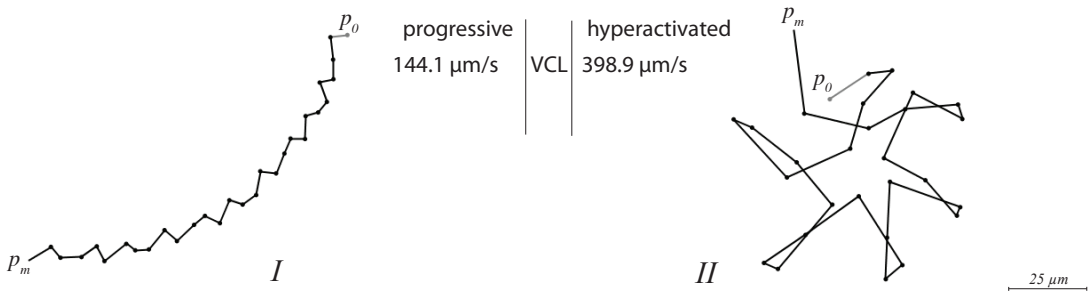

Figure 3.1: *Original Progressive (I) and Hyperactivated (II) Sperm Trajectory. The VCL result of these trajectories are shown.*

3.2 Average Path Velocity VAP

The VAP measure (2.4.1) is often used by investigators to smooth the original trajectory and is the basis of other WHO measure, such as ALH and BCF. This measure works well on progressive trajectories as in Figure 3.2, but has difficulties in more erratic hyperactive trajectories. In II of Figure 3.2 the beginning p_0 and the end p_m of the trajectory cannot be smoothed by VAP. VAP reduces the velocity advantage seen in VCL between a hyperactivated and progressive trajectroy. In the numerical results the hyperactivated trajectory

is now only 1.6 times faster than the progressive sperm.

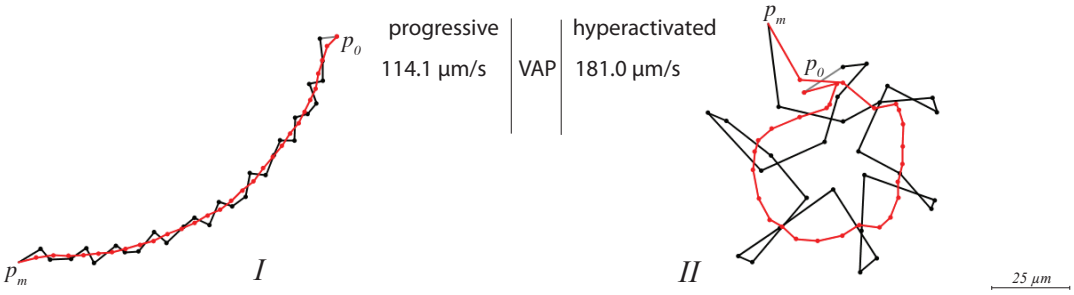

Figure 3.2: *Average Path Velocity VAP*

3.3 Lateral Head Displacement ALH, Beat Cross Frequency BCF

Both, ALH and BCF rely on the average path velocity (VAP) of 3.2. ALH computes the largest perpendicular deviation from the VAP of any point of the trajectory. The resulting distance is multiplied by two. An example of ALH in a hyperactivated trajectory is plotted as a dotted line in Figure 3.3. ALH is too small to plot for the progressive trajctory. ALH assumes the original trajectory crosses over the average path in an oscillating manner and is deceived in erratic or thrashing sperm trajectory patterns, where this regular crossing pattern does not exist.

Similarly, the BCF is a measure of the oscillation of the original sperm trajectory around the average path and is only meaningful if such a movement pattern exists.

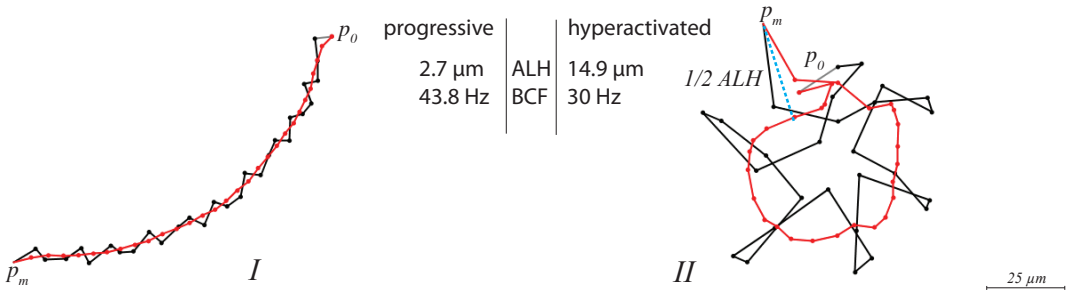

Figure 3.3: *Lateral Head Displacement ALH and Beat Cross Frequency BCF*

3.4 Straight Linear Velocity VSL

This WHO measure is used as an indicator for linearity, by taking the distance between the first point p_0 and last point p_m of the sperm trajectory (Figure 3.4). This measure is vulnerable to directional movement changes in erratic or thrashing motility patterns as observed in hyperactivated sperm. Figure 3.4 picture II shows an example where VSL fails. VSL could have doubled or be cut in half, if p_0 or p_m had changed directions.

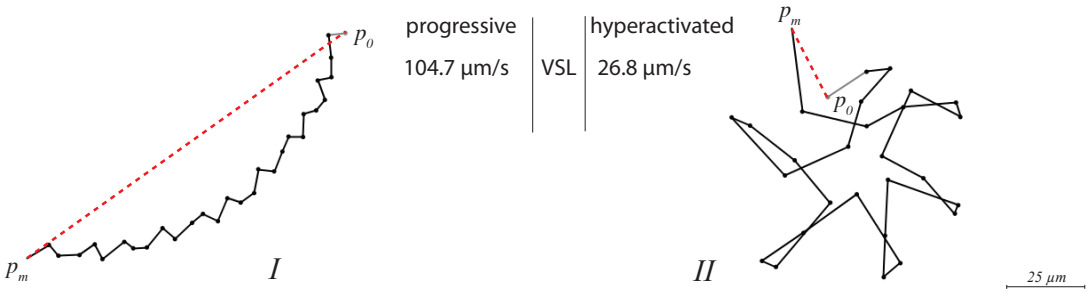

Figure 3.4: *Straight Linear Velocity VSL. This measure is less helpful in hyperactivated sperm trajectories (II).*

3.5 Straightness STR

The last example of a WHO measure is STR, a combined measure of VSL and VAP. It was introduced as an improvement over the linearity measure VSL alone. This measure is derived by dividing VSL by VAP. The result is presented as a percentage. Figure 3.5 displays an example of the original trajectory superimposed by VSL and VAP. The computed STR result for the progressive trajectory is 92%. STR is computed to be 15% for the hyperactivated sperm trajectory example and is for the reasons listed in 3.3 less meaningful for irregular shaped trajectories, as observed in most hyperactivated sperm. For completeness we include a similar measure LIN in this section. LIN is computed by dividing VSL by VCL, and therefore, like STR, inherits the limitations of VSL.

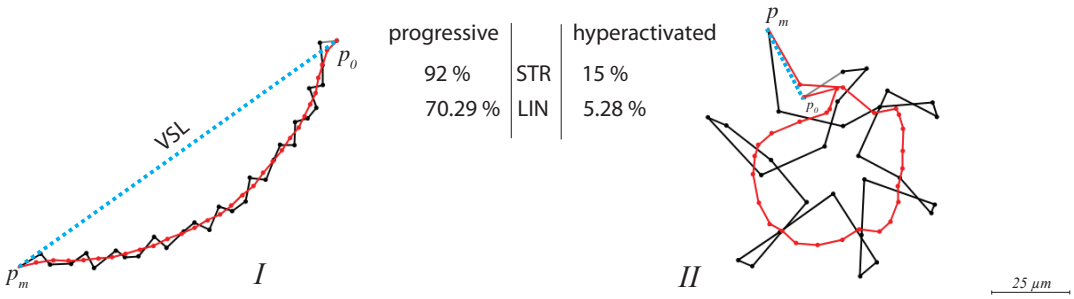

Figure 3.5: *Straightness STR.*

Chapter 4

Approach

This thesis relies on biological data and therefore requires an interdisciplinary approach between computer science and biomedicine. For this study spermatozoa from stallions were chosen, due to their availability and for the safety of laboratory personnel as they are not exposed to infections from handling the samples. In biomedical sciences, most of the results obtained from animal studies can be applied to humans, often with minimal modifications. Rather than computationally capturing all possible hyperactivity patterns, which would have been an almost impossible task, we interpret hyperactive motility of the sperm physiologically as a search pattern to successfully find and fertilize an oocyte. This leads to an algorithm based on the effectiveness of the spermatozoon's searching potential for finding an egg for fertilization. With this model in mind, we refined and tested established measures from the literature together with these new algorithms.

As a brief outline of the upcoming chapter, we present first in section 4.1 the definitions and terminology to help better understand the upcoming chapter. This is followed by a

description of the experimental setup (in section 4.2) and data collection (4.2.5). Section 4.3 discusses validity followed by a discussion of the technique for distinguishing live cells from debris (4.4). Finally we present a detailed description of the proposed classification algorithms in sections 4.5.1 through 4.5.6.

4.1 Definitions and Terminology

The following is a list of basic terminology used in this thesis with their respective definition. Further details are provided within the appropriate algorithm sections.

1: Trajectory Point: The $p_i = (x_i, y_i)$, $(i = 0, ..., m)$ position of the spermatoza head in regard to a x, y coordinate system. p_0 is the first and p_m is the last point.

2: Trajectory or Track: The entire sequence of recorded (x,y) data pairs of one spermatozoon during the data acquisition time of $500\ ms$. The trajectory points of a full trajectory will be labelled $p_0, p_1, ..., p_m$ and consist usually of 30 points ($m = 30$)

3: Segment: The line segment between two chronologically adjacent points $(x_i,\ y_i)$ and $(x_{i+1},\ y_{i+1})$. A trajectory is composed of $m - 1$ segments.

4: Hyperactivated: Classified as red or 1. The phase of a spermatozoon seen in the erratic movement patterns.

5: Transitional: Classified as $yellow$ or 2. The phase of a spermatozoon between being hyperactivated and progressive. Not well defined.

6: Progressive: Classified as $green$ or 3. The initial movement phase of a spermatozoa, seen in a more directed, non-erractic motility.

Classification		
hyperactivated	transitional	progressive
red	yellow	green
1	2	3

Table 4.1: *Classification Terminology*

4.2 Experimental Setup

4.2.1 Experimental Site

All experimental data collections were performed at Colorado State University in Fort Collins, Colorado, Department of Biomedical Sciences, Animal Reproduction and Biotechnology Laboratory under Professor James Graham. Dr. Graham's lab specializes in Male Reproductive Physiology. The sperm trajectory data were obtained from stallion specimens under Animal Care Protocol Approval Number 07-209A-01.

4.2.2 Hardware

A commercial CASA (Computer-aided Sperm Analysis) device by Hamilton Thorne, model HTM-IVOS v10 was used to collect the data. The system consists of the IVOS Analyzer, which integrates a CPU with an optical system (Fig. 4.1) and a camera to track spermatozoa. A laptop computer with a USB frame grabber was interfaced between the camera and an IVOS frame analyzer for analog video clip storage. A microscope with a 10x magnification lens and motorized stage control for the specimen slide is part of the optical system [44]. Slides, coverslips and stage were maintained at $37\ ^oC$ to minimize

artifacts due to temperature fluctuations in the preparations.

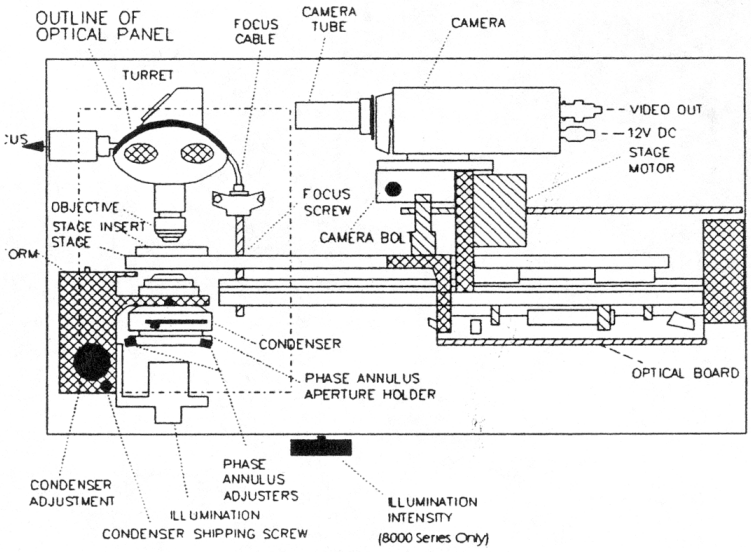

Figure 4.1: *HT IVOS CASA Optical System. On the left side the microscope is shown. Right side depicts the camera used for frame grabbing of the sample. (Hamilton Thorne with permission [44]).*

4.2.3 Calibration and Settings

The Hamilton Thorne IVOS sperm scanner uses a 640 by 480 pixel sensor attached to a microscope with a 10x lens. This results in each pixel representing $1.92\mu m$ (according to the manufacturer). In addition, the device's optic stage was calibrated using a 100 micron grid Makler[1] chamber.

Using the built-in calibration software, the correct magnification was set to be 1.82. The raw data ASCII output file is calibrated in μm. The scale was successfully verified by

[1] An optical flat glass slide with a calibrated etched grid.

reproducing a non−ambiguous parameter as defined by WHO, the straight line velocity VSL (2.2) with our own software and comparing the result with the IVOS sperm scanner's calculation. VSL was chosen, because it simply calculates the distance between the first and last point of a trajectory and is therefore not prone to interpretation errors. Sperm movement is tracked by the sensor as the centroid of a set of pixels of the sperm head with predefined parameters. The location of this centroid is returned as (x, y) data pairs of an orthogonal coordinate system. Frame acquisition rate was set to $60 frames/s$ and 30 frames were acquired equaling $500\ ms$. Minimum cell size was set to 4 pixels. Minimum contrast was 70. Elongation, used to identify spermatozoa from debris and air bubbles, was defined as the ratio of head width to head length. It was set to $12\% < Elongation < 97\%$.

4.2.4 Specimen Preparation

Fresh stallion ejaculates were used to obtain motility data. Each specimen was washed 2 times and the sperm resuspended in TALP dilute to remove debris from the sample and to extend the life of the sperm. Briefly, the sample was first suspended in TALP diluent (Table 9.1) at room temperature. The purpose of the solution is to provide nourishment and prolong the life of the sperm. The specimen was centrifuged at 25 g for 3 minutes. Centrifuging orients cells against the gradient of gravity. Dead cells, because of increased drag, will remain in the middle of the tube, unless they are oriented like the live ones, while live cells end up with high numbers in the pellet. This process increases the concentration of live sperm by approximately 10 to 15%. Another reason for centrifuging is to reduce seminal plasma in the sample . It contains proteins that inhibit capacitation. A sperm density count was performed using spectrophotometry (flow cytometry) as de-

scribed by Hammerstedt [45]. The average sperm count of a stallion is approximately $200 \cdot 10^6 sperm/ml$, approximately 5 times higher than human specimens [25, 100]. This high sperm density would result in an overwhelmingly large number of overlapping trajectories. To reduce ambiguous tracks due to overlap, the sample needed to be diluted to approximately $20 \cdot 10^6 sperm/ml$. Lower density sperm samples also reduce measurement variations and collisions in the glass slide chamber [108]. Finally, a $6\mu l$ sample was placed on a disposable $\frac{1}{2}$" $\times$ 2.0" slide covered with a $\frac{1}{2}$" $\times$ $\frac{1}{2}$" coverslip and analyzed. Experiments [13] have shown that this technique results in a gap of $10\mu m$ distance, larger than the largest diameter ($10\ long\ \times\ 5\ \times\ 2\ \mu m\ deep$) of a stallion sperm, thus confining the sperm to a 2-D space, while still providing ample space for the helical rotating movement. Chamber depth was shown to be critical for sperm concentration calculations, however depth was not significant to detect hyperactive sperm cells, which is the focus here [71, 115]. The volume of the sample and coverslips were kept standardized to allow comparison between all experimental data collection runs [27].

4.2.5 Data Collection

To avoid animal specific bias, specimens from four different stallions were used. Some were used once, others repeatedly, however never more than once a day. The distribution of the sperm in the semen specimens is not homogeneous. Therefore, three measurements were taken from one droplet, each from different locations within the droplet. Data acquisition settings, as described in section 4.2.3, were kept constant for all experiments. Each measurement tracks spermatozoa for $0.5\ s$ and stores the tracking data in two ASCII files on the built-in hard disk. The output data for each trajectory consists of: track identifica-

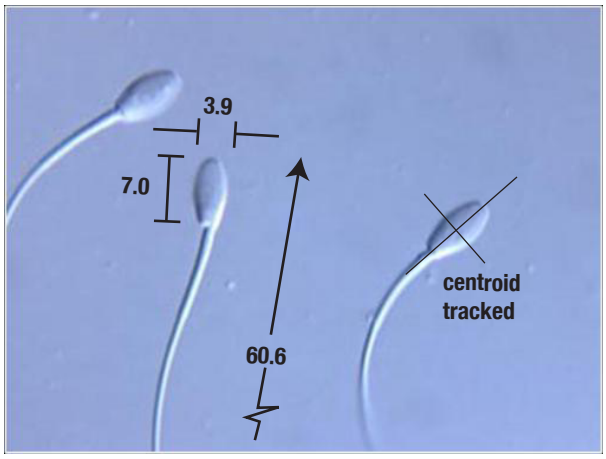

Figure 4.2: *Stallion Spermatozoa. Dimensions of the stallion specimen, Equus caballus, used in this work. Courtesy of Dr. Graham [40]. They are only slightly larger and have a similar morphology than human sperm (Homo sapiens). The centroid position of the sperms' head is tracked by CASA. Scale is in μm.*

tion number, time, trajectory (x, y) coordinate data pairs $(x_0,\ y_0)\ \ldots\ (x_n,\ y_n)$ as well as WHO standardized values of VAP, VSL, VCL, ALH, BCF and STR. A second file lists a summary calculation for all trajectories of one particular recording. The available fields are date, time, VAP, VSL, VCL, ALH, BCF, STR, LIN, ELONGATION, TOTAL_COUNT, MOTILE_COUNT and MOTILE_PCT. The meaning of these acronyms are described in detail in chapter 2 section 2.4. For this thesis, only (x, y) coordinate data pairs are used and WHO data values, such as VCL, are recalculated using the original WHO definition (formula 2.1). The stored ASCII files were transfered via floppy disk for classification analysis.

4.3 Validity Evaluation

In our case of hyperactivity classification of spermatozoa, we have to consider these levels of validity, conclusion, internal, construct and external validity. They are mapped to the different steps seen in figure 4.3.

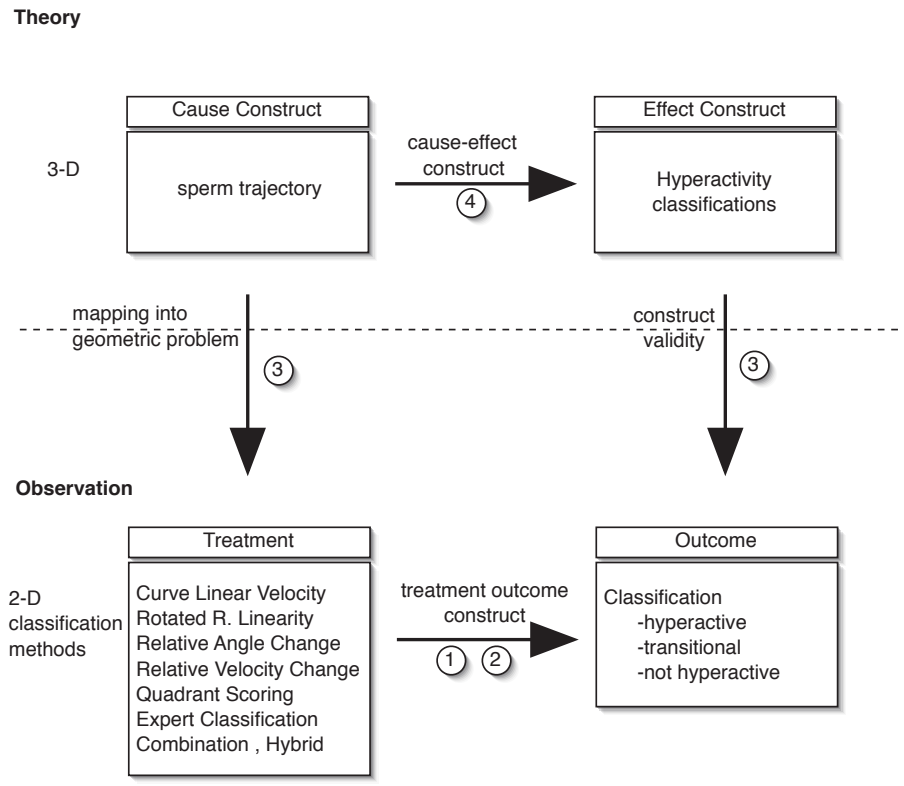

Figure 4.3: *Experimental Principles*

Conclusion Validity ①: This threat deals with the statistical conclusion validity. Conclusion validity was dealt with by using a large number of tests on a large number of sperm.

Internal Validity ②: The internal validity is concerned with the treatment, here the classification algorithms, and the outcome, the classification itself. The data is collected using

Good Laboratory Practice Standards (GLPS) with a calibrated commercial grade sperm scanner (4.2.3).

Construct Validity ③: This validity is concerned about the relationship between theory of sperm classification algorithms and the observation of the actual classification. In the natural biological environment, the spermatoza propel themselves in a 3-dimensional way, however this movement is mapped in the laboratory to a 2-dimensional world. Although the sperms' movement is constrained, it is still an established and appropriate motility measure as shown by other investigators of this field (see section 4.2.4).

External Validity ④: This validity deals with generalization of the results. The experiments do not differ from routine sperm motility tests performed daily in hospitals or veterinary clinics. Moreover we apply the proposed hyperactivity classification algorithm to a study with erectile dysfunction pharmaceuticals to show the feasibility of applying these algorithms in a practical application. We therefore believe that these results may be applicable not only in equine but also in Homo Sapiens.

4.4 Identification Methods

Identification separates live, motile, spermatoza from dead sperm, other cell types or debris. It is a precursor for classification, which is only meaningful on live sperm fulfilling a set of morphological or physiological requirements. The CASA device initially removes objects that do not fit the criteria set forth in $Calibration\ and\ Settings$. One morphological criteria used by CASA is the elongation, defined as the ratio of head width to head length. A ratio of 1 would be a circle and most likely not be a normal sperm head, which is elongated. In this thesis additional measures are used for identification, such as only

sperm with a minimal $VCL \geq 50\mu\ m/s$ are considered. Figure 4.4. shows how sperm are identified in a flowchart.

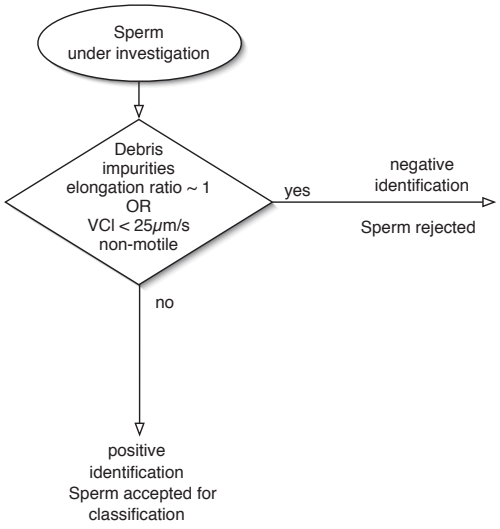

Figure 4.4: *Identification of Spermatoza.*

4.5 Classification Methods

A challenge in classifying biomedical events, such as sperm motility, lies in the non-homogeneous properties of the cells, between cells and over time. It is not feasible for a human operator to observe hundreds of sperm through a microscope in the short time they are motile. Therefore, as in most biomedical experiments, a snapshot of time is used to represent certain behaviors. This approach has been established as a way to capture similar events although the measurements will not be identical. Considering the uncertainty of biomedical measures, any bioinformatic classification algorithm must be robust, have a high level of reproducibility and hold up to the 'gold standard' of manual classification by

experts in the field.

Several approaches are required to capture and describe the motility changes of a sperm. Five new measures and one combined measure are introduced in comparison to one established existing measure. These measures work either by positive classification or elimination of sperm trajectories. Figure 4.5 shows the concept of the developed measures: Rotated Rectangular Velocity in section 4.5.6 , Minimum Bounding Square MBS (4.5.7), Relative Angle Velocity Change RAVC (4.5.2.2), Quadrant Scoring QS (4.5.3), Relative Angle Count RAC (4.5.4) and a combination of the latter, a Logistic Regression Model (4.5.5). For completeness and for comparison we begin with the existing conventional measure, Curvilinear Velocity VCL (4.5.1). For classification of hyperactivity we propose three degrees of hyperactivation: red, yellow and green, where red is a spermatozoid with high probability to be hyperactive, yellow is a transitional spermatozoid less likely to be hyperactive and green is a non-hyperactivated, progressive spermatozoid (see section definitions and terminology 4.1). This is a more realistic approach to classification than existing automated methods, which often only consider two classes: hyperactive and progressive and thus must (mis)classify transitional sperm as either hyperactive or not.

4.5.1 Curvilinear Velocity, VCL

This is an existing measure (2.1) endorsed by the WHO [89]. VCL is a direct measure and the foundation of all derived measures in this research. It captures the absolute distance a spermatozoon traveled during the data acquisition period and is calculated by adding the m segment lengths together and dividing by the measurement duration. The result is presented as velocity in $micrometers\ per\ second$. The capture rate used in this work

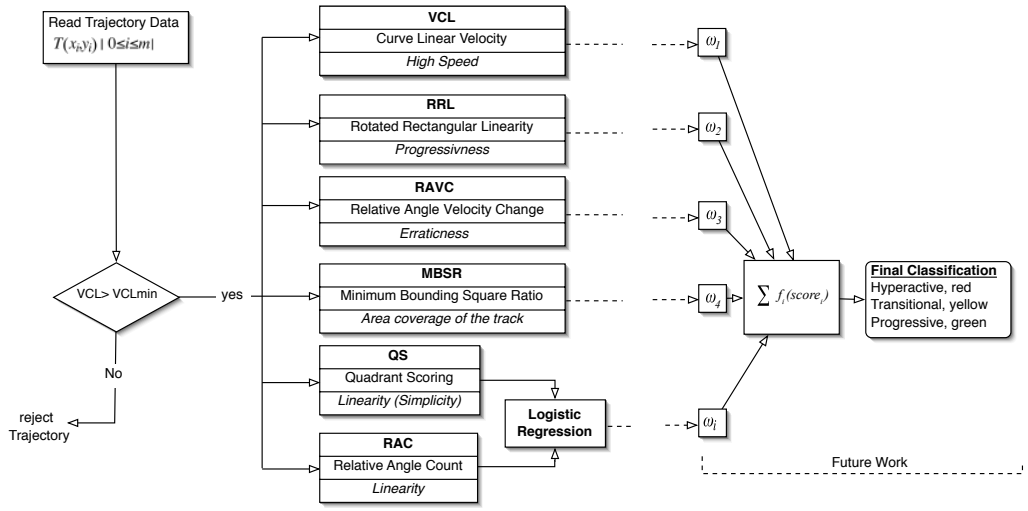

Figure 4.5: *Concept of the proposed Classification Algorithms*

is a constant of $60\ Hz$ with a total recording time of $500\ ms$. It has been shown that the sperm's velocity increases during the hyperactivation phase and VCL is therefore important in defining thresholds from known progressive, or hyperactive data sets [19, 55, 102]. The VCL pseudocode is listed in algorithm 1.

Algorithm 1 Curvilinear Velocity VCL, (T)

1: $m \leftarrow length[T]$
2: $VCL \leftarrow 0$
3: **for** $i = 0$ to $< m$ **do**
4: $\quad d \leftarrow calculate\ segment\ distance\ T[i]$
5: $\quad VCL \leftarrow VCL + d$
6: **end for**
7: **return** VCL

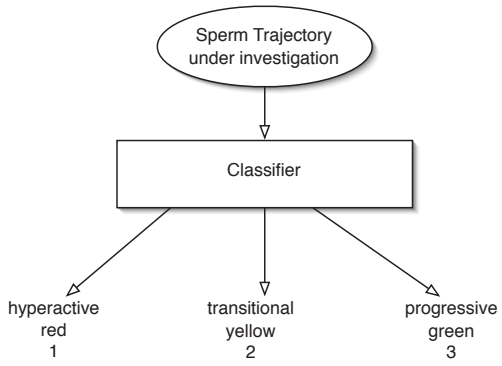

Figure 4.6: *High level classification process*

4.5.2 Relative Angle Velocity Change RAVC

A hyperactivated sperm changes its direction more radically as opposed to a progressive sperm with a more homogeneous smoother trajectory [16, 82]. This physical phenomenon was recognized early on and is listed as the WHO standardized parameter, mean angular displacement MAD (2.4.1). However, as the name indicates, MAD is expressed as a mean over the entire trajectory and will smooth out erratic sperm movement changes, the very feature used to detect sperm hyperactivity, unless they occur often. Often, hyperactivated sperm, especially in the transition stage, make few, but drastic changes in direction. Thus, MAD by itself is not suitable to detect these changes. Mortimer in 1999 [83] extended this measure by multiplying the angle by the length of the following track segment and called it velocity–angle measure, VAM. However, this approach also used a statistical mean over the entire trajectory, concluding the measure cannot discriminate between circling and hyperactivated tracks (2.8.3).

We propose to use a scoring system, rather than statistical means. A score is assigned

to a sperm that exhibits a sudden erratic angular change beyond a set threshold with its following segment larger than a previously set length. Our expectation is that this approach will have a higher specificity ($\frac{True\ Negatives}{True\ Negatives + False\ Positives}$) than MAD or VAM and will even sense transitional sperm motility changes.

The calculation of RAVC is a two step procedure scoring the trajectory segment angles and determining the segmental velocity:

4.5.2.1 Relative Angle Score RAS

The first step is to determine the relative angle θ_k between two consecutive trajectory segments. Let p_0 be the first and p_m be the last data point of a sperm trajectory and p_k be the middle point between p_{k-1} and p_{k+1} for $k = 1, ..., m-1$. Then, the angle θ_k is defined as:

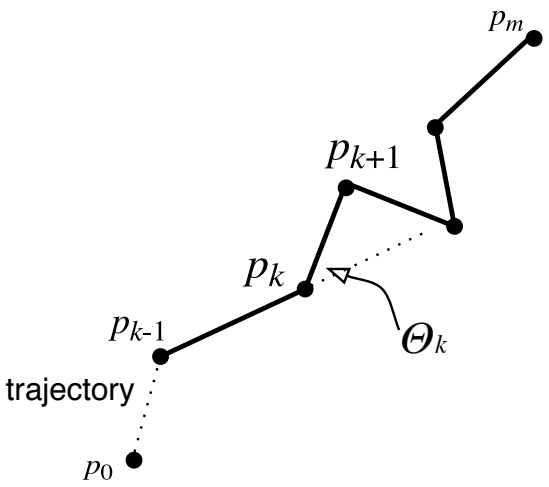

Figure 4.7: *Relative Angle Score RAS. Hyperactivated sperm are defined to have irregular track patterns. RAS captures relative angle changes and is intended to detect inhomogeneous patterns.*

$$\theta_k \;=\; \angle\, p_{k-1}\; p_k\; p_{k+1} \tag{4.1}$$

and finally the relative angle is:

$$\Theta_k \;=\; \pi \;-\; \theta_k \tag{4.2}$$

To capture deviations from straight line motion, we subtract the detected angle θ_k from π. The resulting angle ($\pi \;\leq\; \Theta_k \;\leq\; 2\pi$) will be used to assign scores for RAVC in combination with a trajectory segment (4.5.2.2).

Let R_k be the score assigned to each computed angle:

$$R_k \;=\; \begin{cases} 1 & for\ \Theta_k \;>\; \Theta_{cutoff} \\ 0 & otherwise \end{cases} \tag{4.3}$$

($k = 1, ..., m-1$)

Lastly, the scores R_k are added up to achieve a score for the entire trajectory:

$$RAS \;=\; \sum_{1\,\leq\,k\,\leq\,m-1} \mathrm{R}_k \tag{4.4}$$

Algorithm 2 shows the pseudocode for RAS.

Algorithm 2 Relative Angle Score RAS, (T)

1: $m \leftarrow length[T]$
2: $RAS \leftarrow 0$
3: **for** $k = 0$ to $< m$ **do** {go though all segments in T}
4: $\quad \Theta_k \leftarrow calculate\ angle\ (\pi - \angle\ p_{k-1}\ p_k\ p_{k+1})$
5: $\quad$ **if** $\mid \Theta_k \mid \geq \Theta_{cutoff}$ **then**
6: $\quad\quad RAS \leftarrow RAS + 1$
7: $\quad$ **end if**
8: **end for**
9: **return** $RAS\ Score$

4.5.2.2 RAVC

The angle velocity change, RAVC (figure 4.8), combines erratic angular movement changes (as calculated in section 4.5.2.1), with the velocity changes of each trajectory segment. Let the adjacent trajectory segment velocity be $SVCL_k(p_k, p_{k+1})$, where $p_k = (x_k, y_k)$, $p_{k+1} = (x_{k+1}, y_{k+1})$, and Δt be the recording time ($k = 0,\ ...\ m-1$). The segment velocity $SVCL_k$ is calculated similar to VSL (2.2):

$$\text{S}VCL_k = \frac{\sqrt{(x_{k+1} - x_k)^2 + (y_{k+1} - y_k)^2}}{\Delta t} \tag{4.5}$$

Then the score C_k for each segment S_k is calculated as follows:

$$\text{C}_k = \begin{cases} 1 & for\ \Theta_k > \Theta_{cutoff}\ or\ SVCL_k > SVCL_{threshold} \\ 0 & otherwise \end{cases} \tag{4.6}$$

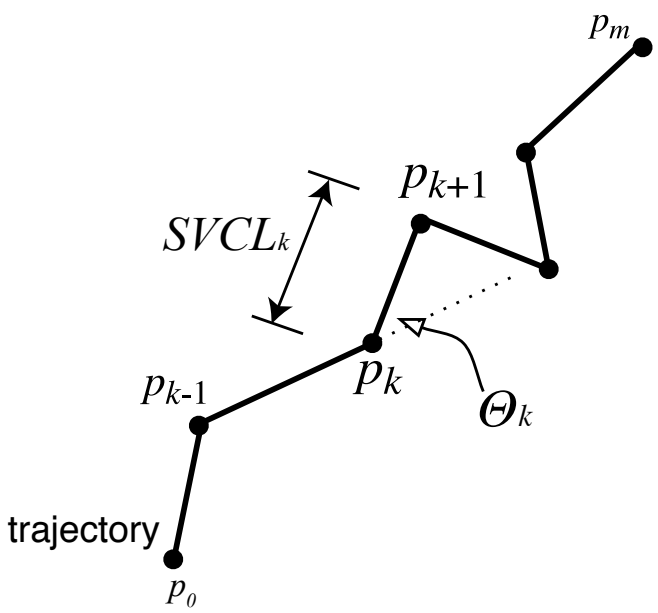

Figure 4.8: *Relative Angle Velocity Change RAVC. An adjacent movement increment is used in conjunction with the angular change. This helps to differentiate hyperactivated sperm from progressive sperm with large RAC, but small incremental movements.*

A score of 1 is assigned if Θ_k and its adjacent segment velocity $SVCL_k$ reach predefined thresholds. Thresholds for the angle Θ_k and velocity $SVCL_{threshold}$ may have different threshold values.

Lastly, the scores C_k are added up to achieve a score for the entire trajectory:

$$RAVC = \sum_{1 \leq k \leq m-1} \mathrm{C}_k \tag{4.7}$$

Algorithm 3 Segment Velocity SVCL, (T)

$m \leftarrow length[T]$
$SVCL\ score \leftarrow 0$
for $k = 0$ to $< m$ **do**
  $SVCL_k \leftarrow calculate\ segment\ velocity$
  if $SVCL_k \geq threshold$ **then**
    $SVCL\ score \leftarrow SVCL\ score + 1$
  end if
end for
return SVCL score

Algorithm 4 Relative Angle Velocity Change RAVC, (T)

1: $m \leftarrow length[T]$
2: $SVCL\ score \leftarrow$ **false**
3: $RAS\ score \leftarrow$ **false**
4: **for** $i = 0$ to $< m$ **do**
5: $\Theta_k \leftarrow calculate\ angle\ (\pi - \angle\ p_{k-1}\ p_k\ p_{k+1})$
6: **if** $\mid \Theta_k \mid \geq \Theta_{cutoff}$ **then**
7: $RAS\ score \leftarrow$ **true**
8: **end if**
9: $SVCL_k \leftarrow calculate\ segment\ velocity$
10: **if** $SVCL_k \geq threshold$ **then**
11: $SVCL\ score \leftarrow$ **true**
12: **end if**
13: **if** RAS **true** OR $SVCL$ **true then**
14: $RAVC \leftarrow RAVC\ + 1$
15: **end if**
16: **end for**
17: **return** $RAVC\ Score$

4.5.3 Quadrant Scoring QS

Quadrant scoring (QS) is an attempt to explore whether a very simple algorithm can be utilized to classify sperm trajectories. QS counts the occurrences of the trajectory turning points relative to the previous point in the four quadrants, I, II, III and IV of a Cartesian coordinate system. The resulting four scores could be useful in interpreting circular or progressive movements. The case of $S_I \sim S_{II} \sim S_{III} \sim S_{IV}$ could be interpreted as a circular motion as observed in hyperactivated sperm, while a concentration of scores in one or two quadrants could indicate smoother, progressive sperm movement.

Conjecture 1: Trajectories with a concentration of QS scores in two or less quadrants may be *progressive*.

Conjecture 2: Trajectories with a distributed QS scores in more than three quadrants may be *hyperactive*.

This requires a measurement of the dispersion of the data, which can be measured by its standard deviation σ. A low σ indicates a distribution of QS among the quadrants (hyperactive), while a high σ shows a concentration of QS in fewer quadrants (progressive).

The standard deviation is defined as: $\sigma = \sqrt{\frac{1}{n}\sum_{i=1}^{n}\left(QS_i - \overline{QS}\right)^2}$. Where σ is the standard deviation, n the number of data points (here four quadrants), QS_i the quadrant score of the appropriate quadrant 1 through 4 and $\overline{QS}$ is the mean of $(QS_1 + QS_2 + QS_3 + QS_4)/4$.

Let p_k be a previous point of the sperm trajectory, p_{k+1} the next point of the track and $\overrightarrow{V}_{QS} = (QS_1, QS_2, QS_3, QS_4)$ the quadrant score sum vector and $p_0\ , ..., p_m$ be the vertices in the trajectory. Then $\overrightarrow{V}_{QS}$ is calculated by:

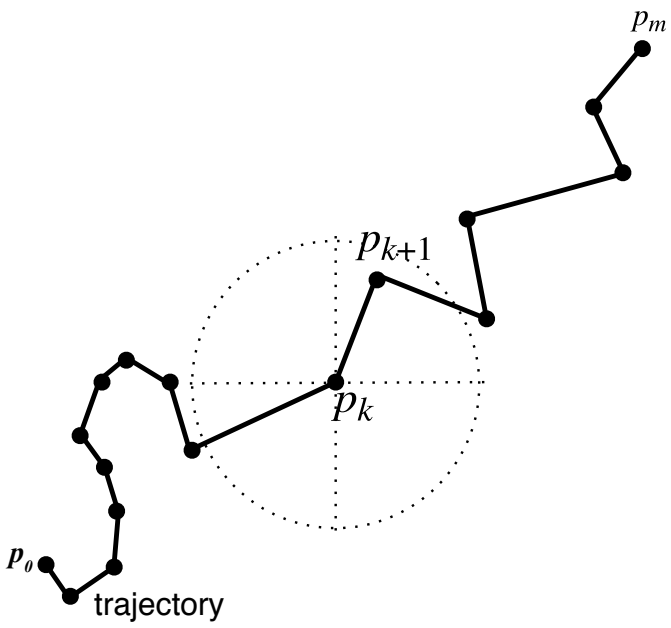

Figure 4.9: *Quadrant Scoring QS. The intend of this proposed measure is to show the effectiveness of a simple algorithm for hyperactivity classification.*

$$\overrightarrow{V}_{QS} = \sum_{i=0}^{m-1} \overrightarrow{q}\,(p_i\ ,\ p_{i+1}) \tag{4.8}$$

where $\overrightarrow{V}_{QS}$ is the vector quadrant score sum and $\overrightarrow{q}\,(p_i\ ,\ p_{i+1})$ the score for each individual segment (4.9).

$$\overrightarrow{q}\left(p_i\ ,\ p_{i+1}\right) = \begin{cases} (1,0,0,0) & for\ x_{k+1} - x_k\ \geq\ 0\ and\ y_{k+1} - y_k\ >\ 0 \\ (0,1,0,0) & for\ x_{k+1} - x_k\ <\ 0\ and\ y_{k+1} - y_k\ \geq\ 0 \\ (0,0,1,0) & for\ x_{k+1} - x_k\ \leq\ 0\ and\ y_{k+1} - y_k\ <\ 0 \\ (0,0,0,1) & for\ x_{k+1} - x_k\ >\ 0\ and\ y_{k+1} - y_k\ \leq\ 0 \end{cases} \tag{4.9}$$

The QS results are compared using standard deviation σ .

$$\sigma\ =\ \sqrt{\frac{1}{n}\sum_{i=1}^{n}\left(QS_i\ -\ \overline{QS}\right)^2} \tag{4.10}$$

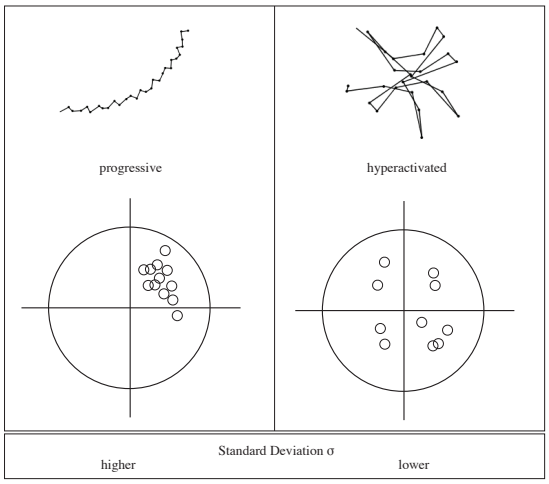

Figure 4.10: *QS Interpretation illustrates the behavior of hyperactivated and progressive sperm track example. A progressive track will most likely score in 1 or 2 quadrants, while a hyperactivated track will have scores distributed among the four quadrants*

where $n = 4$ represents the four quadrants. QS_i is the individual Quadrant Score and $\overline{QS}$ the average of the individual scores. Algorithm 15 summarizes the steps above.

Algorithm 5 Quadrant Scoring QS

$(Q_{1...4}) \leftarrow 0$
for $i = 1$ to $< m$ **do**
  $location \leftarrow (x_{k+1}, x_k, y_{k+1}, y_k)$
  if $location = first\ quadrant$ **then**
    $Q_1 \leftarrow Q1 + 1$
  else if $location = second\ quadrant$ **then**
    $Q_2 \leftarrow Q2 + 1$
  else if $location = third\ quadrant$ **then**
    $Q_3 \leftarrow Q3 + 1$
  else if $location = fourth\ quadrant$ **then**
    $Q_4 \leftarrow Q4 + 1$
  end if
end for
$calculate\ standard\ deviation(Q_{1...4})$
return $(Q_{1...4}), standard\ deviations$

4.5.4 Relative Angle Count RAC

The motivation for this is similar to the Relative Angle Score RAS in section 4.5.4, but with the emphasis on the flagellar motion of the spermatozoa tail, rather than an absolute angle threshold. The helical tail movement is observed in the 2D as an almost symmetrical left-right motion. If the sperm is moving in a progressive fashion, the observed left-right movement should cancel itself. On the contrary, an erratic movement should require an asymmetrical number of beats. The algorithm computation is similar to RAS (see algorithm 2) with the exception of replacing the angle thresholding with a sign function.

Let R_k be the score assigned to each computed angle and let $sgn(\Theta)$ denote the sign of Θ.

$$R_k = \begin{cases} 0 & for\ \text{sgn}\,(\Theta_{k+1}) \neq \text{sgn}\,(\Theta_k) \\ 1 & otherwise \end{cases} \tag{4.11}$$

Lastly, the scores R_k are added up to achieve a score for the entire trajectory:

$$RAS \ = \sum_{1 \leq k \leq m-1} \mathrm{R}_k \tag{4.12}$$

The pseudocode for RAS is listed in algorithm 6.

Algorithm 6 Relative Angle Count RAC, (T)

1: $m \leftarrow length[T]$
2: $RAC \leftarrow 0$
3: **for** $k = 1$ to $< m$ **do** {go though all segments in T}
4: $\quad \Theta_k \ \leftarrow calculate\ angle\ (\pi - \angle\ p_{k-1}\ p_k\ p_{k+1})$
5: $\quad \Theta_{k+1} \ \leftarrow calculate\ angle\ (\pi - \angle\ p_k\ p_{k+1}\ p_{k+2})$
6: $\quad$ **if** sgn $(\Theta_{k+1}) \ =$ sgn (Θ_k) **then**
7: $\quad\quad RAC \leftarrow RAC \ + 1$
8: $\quad$ **end if**
9: **end for**
10: **return** $RAS\ Score$

4.5.5 Logistic Regression Model

In order to investigate if the performance of individual algorithms could be improved by combining them, we turned to a logistic regression model. Logistic regression [18] is used increasingly in medical and biomedical problems to examine effects of one or more variables. Here we look at the effects of combining two algorithms, RAC and QS, both capturing different features of the sperm trajectory. RAC scores a deviation from the left-right movement of the sperm trajectory by adding a score of one (section 4.5.4). This captures the regularity of the whipping motion of a progressive sperm flagellum, normalized as a percent of the number of segments. QS describes the relative occurrence of the sperm location within an orthogonal four quadrant system, expressed as a standard devi-

ation (4.5.3). In this logistic regression application, the binary response variable can take on only two possible outcomes, 1 or 0, corresponding to hyperactivated and progressive states. We initially will classify between hyperactive and progressive sperm trajectories. After the logistic regression has been applied, transitional margins will be determined on the basis of the biological properties of trajectories ambiguously classified by the logistic model. Specifically, several investigators in the past have published criteria for hyperactivated and progressive sperm trajectories [70, 79, 91, 119]. Transitional sperm trajectories are either not mentioned at all or investigators disagree on their criteria [13, 78, 111]. This approach improves the analyses in the literature. Consider the following logistic regression model (equation 4.13). As mentioned above, the response variable is binary 1, 0 and the probabilities are π and $\pi - 1$.

$$\mathrm{E}\left[Y_i\right] \;=\; \pi_i \;=\; \frac{\exp\left(\beta_0 \;+\; \left[\beta_1, \beta_2\right] X_i\right)}{1 \;+\; \exp\left(\beta_0 \;+\; \left[\beta_1, \beta_2\right] X_i\right)} \tag{4.13}$$

where $\mathrm{E}\left[Y_i\right]$ is the expected response and X_i are the observations. The index i represents the observed trajectories. The probability is

$\pi_i \;=\; P\left(Y_i = 1\right)$ and $1 - \pi_i \;=\; P\left(Y_i = 0\right)$ and $\beta_0, \beta_1, \beta_2$ are the coefficients of the logistic regression model.

$$\text{with } X_i \;=\; \begin{bmatrix} RA\mathrm{C} \\ Q\mathrm{S} \end{bmatrix} \text{ and } \pi = \tfrac{1}{2} \text{ we set:}$$

$$\pi \;=\; \frac{1}{2} \;=\; \frac{\exp\left(\beta_0 \;+\; \beta_1 RAC \;+\; \beta_2 QS\right)}{1 \;+\; \exp\left(\beta_0 \;+\; \beta_1 RAC \;+\; \beta_2 QS\right)} \tag{4.14}$$

To solve for x we set $x \;=\; \exp\left(\beta_0 \;+\; \beta_1 RA\text{C} \;+\; \beta_2 Q\text{S}\right)$. The equation becomes $\frac{1}{2}\left(1 + \exp\left(x\right)\right) \;=\; \exp\left(x\right)$. This reduces to $1 \;=\; \exp\left(x\right)$, thus $x = 0$.

Back-substituting, the line $0 \;=\; \beta_0 \;+\; \beta_1 RA\text{C} \;+\; \beta_2 Q\text{S}$ divides trajectories with $\pi \;>\; \frac{1}{2}$ and $\pi \;<\; \frac{1}{2}$.

The logistic regression coefficients $\beta_0, \beta_1, \beta_2$ are found using the command lrm in R Statistical Computing Toolset [37, 99]

4.5.6 Rotated Rectangular Linearity RRL

The goal of this new measure is used to express the linearity, or progressiveness, of a sperm trajectory and therefore allow the elimination of non-hyperactivated sperm. Currently, the WHO definitions of VSL, LIN and STR are considered the gold standard [13, 60, 71, 79, 122]. The straight linear velocity, as defined by WHO, takes only the first and last point into account (equations 2.2, 2.6 and 2.7). Clearly, this ignores all data points in between and will misclassify sperm trajectories which make a final turn towards the end of the recording while otherwise exhibiting linear motion. However, the Rotated Rectangular Linearity RRL measure uses a tight fitting rectangle, creating an envelope surrounding the track. This approach is more robust than VSL and is less prone to errors produced by reversal of direction of the sperm trajectory. It does not penalize tracks with turns, because

it will always return the maximal extent a sperm has travelled. It is calculated similarly to A_{MBS}, with the exception of rotating the array of trajectory points in 0.1 radiant increments over $\frac{\pi}{2}$, while calculating the bounding rectangle (a, b) for each iteration and retaining the maximal side length. The RRL represents the furthest distance the sperm was able to travel (Figure 4.11). The following details the computation of RRL. Let Θ be the angle, by which the trajectory is turned. T_Θ is then the new rotated trajectory. $(x_{\min}(\Theta)\ , y_{\min}(\Theta)\ )$ are the respective values of a minimum point and $(x_{\max}(\Theta)\ , y_{\max}(\Theta)\ )$ are the respective maximum values of a point of the rotated trajectory T_Θ.

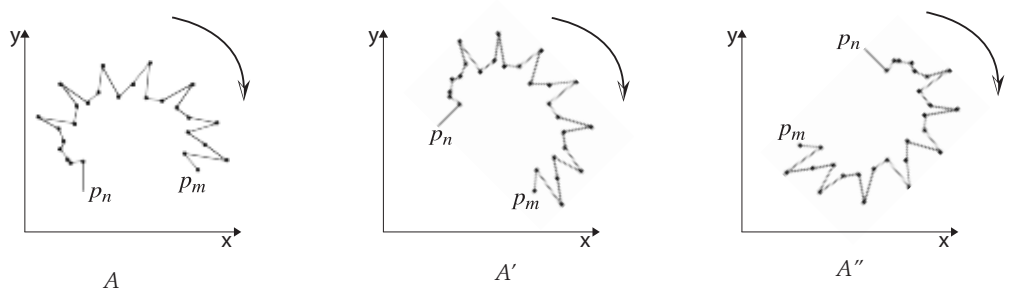

Figure 4.11: *Rotated and transposed trajectories are equivalent, wen using RRL . The RRL measure is spatially independent and robust.*

The minimum $x_{\min}(\Theta)$ coordinate of a point of the rotated trajectory T_Θ is found by:

$$x_{\min}(\Theta)\ = min\ \{x \mid x\ is\ the\ x - coordinate\ of\ a\ point\ of\ T_\Theta\ \} \tag{4.15}$$

The maximum $x_{\max}(\Theta)$ coordinate of a point of the rotated trajectory T_Θ is found by:

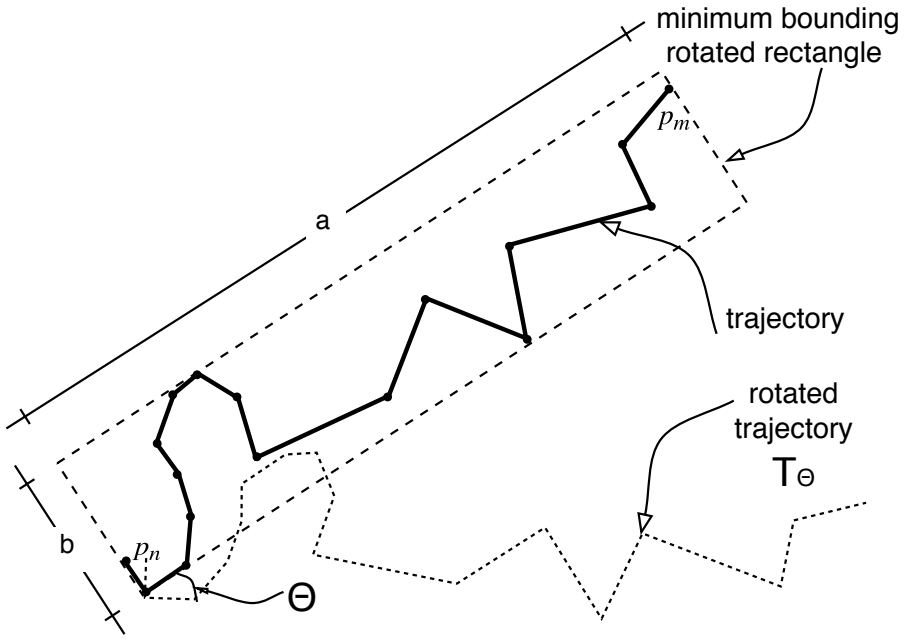

Figure 4.12: *Minimum Bounding Rotated Rectangle (RRL). The longest side of the rectangle,* $max(a, b)$*,reflects the furthest extend, the sperm was able to reach. It is a proposed new measure of linearity as improvement over LIN and STR.* Θ *is the angle, by which the trajectory is turned.*

$$x_{\max}(\Theta) = max\ \{x \mid x\ is\ the\ x - coordinate\ of\ a\ point\ of\ T_\Theta\} \tag{4.16}$$

The minimum $y_{\min}(\Theta)$ coordinate of a point of the rotated trajectory T_Θ is found by:

$$y_{\min}(\Theta) = min\ \{y \mid y\ is\ the\ y - coordinate\ of\ a\ point\ of\ T_\Theta\} \tag{4.17}$$

The maximum $y_{\max}(\Theta)$ coordinate of a point of the rotated trajectory T_Θ is found by:

$$y_{\max}(\Theta) = max\ \{y \mid y\ is\ the\ y - coordinate\ of\ a\ point\ of\ T_\Theta\} \tag{4.18}$$

$$a(\Theta) = x_{\max}(\Theta) - x_{\min}(\Theta) \tag{4.19}$$

Then $a(\Theta)$ is the length of the side parallel to the $x - axis$ of the minimum bounding rectangle for T_Θ having sides parallel to the axes.

$$b(\Theta) = y_{\max}(\Theta) - y_{\min}(\Theta) \tag{4.20}$$

Then $b(\Theta)$ is the length of the side parallel to the $y - axis$ of the minimum bounding rectangle for T_Θ having sides parallel to the axes.

$$dist(\Theta) = \max\{a(\Theta),\ b(\Theta)\} \tag{4.21}$$

Where $dist(\Theta)$ is the longest side of the enveloping rectangle.

The longest rectangular side (LRS) over a rotated trajectory over $\frac{\pi}{2}$ is:

$$LRS = \max\left\{dist(\Theta) \mid 0 \leq \Theta \leq \frac{\pi}{2}\right\} \tag{4.22}$$

Finally, RRL is computed by dividing LRS by VCL (2.1), expressed as percentage. A larger LRS would be an indicator for a progressive sperm and will result in a larger RRL.

$$RRL = \frac{\max\left\{dist(\theta) \mid 0 \leq \theta \leq \frac{\pi}{2}\right\} \cdot 100}{VCL} \tag{4.23}$$

The pseudo code to compute RRL is listed in algorithm 7.

In figure 4.13 a hyperactivated trajectory example (Ia) is altered to show the improvements of RRL versus LIN. The trajectories Ia and Ib are identical with the exception of swapping the point p_m with p_{m-2}, with the effect, that the trajectory tail moved back a small step. The envelope, or the extent this particular sperm was able to swim increases

Algorithm 7 Rotated Rectangular Linearity RRL (T)

$a \leftarrow 0$ $\quad \triangleright first\ side\ of\ rectangle$
$a_{temp} \leftarrow 0$
$b \leftarrow 0$ $\quad \triangleright second\ side\ of\ rectangle$
$b_{temp} \leftarrow 0$
for $\Theta \geq 0$ *to* $\Theta \leq \pi/2$ *by increment* **do**
  for $i = 0$ to m **do**
    $a \leftarrow\ find\ difference(x_{max}, x_{min})\ of\ T[\,]$
    $b \leftarrow\ find\ difference(y_{max}, y_{min})\ of\ T[\,]$
    if $a > a_{temp}$ **then**
      $a_{temp} \leftarrow a$
    end if
    if $b > b_{temp}$ **then**
      $b_{temp} \leftarrow b$
    end if
  end for
end for
$longestSide \leftarrow max(a, b)$
$RRL \leftarrow longestSide * 100/VCL$
return RRL

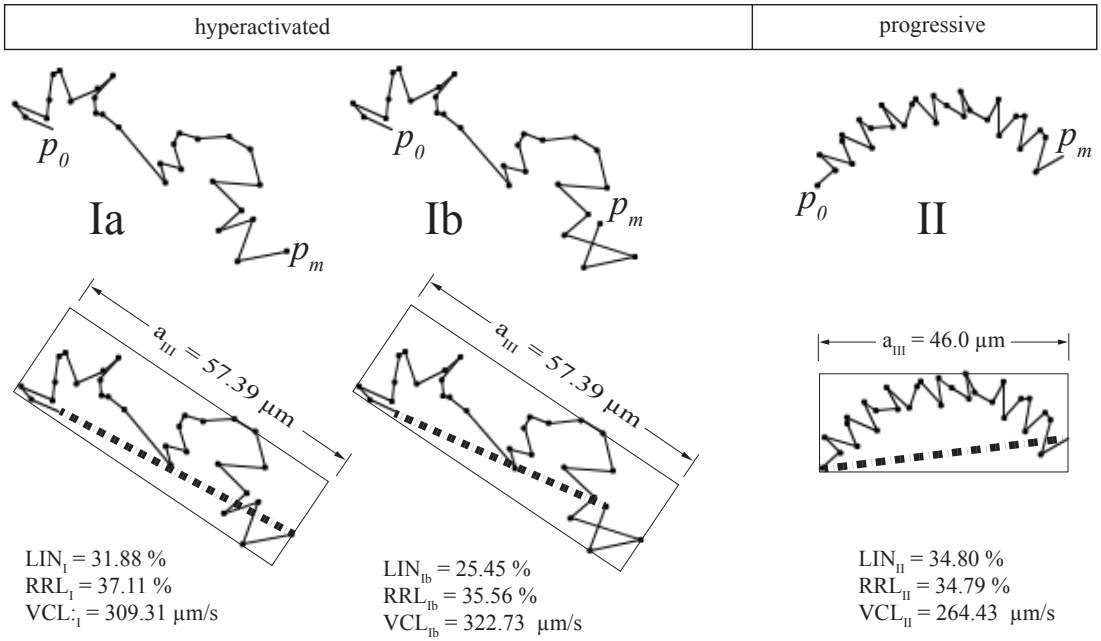

Figure 4.13: *Effect of linearity on the trajectory. Two trajectory examples (I, II) with comparable LIN. Track Ia and Ib are identical with the exception that points p_m and p_{m-3} are swapped, to reverse the track's direction, without changing the geometric position of the furthest points. Dotted line is the straight linear velocity (see 2.2). Note how RRL is unaffected by the slightly altered track Ib, in contrast to a 20.17 % in the LIN measure.*

only slightly by 1.55% from 37.11%. But the existing measure LIN falsely reduces this trajectory with a 20.17% penalty. Trajectory II has a similar RRL and LIN but LIN or RRL alone cannot distinguish between hyperactivated and progressive sperm tracks. This effect is more dominant in hyperactivated than progressive trajectories (Fig. 6.11).

4.5.7 Minimum Bounding Square Ratio, MBSR

The appearance of a hyperactivated sperm trajectory is frequently illustrated as having a thrashing, star−spin appearance (Table 2.7). Rather than trying to explain and computationally calculate the many different shapes of hyperactivated sperm tracks, we interpret the erratic movements as a search pattern of the spermatozoa to reach the oocyte for fertilization. For example, a hyperactivated sperm with an erratic zig−zag trajectory pattern would cover a larger area than a progressive spermatoza moving almost linearly (Figure 4.14). Let this search area be A_{hull}. In order to calculate how effectively the spermatoza is searching, we have to define another, larger area, that we call the $exploration\ region$. It is intuitive to use for this new area boundaries set by the spermatozoa itself, like the tightest fit square,A_{MBS}, rather than coming up with, for example, average threshold values. Not only will each spermatoza set its own $exploration\ region$, it also will fit the physiological motility properties of the sperm, where a hyperactivated sperm with erratic motility patterns will have a larger search area A_{hull}, than a progressive sperm with a smaller A_{hull} (Figure 4.15). Thus, we can now compare the area of the trajectory, A_{hull} with the area of the $exploration\ region$, the minimum bounding square, A_{MBS} and are able to calculate the search effectiveness of the sperm, called $MBSR$. Consequently, we are independent of the actual pattern of the sperm trajectory and have a potential tool to classify the sperm's

motility.

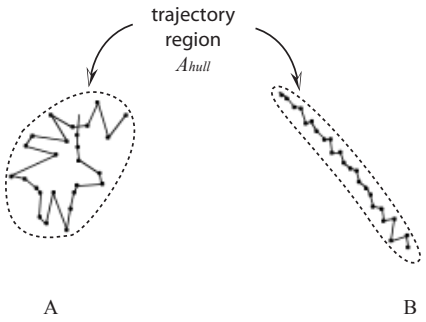

Figure 4.14: *Sperm Trajectory Search Area Coverage. A zig−zag pattern of a hyperactivated sperm (A) covers more area (dashed line) than a progressive sperm (B).*

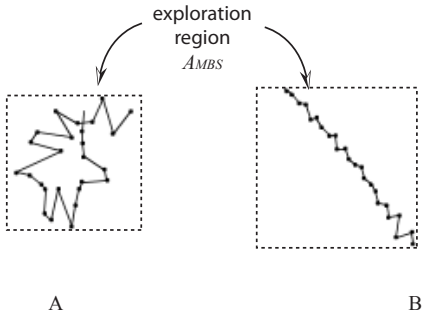

Figure 4.15: *Sperm Trajectory Exploration Region MBS. The zig−zag pattern of a hyperactivated sperm (A) covers a larger portion of the Minimum Bounding Square area of (A) (dashed line) than a progressive sperm (B).*

Next, the trajectory's search area A_{hull} needs to be defined. We use a set of joint convex hulls, an envelope of points of the trajectory, to achieve this goal. The following

sections describe the formal computational approach for minimum bounding square ratio $MBSR$. It is divided into the calculation of the trajectory's search area A_{hull} (4.5.7.1), followed by the calculation of the $exploration\ region$, the minimum bounding square, A_{MBS} (4.5.7.2) and concluded with the calculation of the Minimum Bounding Square Ratio, $MBSR$ (4.5.7.3).

4.5.7.1 Trajectory Hull, A_{hull}

We decided to use convex hulls as an area approximation for the coverage calculation of the trajectory. Approximation is a reasonable approach, since the sperm trajectories are biomedical measurements and represent only the momentary situation when they were recorded. Additional recordings, even from the same spermatoza, will have similar characteristics but will not be identical. The definition of a convex hull can be imagined by picturing the points of the sperm trajectory as nails sticking out of the plane. Snapping an elastic band around the nails will minimize its length, contain all the points (nails) and describe the vertices of the convex hull of the trajectory. Therefore, the convex hull of a set of sperm trajectory points is the smoothed envelope of the area containing all the points of its trajectory.

A single convex hull, enveloping the entire trajectory points, might be suitable for circular sperm patterns, but will overstate the trajectory hull,A_{hull} for a half$-$moon like track shape. To better follow the contour of the sperm trajectory, we propose using multiple convex hulls connected with each other. The following describes an A_{hull} calculation, suitable to calculate a single, or multiple connected convex hulls, representing the trajectory search area A_{hull}. Connected or joint convex hulls are convex hulls sharing one point for the first

and the last hull and two points for middle hulls. Figure 4.16 illustrates a sperm trajectory search area represented as a set of joint convex hulls.

Let A_{hull} be the entire search area of the trajectory and A_i be a sub convex hull of A_{hull}, if multiple convex hulls exist. Let the number of desired hulls be h and $m + 1$ the total number of sperm trajectory points. Chapter 6 section 6.8.2 discusses examples of the effect of the number of hulls on the trajectory hull area A_i. To cover the case of multiple convex hulls, $h > 1$, the count of points must be extended by $h - 1$ points to compensate for the shared points connecting the hulls. The number of the hull points c_{hull} is then obtained by adding the desired number of hulls to the maximum number of trajectory points and dividing the result by the desired number of hulls. The floor function guarantees a next lower integer result.

$$c \; = \; \left\lfloor \frac{(m+h)}{h} \right\rfloor \tag{4.24}$$

Require $c \; \geq \; 3$ as the minimum required to form a convex hull.

Consider the remainder points r, if they exist, as:

$$r \; = \; (m \; + \; h) \; \text{mod} \; h \tag{4.25}$$

For $r = 0$, a single convex hull, form the hull as follows:

$$hull\left(p_0 \ldots p_{c-1}\right),\ hull\left(p_{c-1} \ldots p_{2c-2}\right),\ \ldots,\ hull\left(p_{m-c+1} \ldots p_m\right) \tag{4.26}$$

Here p_0 is the first and p_{c-1} is the last point of the first hull and $hull(p_i...p_j)$ denotes the convex hull of the points $p_i, p_{i_+1}...p_m$. c is the number of hulls as calculated in 4.24. The point p_{m-c+1} is the first point and p_m the last point of the last convex hull of the trajectory.

If $r = 1$ there is one additional data point. It will be added to the last convex hull:

$$hull\left(p_0 \ldots p_{c-1}\right),\ hull\left(p_{c-1} \ldots p_{2c-2}\right),\ \ldots,\ hull\left(p_{m-c} \ldots p_m\right) \tag{4.27}$$

For $r \geq 2$ a new convex hull can be formed at the end of the trajectory. The minimum of three points for a convex hull is satisfied even for $r = 2$, since there is one shared point from the previous hull:

$$hull\left(p_0 \ldots p_{c-1}\right),\ hull\left(p_{c-1} \ldots p_{2c-2}\right),\ \ldots,\ hull\left(p_{m-r} \ldots p_m\right) \tag{4.28}$$

The point p_{m-c} is the first point and p_m the last point of the last convex hull of the trajectory. Note: An additional hull is added.

The final number of hulls n is:

$$n = \begin{cases} h & for\ r = 0, 1 \\ h + 1 & for\ r \geq 2 \end{cases} \tag{4.29}$$

The area A_{hull} covered by the sperm trajectory is expressed by summing the areas of the sub convex hulls A_i:

$$A_{hull} = \sum_{i=1}^{h} A_i \tag{4.30}$$

Here A_i is the area of the $i - th$ convex hull. The area of this planar convex polygon is then computed using standard computational geometry formulas [90]. The pseudocode to obtain the trajectory hull A_{hull} is shown in algorithm 8.

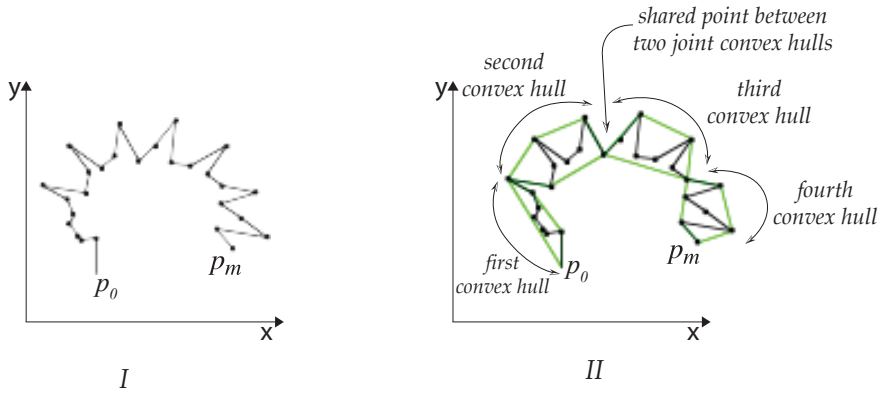

Figure 4.16: *Trajectories Hull A_{hull}. I : Sperm trajectory. II : Trajectory with four joint convex hulls. The sum of these fours convex hulls captures an approximation of the search area A_{hull} described by the sperm trajectory.*

Algorithm 8 Trajectory Hull Area A_{hull}, (T, m, h)

Require: $(m \geq 3)$ AND $(1 \leq h \leq \lfloor \frac{m}{2} \rfloor)$ ▷ *minimum convex hull conditions*

$A_{hull} \leftarrow 0$
$A_{temp} \leftarrow 0$
$h \leftarrow desired\ number\ of\ hulls$
while points remain **do**
  $put\ points\ into\ hull\ until\ all\ points\ are\ used$
  if $remaining\ points \geq 2$ **then**
    $T_{hull} \leftarrow hull\ points$
    $T_{convex\_hull} \leftarrow compute\ convex\ hull\ of\ T_{hull}$
  else
    $add\ remaining\ points\ to\ previous\ hull$
  end if
  $A_{temp} \leftarrow calculate\ A_{hull}\ of\ T_{convex\_hull}$
  $A_{hull} \leftarrow A_{hull} + A_{temp}$
end while
return A_{hull}

4.5.7.2 Exploration Region A_{MBS}

Next we have to define the computation of the area of the $exploration\ region$, A_{MBS}. As mentioned in section 4.5.7 it is a reasonable approximation to set the $exploration\ region$, which the trajectory has to cover in its search by the track itself. Thus, the spermatozoa defines the trajectory coverage, A_{hull} and $exploration\ region$, A_{MBS} according to its own individual capabilities, without setting thresholds. A minimum bounding square surrounding the trajectory serves this purpose well. It represents the largest area a sperm could have covered within the data acquisition period.

The A_{MBS} is computed by finding the minima and maxima in the $x-$ and $y-axis$ (Figure 4.17).

Let $T = \{p_o, ... , p_m\}$ be the time ordered set of sperm trajectory points and $x_{\min}(T)$ be the minimum x−coordinate of a point of the trajectory T.

The minimum x_{min} coordinate of a point of the trajectory T is found by:

$$x_{\min}(T) = min\ \{x \mid x\ is\ the\ x - coordinate\ of\ a\ point\ of\ T\ \} \tag{4.31}$$

The maximum x_{max} coordinate of a point of the trajectory T is found by:

$$x_{\max}(T) = max\ \{x \mid x\ is\ the\ x - coordinate\ of\ a\ point\ of\ T\ \} \tag{4.32}$$

The minimum y_{min} coordinate of a point of the trajectory T is found by:

$$y_{\min}(T) = min\ \{y \mid y\ is\ the\ x - coordinate\ of\ a\ point\ of\ T\ \} \tag{4.33}$$

The maximum y_{max} coordinate of a point of the trajectory T is found by:

$$y_{\max}(T) = max\ \{y \mid y\ is\ the\ x - coordinate\ of\ a\ point\ of\ T\ \} \tag{4.34}$$

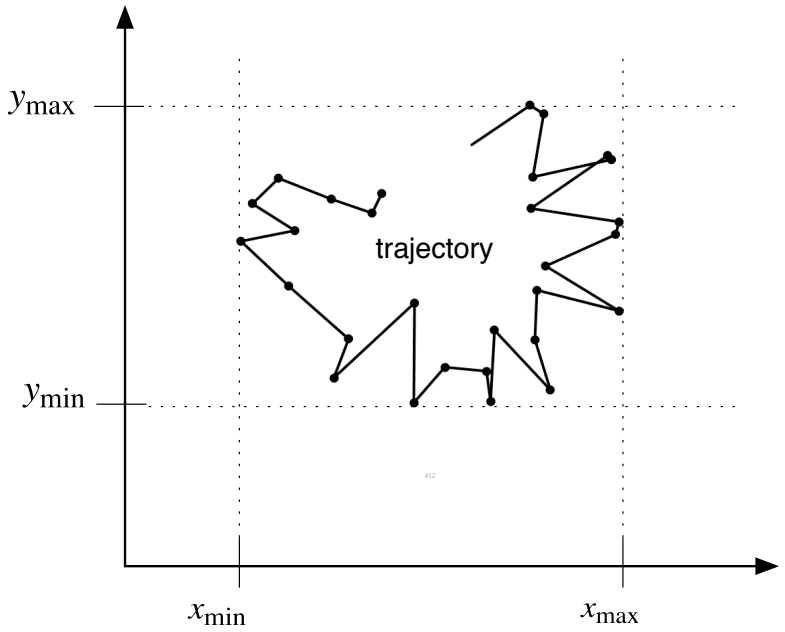

Figure 4.17: *Orthogonal Minimum Bounding Square, A_{MBS}, Calculation. A_{MBS} represents the furthest possible extend of an $exploration\ region$ the spermatozoa could have reached.*

The four coordinates $(x_{min}, y_{min}, x_{max}, y_{max})$ will describe a rectangle, which might

resemble A_{hull} of a linear progressive trajectory, defeating the conjecture of a smaller $exploration\ region$ coverage by progressive sperm. To compensate for this problem, we choose the largest side of this rectangle to form the minimum bounding square, thus restoring the physiological properties. The minimum bounding square area ($exploration\ region$) is calculated as taking the largest side of the rectangle to form a square:

$$A_{MBS} \ = \ \left(\max\left\{x_{\max}\left(T\right) \ - \ x_{\min}\left(T\right), \ y_{\max}\left(T\right) \ - \ y_{\min}\left(T\right)\right\}\right)^2 \tag{4.35}$$

The algorithm 9 shows the pseudocode for computing the orthogonal MBS.

Algorithm 9 Trajectory Exploration Region (Orthogonal) MBS_{orth}, (T)

$A_{MBS} \leftarrow 0$
$longestSide \leftarrow 0$
for $i = 0$ to m **do**
    $a \leftarrow \ find\ difference(x_{max}, x_{min})\ of\ T[\,]$
    $b \leftarrow \ find\ difference(y_{max}, y_{min})\ of\ T[\,]$
    $longestSide \leftarrow max(a, b)$
end for
$A_{MBS} \leftarrow longestSide\ squared$
return $A_{MBS_{orth}}$

The MBS algorithm above returns smaller A_{MBS} for trajectories not parallel to the arbitrary axes of the CASA coordinate system. This error can reach a factor of $\sqrt{2}$ for progressive sperm tracks running diagonally to the coordinate axes . To compensate for this error and enchance accuracy, we use an improved version of computing A_{MBS} algorithm 9, rotating the trajectory until the largest A_{MBS} is found. The consideration of rotated trajectories makes A_{MBS} independent of the trajectories' orientation relative to the artificial

CASA axes. The pseudocode of the rotated A_{MBS} is listed in algorithm 10. Details on the trajectory rotation are described in section 4.5.6.

Algorithm 10 Trajectory Exploration Region (Rotated) MBS_{rot}, (T)

```
a ← 0                                   ▷ first side of rectangle
a_temp ← 0
b ← 0                                   ▷ second side of rectangle
b_temp ← 0
for Θ ≥ 0 to Θ ≤ π/2 by increment do
    for i = 0 to m do
        a ← find difference (x_max, x_min) of T[ ]
        b ← find difference (y_max, y_min) of T[ ]
        if a > a_temp then
            a_temp ← a
        end if
        if b > b_temp then
            b_temp ← b
        end if
    end for
end for
longestSide ← max(a, b)
MBS_rot ← longestSide squared
return MBS_rot
```

4.5.7.3 MBSR

Finally, to express the search efficiency of each spermatozoon, we compute the proportion of search area covered versus size of the full exploration region as the trajectory hull area A_{hull}(4.30) and $exploration\ region, A_{MBS}$ (4.35.) Figure 4.18 illustrates the MBSR algorithm:

$$MBSR = \frac{A_{hull}}{A_{MBS}} \tag{4.36}$$

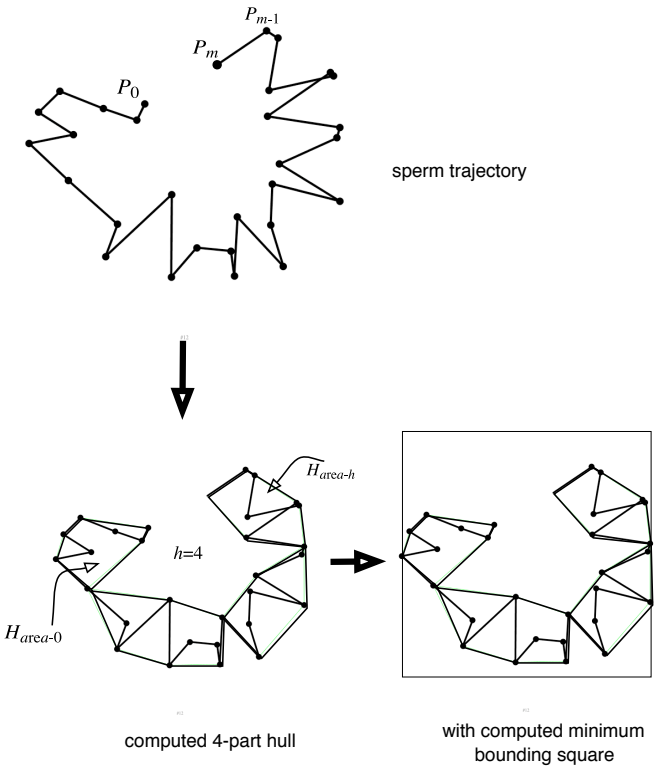

Figure 4.18: *Minimum Bounding Square Ratio(MBSR). Combining both the A_{hull} area with the A_{MBS} is a the new proposed measure of hyperactivity, reflecting the effectiveness on how well the possible search area was covered by the spermatozoa.*

Algorithm 11 Minimum Bounding Sqaure Ratio MBSR, (T)

1: $MBSR \leftarrow 0$
2: $MBSR \leftarrow A_{hull} * 100/A_{MBS}$
3: **return** MBSR

Chapter 5

Comparative Example of New Measures

In this chapter we apply the new proposed measures of QS (4.5.3), RAC (4.5.4), RRL (4.5.6) and MBSR (4.5.7) side-by-side on two stallion sperm trajectory examples for better comparison. The numerical results for the particular new measure are also presented along with a graphical representation. The scale of the figures is indicated by the $25\mu m$ bar included in all the figures of this chapter.

5.1 Minimum Bounding Square MBSR

The minimum bounding square ratio is computed by calculating the trajectory hull and exploration region. The minimum bounding square MBS is calculated in two versions. The first version (section 5.1.2) computes the MBS surrounding the sperm trajectory as recorded by the CASA device within its arbitrary assigned coordinate system. An MBS obtained in this manner is not guaranteed to result in the maximum possible square, especially in diagonally oriented sperm trajectories. The second version compensates for this error by

(section 5.1.3) rotating the sperm trajectory until a maximal rectangle is detected.

5.1.1 Trajectory Hull

The trajectory search area A_{hull} is computed as a four part joint convex hull. Figure 5.1 provides an example of A_{hull} for a progressive ($91.23\mu m^2$) and a hyperactivated ($602.18\mu m^2$) sperm trajectory (green line). Note in comparison to a progressive trajectory the 6.6 times larger A_{hull} of the hyperactivated sperm track. The overlapping of individual convex hulls in the hyperactivated sperm trajectory is a desirable effect, given that it increases the A_{hull} of this type of sperm trajectory.

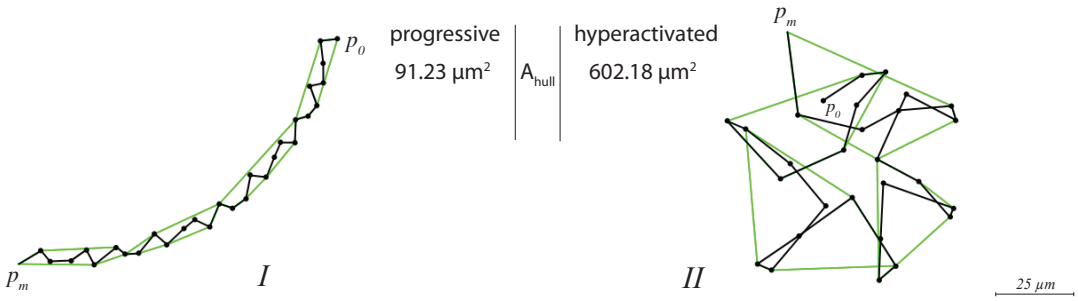

Figure 5.1: *Trajectory region area with a 4-point joint convex hull*

5.1.2 MBS and MBSR non-rotated trajectory

The exploration region A_{MBS} of the sperm trajectory is computed by calculating the minimum bounding rectangle enveloping the trajectory. The largest side of this rectangle is then used for A_{MBS}. Figure 5.2 illustrates a A_{MBS} for a progressive ($1707.34\mu m^2$) and a hyperactivated ($992.82\mu m^2$) sperm trajectory. The MBSR is then the ratio in percent

between A_{hull} and A_{MBS}, in the example 5.34% for the progressive and 60.65% for the hyperactivated sperm. Note the 11 fold difference between the two types of sperm trajectories.

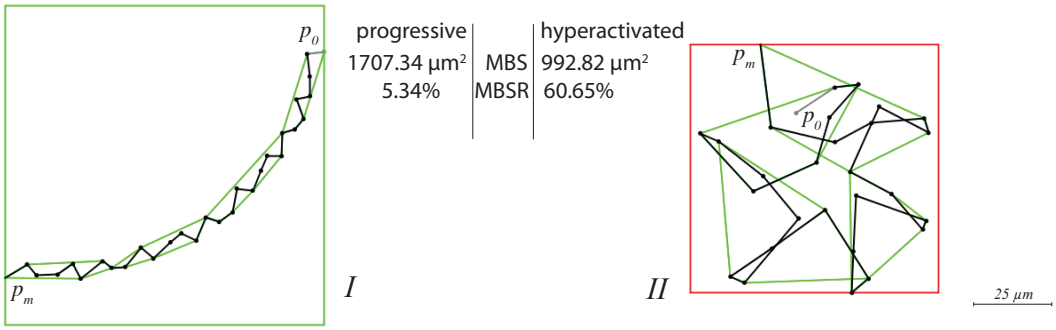

Figure 5.2: *Minimum Bounding Square MBSR on a non-rotated sperm trajectory set.*

5.1.3 MBS and MBSR rotated trajectory

The orientation of the sperm trajectory in regard to the coordinate system can affect the size of the A_{MBS} (Chapter 4 section 4.5.6). To compensate for this error the trajectory is rotated over $\pi/2$ and the largest rectangle is retained. Again, the largest side of this rectangle is used for the A_{MBS}. Figure 5.3 provides an example of a A_{MBS} obtained from a rotated trajectory. Note how the progressive trajectory in comparison to the non-rotated example of Figure 5.2 needed to be rotated over almost $\pi/2$ until the maximal area (2561.11) was detected. In this example, the rotated MBS compensated for an error of approximately 50% over the non-rotated method in the progressive example, helping to differentiate better between progressive and hyperactivated sperm, by reducing the MBSR from 5.34% in Figure 5.2 down to 3.56%.

The non-rotated hyperactivated trajectory of Figure 5.2 already produces, as desired, a large MBSR. The hyperactivated sperm trajectory example of 5.3 shows that the rotation keeps the large MBSR. The hyperactivated sperm trajectory required only a minor rotation to detect the maximal A_{MBS} of $1026.20\mu m^2$, a small increase in comparison to the non-rotated A_{MBS} of 992.82%. The resulting MBSR remained approximately the same with 58.11% versus 60.65% for the non-rotated track.

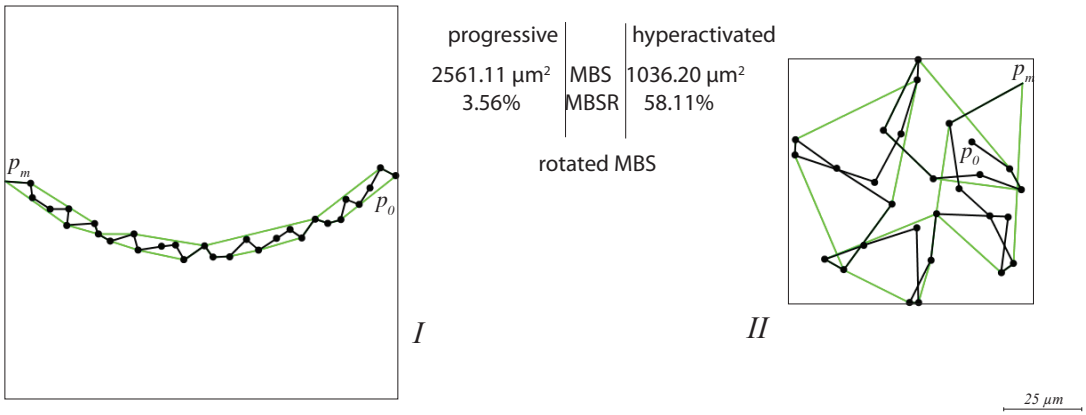

Figure 5.3: *Minimum Bounding Square MBSR on a rotated sperm trajectory set*

5.2 Rotated Rectangular Linearity RRL

RRL is an improvement of the existing WHO measure LIN. It is computed in the same fashion as the rotated A_{MBS}, but as LIN, divided by VCL. The result is presented in percent. Figure 5.4 shows the computed minimum bounding rectangle used for RRL calculation on a progressive and hyperactivated trajectory. RRL improved the LIN from 5.28% to 16.27%. As seen in the chart, RRL is less prone to directional changes of the first (p_0) and last point

(p_m) of the trajectory. For this progressive example, RRL (70.28%) is identical to LIN (70.28%), since the first and last point of the trajectory are part of the VSL and are also part of the minimum bounding rotated rectangle. RRL is an improvement for hyperactivated sperm trajectories and returns the same or better values for progressive sperm. The progressive trajectory example of Figure 5.4 (21.43%) example exhibits few movements in the same direction, an indication for a linear moving sperm. In contrast, in the hyperactivated sperm direction changes are frequent (66/67%).

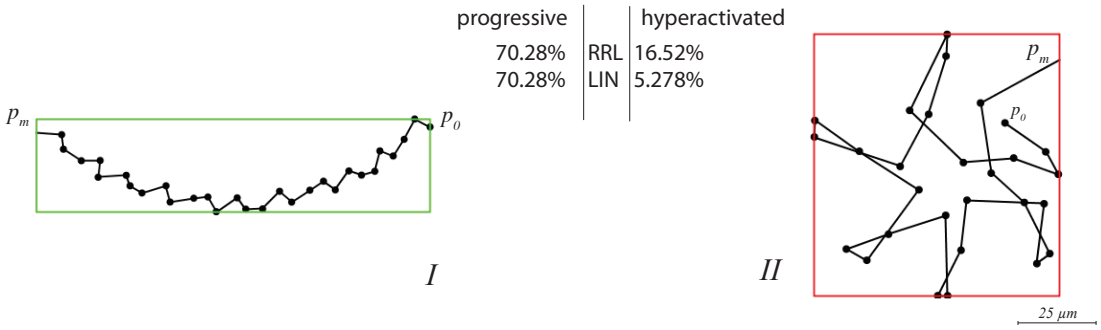

Figure 5.4: *Rotated Rectangular Linearity RRL*

5.3 Relative Angle Score RAS

RAC is an indicator for symmetrical movement of the sperm, by canceling relative left-right and right-left movements of two consecutive points of the sperm trajectory, but scoring one otherwise (Chapter 4 secton 4.5.4). A red dot, starting from p_0 of the trajectory in Figure 5.5 indicated a movement of the sperm in the same direction. A green dot identifies a left-right or right-left movement that is not being scored. The scoring result is normalized

over the entire amount of point of the trajectory to compensate for differences in the number of points.

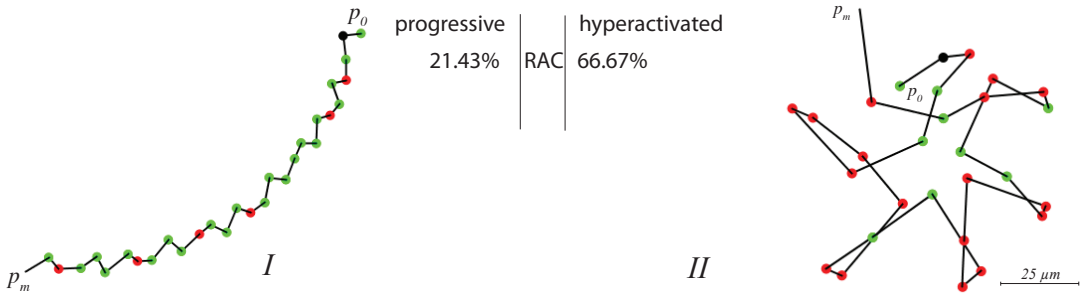

Figure 5.5: *Relative Angle Score RAS. A red dot follows two prior consecutive angles with the same sign. Change in color indicates a change in the direction of the sperm trajectory angle. The progressive trajectory (I) has 6 occurrences, where consecutive angles have the same sign. The hyperactive trajectory (II) has 18 occurrences where consecutive angles have the same sign.*

5.4 Quadrant Score QS

QS is another linearity measure, by scoring the relative occurrence of the next point of the sperm trajectory in the quadrants of a Cartesian coordinate system. The scores are kept for each quadrant and the result is returned as standard deviation. To illustrate the effect of QS on a sperm trajectory we assigned a different color for each quadrant (I=red, II=blue,III=green,IV=yellow) and plotted these colors for the points of a progressive and hyperactivated sperm trajectory (Figure 5.6). The individual quadrant scores are plotted in the corners of the chart.

The transitional sperm trajectory has a more linear pattern and scores mainly in the second (8) and third quadrant (18), seen in the blue and green dots. There are only three

scores in the fourth quadrant. This is reflected in the QS score of 7.89. By contrast, the relative position of the hyperactivated sperm trajectory points occur almost evenly in all quadrants, seen in the almost evenly distributed color dots in the hyperactivated trajectory.

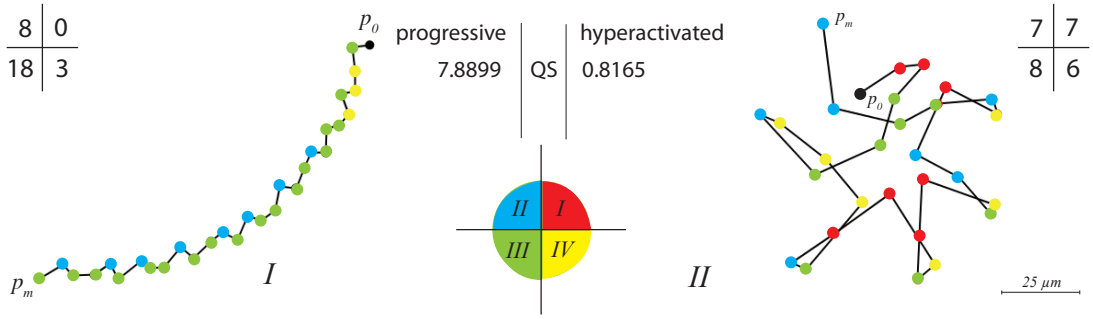

Figure 5.6: *Quadrant Score QS*

Chapter 6

Evaluation and Validation of Classification Approaches

Each classification algorithm underwent an analysis on training data and on a random test data set. The training data set was used to determine boundaries for hyperactivated and progressive sperm tracks as well as transitional trajectories. Performance was then measured on the test data set. Descriptive statistics are used to present these results. Results are individually summarized in a table which reports correct classifications as well as misclassifications. A diffusion matrix summarizes classification performance. For validation, we retrospectively examined the test data using a box plot with the previously detected boundaries overlaid. Finally, a summary histogram is presented to compare the side-by-side and ranked performance of the existing and novel classification algorithms developed.

This chapter is organized as follows: First, the general criteria for the trajectory data sets in this analysis are presented (section 6.1), followed by a detailed description of the training

data (6.1.1) trajectories and test data trajectories in section 6.1.2. The analysis begins with results on the existing and widely used VCL method 6.2, then RRL is compared directly with the existing LIN measure (6.3). In section 6.4, RAVC results are presented. Section 6.5 and 6.6 cover the analysis of RAC and Qs respectively, and the combining of these two measures using logistic regression is presented in section 6.7. Lastly, the MBSR results are described in section 6.8 with details of the trajectory hull (6.8.1), optimal trajectory joint convex hulls (6.8.1) and expected MBSR values in section 6.8.2.

6.1 Spermatozoa Trajectory Data

The trajectory data were collected from a pool of seven different stallions over the course of several months. Some stallions were used multiple times, however, no samples were ever collected on the same day. Fresh ejaculate was always obtained and processed as described in section 4.2.4.

6.1.1 Training Data Set

As discussed in chapter 2, there is no consensus among experts in the field for the definition of hyperactivated or progressive trajectories. This makes transitional trajectories, by nature the state of the sperm on the verge between progressive and hyperactivation, even more difficult to standardize and classify. To reduce ambiguity in the selection of sperm patterns of our control dataset, we therefore decided on two (hyperactivated and progressive), rather than three classifications including transitional trajectories. One file containing 40 hyperactivated and one file containing 40 progressive trajectories classified by experts in the field were used as controls to detect boundaries and thresholds. The trajectories came

from five different stallions, sampled on five different laboratory days. The training data contained untreated and treated specimens, randomly selected for each group of hyperactivated and progressive trajectories. The treated trajectories were obtained from the MBSR application described in Section 7.

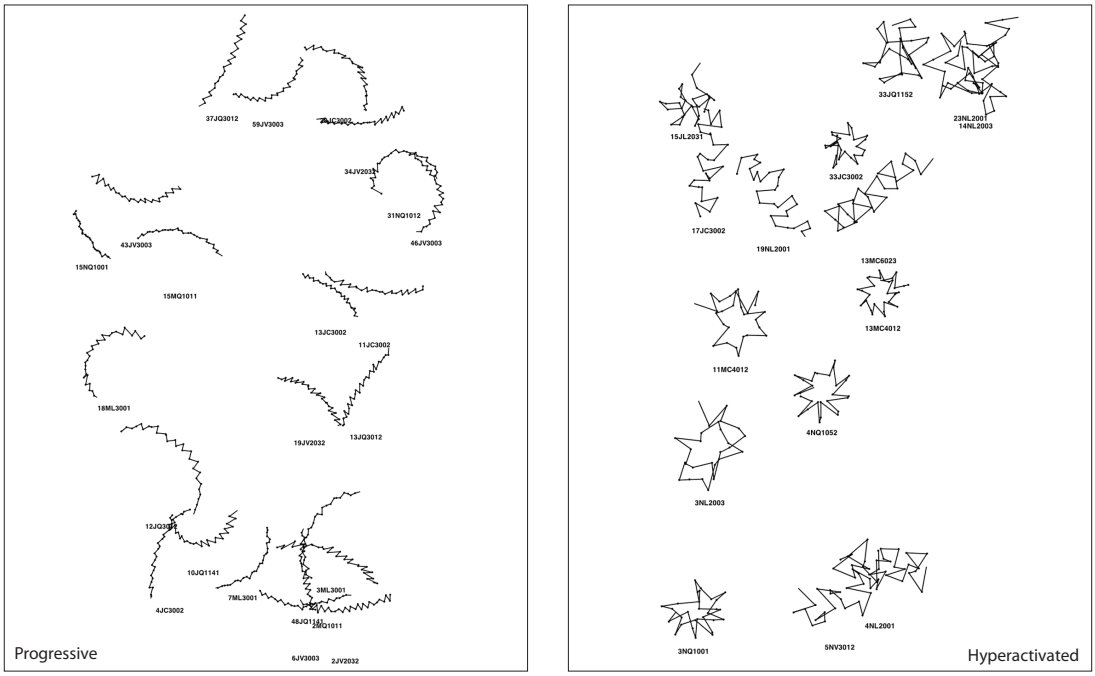

Figure 6.1: *Training Data Set Excerpt. The whole file contains forty expert selected hyperactivated and forty progressive trajectories. A similar excerpt of the same files with trajectory convex hulls and Minimum Bounding Rectangle can be found in appendix 9.1*

6.1.2 Test Data Set

The trajectories in the test data file came from two stallions, different from the ones used in the training data described above. The test data included four random files containing

18, 21, 52 and 47 trajectories. To retain the biological validity of the test data, all measurements of the droplet were included without further processing the data. Two of the files were pharmaceutically treated samples and two were untreated. The test data was classified by experts in the field into hyperactivated, transitional and progressive trajectories. The test data was first classified into hyperactivated and then progressive trajectories, so more ambiguous transitional trajectories were determined last. A trajectory was excluded from the classification, if either the expert or the algorithm decided it was unclassifiable. "Unclassifiable" was defined to be too small in the printout for the expert in the field and not meeting a threshold of $50\mu m/s$ for the algorithms. This resulted in one more rejection of a progressive trajectory reducing the classifiable sperm trajectories to 29 hyperactive, 25 transitional and 70 progressive trajectories.

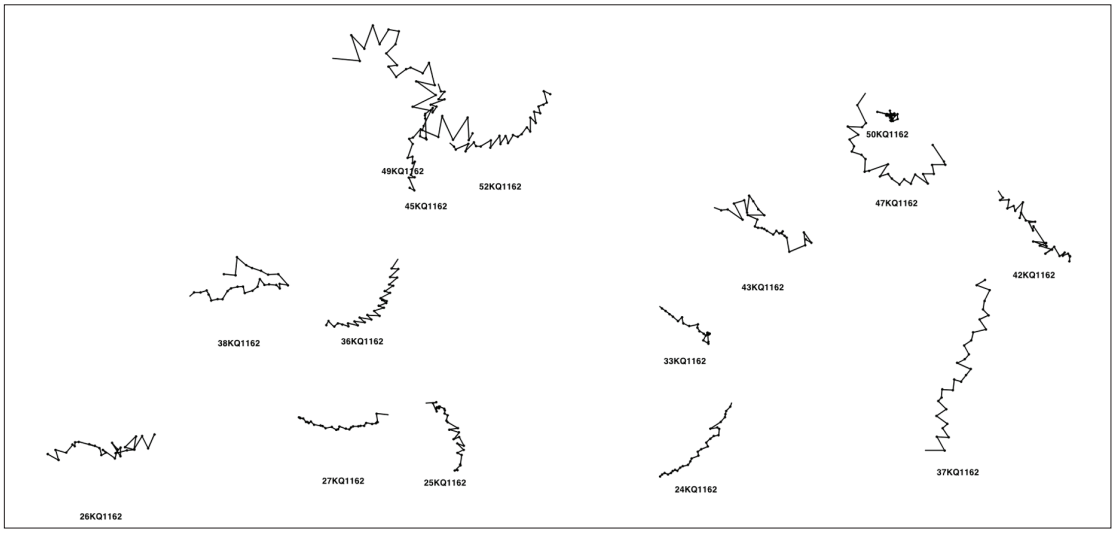

Figure 6.2: *Test Data Set Excerpt. The file is composed of 138 random trajectories from 4 droplet scans of 2 stallions, different from the ones used in the training data set. A similar excerpt of the same file classified can be found in appendix 9.2*

hyperactivated	transitional	progressive	classified total	rejects	Total Tracks
29	25	71	125	13	138

Table 6.1: *Test Data Trajectories Expert Classification Results. Note: An individual algorithm can increase the number of rejected trajectories. The total number of classifiable tracks are listed within the individual algorithm section.*

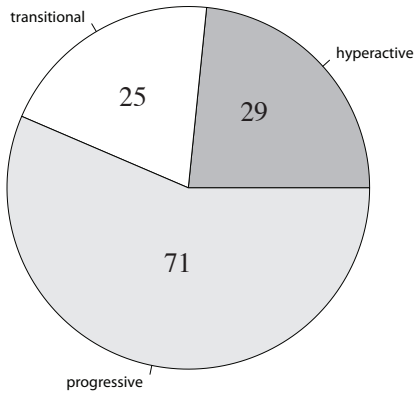

Figure 6.3: *Training Data Classifiable Tracks represent a typical mixture of progressive and hyperactivated trajectories.* $n = 125$. *One more progressive trajectory was rejected by the algorithm threshold of* $50\mu m/s$ *reducing the progressive set to 70 classifiable trajectories.*

6.1.3 Diffusion Matrix

The classification results of each algorithm were mapped into a diffusion matrix. The x-axis represents the classification of the expert in the field (True Classification) and the y-axis the classification of the algorithm. The classification levels are labelled in the colors red, yellow and green according to Figure 6.4. The upper left hand corner shows the classification agreement of hyperactivated sperm (red) and the lower right corner the one for progressive. The individual classification results as well as the absolute values and percent-

ages and the all-over classification performance of each algorithm tested are presented. The center displays the results for matches for transitional sperm trajectories. The horizontal gray arrow represents the location of false positives, meaning trajectories wrongly classified as hyperactive by the algorithm. The vertical arrow is the location of false negatives, where hyperactivated trajectories are missed as such by the algorithm. The diagonal gray arrow indicates the location of correctly classified sperm trajectories (Figure 6.4). Expert classification is synonymous with true classification in the diffusion matrix.

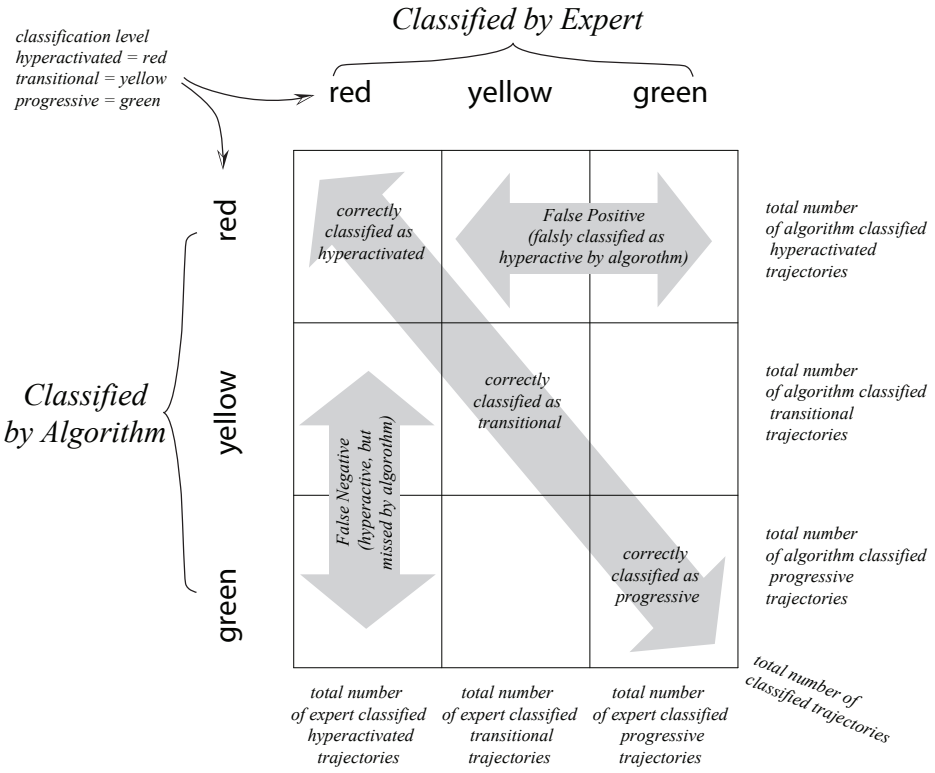

Figure 6.4: *Diffusion matrix explanations.*

6.1.4 Classification Boundaries

The training data served as a basis to define threshold boundaries for hyperactivated, transitional and progressive trajectories. Although the training data did not contain transitional trajectories, biologically, these transitional trajectories are defined to occur between the progressive and hyperactivated state. For VCL (6.2), RRL (6.3), RAVC (6.4), RAC (6.5) and QS (6.6) box plots were utilized for boundary detection. Two box plots, one representing the hyperactivated and one the progressive sperm trajectories of the training data set, were produced from each algorithm. In an ideal case, a clear separation of the minimum or maximum whiskers of these box plots was observed. In such a case, the range between the minimum and maximum of either the hyperactivated and progressive box plot whisker was used as transitional threshold. If there was an overlap between the two box plots, we either used the minimum to maximum whiskers as threshold, or the quartiles, whichever resulted in the smaller range.

For the logistic linear regression (6.7) a band around the computed regression line was used as threshold boundaries.

Similarly for MBSR (6.8.3), a band surrounding the the intersection of the MBSR thresholds of hyperactivated and progressive training data trajectories were used.

6.1.5 Retrospective Threshold Analysis

After completion of the classification analysis of each algorithm, we applied the computed classification boundaries from the training data to the test data, including transitional trajectories, in an effort to find out if a different set of thresholds could have improved the classification outcome. First we looked at the statistical distribution of hyperactivated, tran-

sitional and progressive sperm trajectories of the test data after applying each algorithm. Next, we examined the effect on the test data as a result of changing the upper or lower threshold bound computed from the training data and whether or not the three classifications of hyperactivated, transitional and progressive could have been improved. After that, we looked at the effect of individually changing the upper or lower threshold bound and at shifting the threshold band. Subsequently, we looked at the threshold impact, of classification on only hyperactivated and progressive trajectories, without transitional tracks. Transitional sperm trajectories have been problematic to classify throughout this dissertation, because of the lack of definition for this sperm group. Figure 6.5 shows the labeling used in this retrospective analysis of VCL, RRL, RAC, QS and MBSR. For the retrospective analysis of the logistic regression a new regression line was computed based on the test data and plotted together with the regression line from the training data and will be discussed in more detail within the results of each tested algorithm.

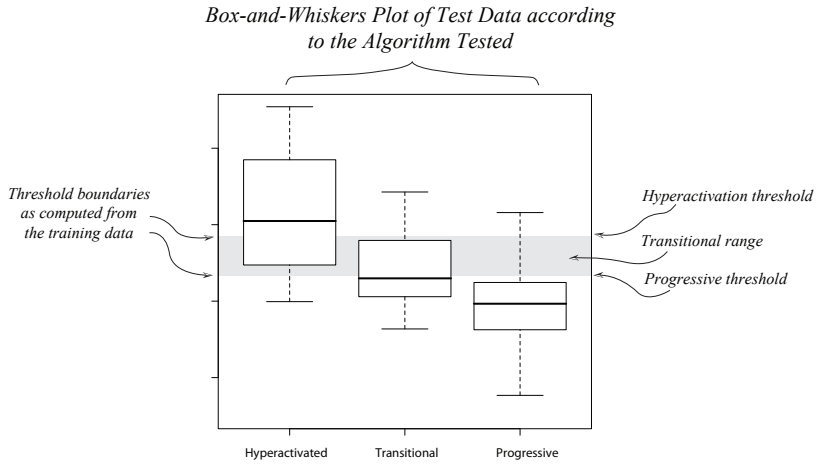

Figure 6.5: *Labeling Example for Retrospective Analysis Explanations for VCL, RRL, QS and MBSR algorithms.*

6.2 Curvilinear Velocity Analysis, VCL

This measure in conjunction with LIN is currently the gold standard to classify hyperactivated sperm and is included here for completeness and comparison. The velocity of hyperactivated sperm was reported by several investigators to be substantially higher than in progressive sperm [3, 13, 59].

Threshold Boundaries: Figure 6.6 compares hyperactive and progressive trajectories of the training data set. Two distinct separate distributions of progressive and hyperactivated sperm trajectories are visible (Figure 6.6 and 6.7). According to section 6.1.4 , we decided to use the maximum value of the progressive set ($258.98\ \mu m/s$) as the upper boundary for progressive sperm and the minimum of the hyperactivated control trajectory ($295.52\ \mu m/s$) set as lower boundary of hyperactivated sperm trajectories (Table 6.2). The transitional sperm trajectories will fall in between as $295.52\ \mu m/s\ > Transitional\ > 258.98\ \mu m/s$.

	Hyperactivated	Progressive
Min.	295.52212	87.28792
Max.	598.16099	258.97935
Median	426.83725	169.31328
Mean	427.58152	168.95088

Table 6.2: *VCL Training Data Statistics. Values in $\mu m/s$.*

Classification Analysis: The diffusion matrix analysis of Figure 6.8 on the test data exhibits a different observation than the one on the training data. Only 51.72% of hyperactivated and 20% of transitional sperm trajectories of the test data were correctly classified.

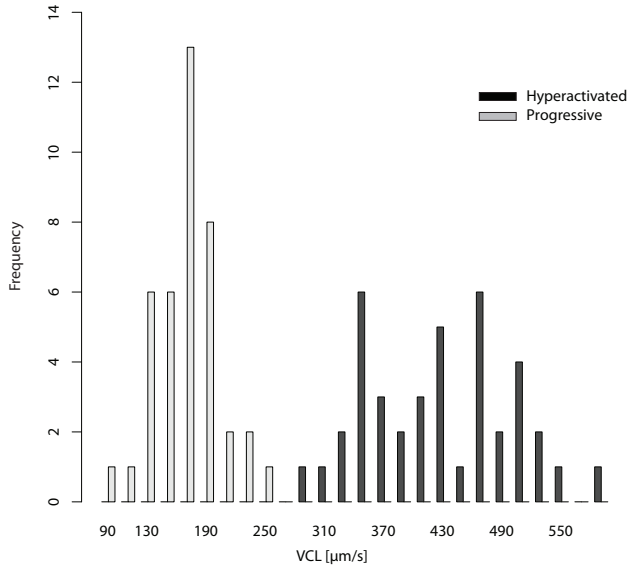

Figure 6.6: *Training data VCL histogram containing* $2\ x\ 40$ *progressive and hyperactivated sperm . Hyperactivated: Mean:* $427.58 \pm 74.40\mu m$; $Median$: $426.84\mu m$; $Min.$: $295.52\mu m$; $Max.$: $598.16\mu m$. *Progressive: Mean:* $168.95 \pm 32.35\mu m$; $Median$: $169.31\mu m$; $Min.$: $87.29\mu m$; $Max.$: $258.98\mu m$

However, VCL was able to classify 91.43% of the progressive trajectories. Seven sperm trajectories were falsely classified as being hyperactivated (False Positives) and 14 trajectories were missed by the algorithm as being hyperactivated (False Negatives). The total correct classification rate was 84 out of 124 trajectories or 67.74%. This is a poor result, especially when considering that VCL is currently the gold standard for sperm hyperactivity classification.

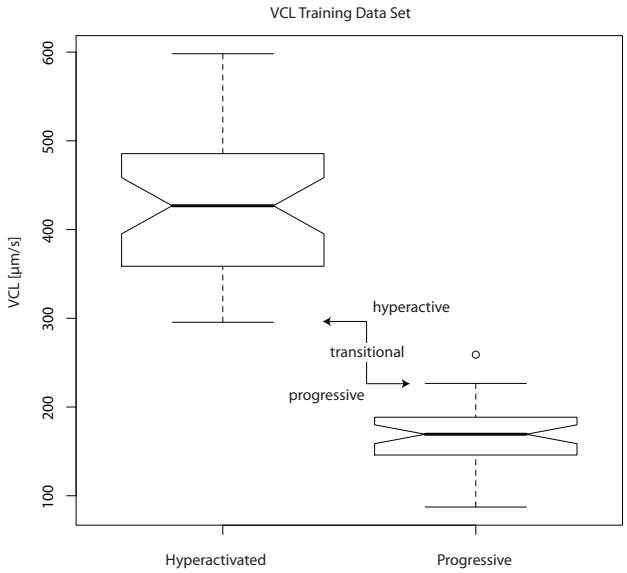

Figure 6.7: *VCL Training Data Box Plot. Hyperactive and progressive VCL sperm trajectory values are clearly separated.*

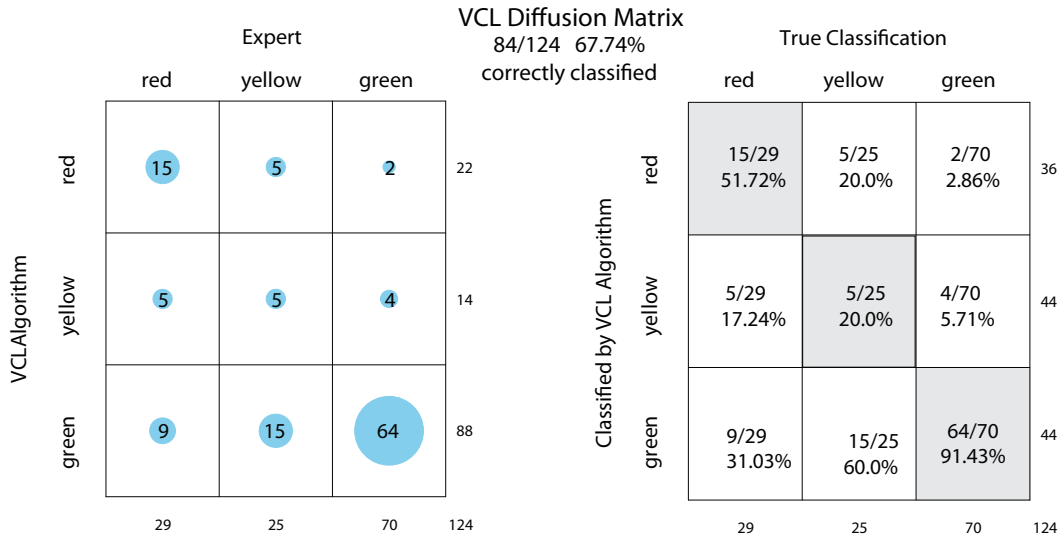

Figure 6.8: *VCL Classification Matrix.*

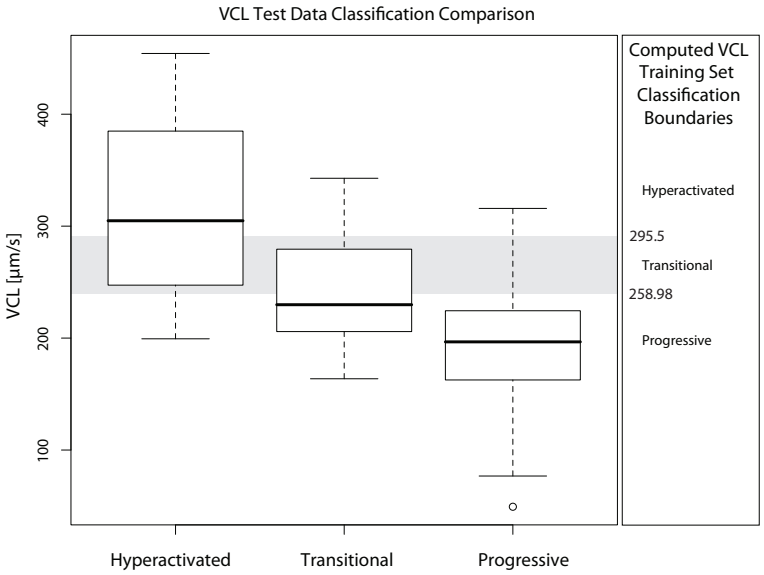

Figure 6.9: *VCL Retrospective Analysis. Contrary to the training data set, the VCL ranges of hyperactivated, transitional and progressive classification groups in the test data markedly overlaps and is a reason for the inadequate classification performance of this algorithm.*

Retrospective Analysis: The reason for the poor performance of the classification using VCL can be seen in a retrospective analysis of Figure 6.9 of the test data. We plotted the distributions of the three classification groups of hyperactivated, transitional and progressive sperm trajectories and superimposed the threshold boundaries detected from the training data set. Contrary to the training data set, the test data does not display a clear separation between hyperactivated and progressive classification groups as seen in the training data. For example, almost half of the transitional trajectories lie within three quartiles of the progressive classification group and more than three quarters are within the hyperactivated group. This makes a distinction between these three classification groups impossible

using the VCL method. Choosing a different lower bound threshold could have improved hyperactivation classification at the expense of progressive and transitional sperm trajectories. Without the transitional trajectory group, VCL might have been a better, but not ideal candidate as a hyperactive and progressive classifier.

6.3 Rotated Rectangular Linearity RRL in comparison with LIN

Hyperactivated sperm trajectories have erratic movement patterns, resulting in reduced linearity (LIN). The linearity measure can therefore be used to eliminate progressive sperm trajectories from the pool of sperm trajectories of hyperactivated, transitional and progressive sperm. In this section we present the advantage of RRL over LIN. Rotated Rectangular Linearity (RRL) removes an imperfection of the existing sperm linearity, LIN measure (Chapter 4 Section 4.5.6). In this section we evaluate RRL and LIN in a side-by-side comparison. First, we examine the effect of RRL on hyperactivated and progressive sperm trajectories of the test data set (Figure 6.10). Since both measures, LIN and RRL, compute a similar feature of the sperm trajectory (Chapter 2 Section 2.6 and Chapter 4 Section 4.5.6), we subtracted the result of LIN from RRL and plotted the difference as relationship to the velocity (VCL) of the sperm trajectory. A positive value is to be expected, if RRL indeed returns in a larger value than LIN and a negative difference otherwise. The existing LIN measure underreported the linearity in almost all hyperactivated trajectories (black triangles) by 10 - 18% of the training data set. LIN even underestimated the more linear progressive trajectories, especially in trajectories with higher velocity of approximately $200\mu m/s$. Give that RRL and LIN are related, we expect similar classification performance. The advantage of RRL is the robustness in reliably returning a linearity measure

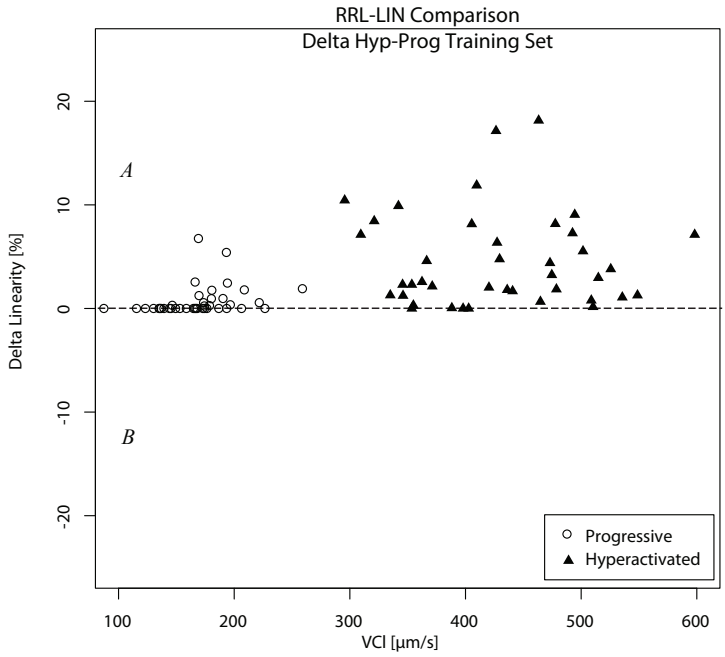

Figure 6.10: *RRL-LIN Comparison of the training data set. The chart shows* $\Delta(RRL-LIN)$*. The current standard measure LIN underreports linearity, expecially in shorter hyperactivated trajectories.* A*: LIN underreported the track linearity.* B*: RRL underreported the track linearity.*

even in erratic hyperactivated sperm trajectories, were LIN falls short.

Threshold Boundaries: The RRL and LIN threshold boundaries (Figure 6.11) were found by using the small overlap of their whiskers observed in the box plot in the training data. The LIN thresholds boundaries are therefore $hyperactive \leq 31.36\%$, $progressive \geq 37.66\%$ with transitional trajectories falling in between. RRL increases the linearity of hyperactivated sperm trajectories (Figure 6.10) and poses the risk of diminishing the linearity differences achieved by the LIN measure. The benefit of RRL is the robustness and not being less affected by directional changes of the first or last points of the trajectory.

The risk did not materialize. RRL reduces the range of hyperactivated (min-max range $13.93\% - 39.96\%$ for RRL vs. $1.5\% - 37.66\%$ for LIN) and in progressive trajectories (min-max range $36.77\% - 86.21\%$ for RRL vs. $31.36\% - 86.28\%$ for LIN . The RRL threshold boundaries are $hyperactive \leq 36.77\%$, $progressive \geq 39.96\%$ and as before with the LIN measure, transitional trajectories falling in between.

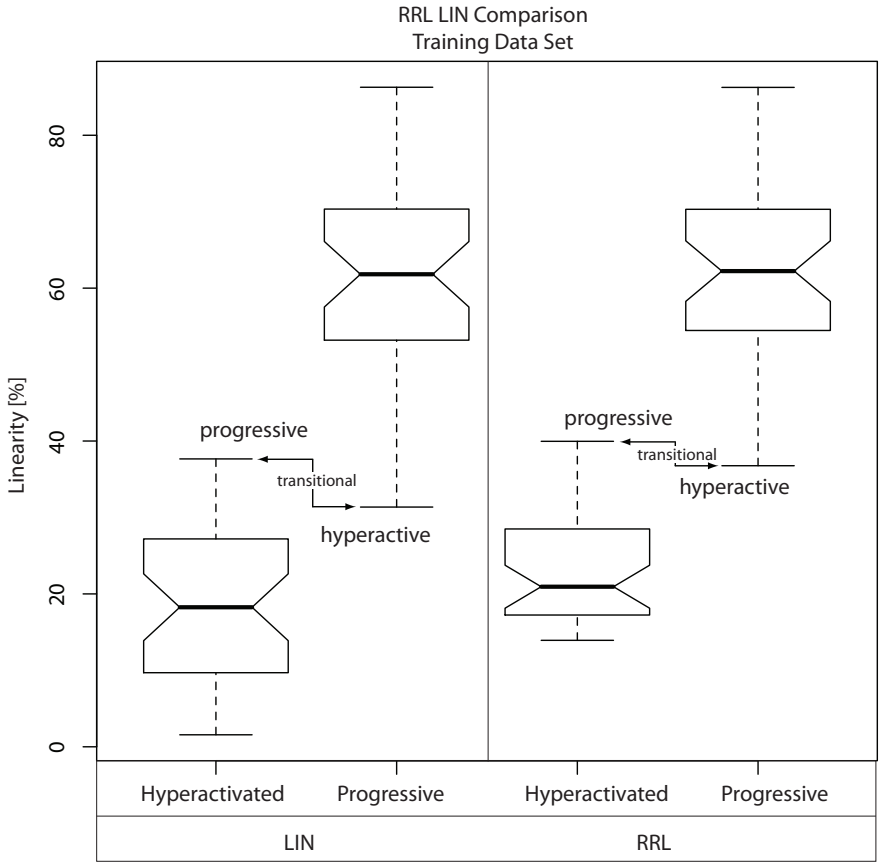

Figure 6.11: *RRL LIN Comparison on the Control. RRL reduces the range in both, the hyperactivated and progressive sperm trajectories of the training data set.*

	RRL		LIN	
	Hyperactivated	Progressive	Hyperactivated	Progressive
Min.	13.926153	36.76923	1.569333	31.36088
Max.	39.960688	86.26163	37.660138	86.27990
Median	20.941179	62.22934	18.253005	61.81596
Mean	22.837008	62.63089	18.350469	61.95868

Table 6.3: *RRL - LIN Training Data Statistics.*

Classification Analysis: Table 6.4 summarizes the classification results of RRL versus LIN. The new proposed RRL measure was able to improve hyperactivation classifiaction by approximately 10 percentage points from 82.76% to 93.10%. No improvement was observed in the transitional classification and a slight reduction of approximately 3% from 98.59% for LIN to 95.77% for RRL was seen.

The diffusion matrix (Figure 6.12) again displays the excellent classification performance of hyperactivated and progressive sperm trajectories only. But transitional trajectories are poorly classified (24%) and come with a high number of false positives ($15/25,\ 60\%$), where RRL classifies a trajectory incorrectly as hyperactive, and a low number of false negatives (2). While the false positive number is high, it mainly resulted from a misclassification of transitional trajectories, whose boundaries were difficult to define to begin with (section 6.1.1). More importantly, no hyperactivated sperm trajectories were misclassified as progressive or vice versa. Overall detection performance for both, RRL and LIN was the same with 80.65%. While the overall classification rate is the same, RRL classified hyperactive trajectories with 27/29 (93.10%) better than LIN with 24/29 (82.76%). These results show that both methods can distinguish well between hyperactive and progressive sperm, with RRL having an edge over LIN in the more important classification of hyperactivated

sperm trajectories, but both fail in detecting transitional sperm trajectories.

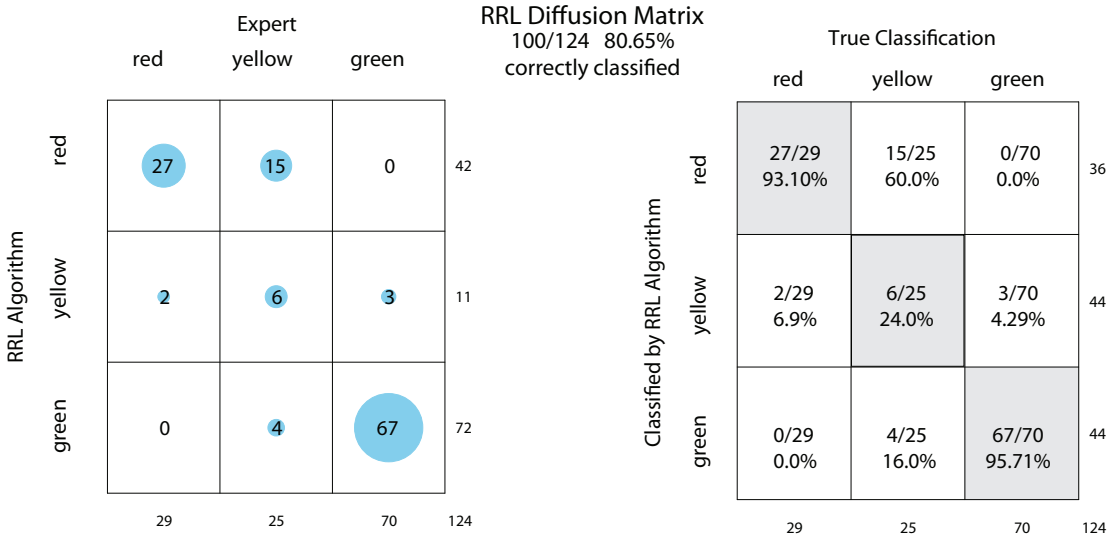

Figure 6.12: *RRL Diffusion Matrix.*

	RRL- LIN Results Correct Classification						
	Absolute			Percent			
Algorithm	hyperactivated	transitional	progressive	hyperactivated	transitional	progressive	n
RRL	27	6	67	93.10	24.0	95.71	124
LIN	24	6	70	82.76	24.0	100	124

Table 6.4: *RRL and LIN Classification Summary.*

Retrospective Analysis: Figure 6.13 displays the retrospective analysis of the test data with RRL training data boundaries. As in the training data, RRL separated the hyperactivated from the progressive trajectory classification group ($RRL_{hyper-max} = 37.82\%$ and $RRL_{progressive-min} = 38.55\%$). This explains the high positive classification rate for these two groups. As with VCL before, the transitional trajectories are also a continued problem

for RRL. Almost three quartiles of the transitional trajectories lie within the hyperactivated group and approximately one quartile within the progressive classified trajectory section.

The upper threshold boundary (39.35%) detected by the training data almost perfectly classifies progressive trajectories and missed only one out of 70 progressive trajectories. Similarly, the lower bound (36.76%) captures all but two of 29 hyperactivated sperm trajectories. Little can be done to improve these boundaries without diminishing the already poor performance on the transitional sperm group. Any shift of the boundaries to improve transitional trajectory classification would come at the expense of hyperactivated or progressive sperm trajectories.

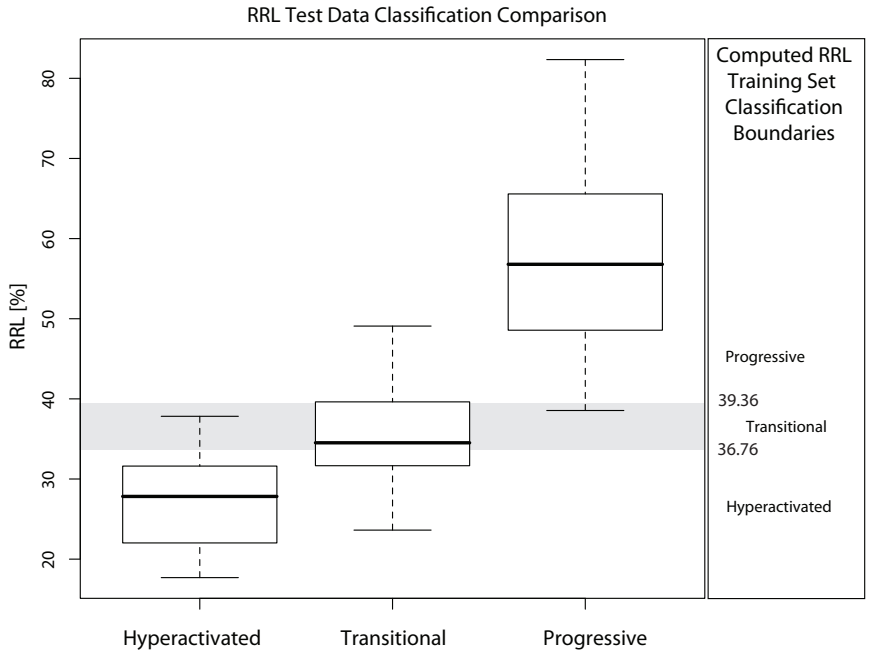

Figure 6.13: *RRL Retrospective Analysis*

As for the VCL algorithm before, RRL maybe best used for hyperactivated and progressive trajectory classification, without considering transitional sperm trajectories.

Again as with VCL before, without transitional sperm trajectories, RRL may be an excellent method to classify hyperactivated and progressive sperm.

6.4 Relative Angle Velocity Change RAVC

We examined 1079 hyperactivated and 1105 progressive segment angles of sperm trajectories of the training data set (Figure 6.14 part I). No significant difference between hyperactivated and progressive angles was found ($p = 0.6412$). This confirms parts of the findings of Mortimer et al. [83], who created a similar new measure called VAM by multiplying trajectory angles with segment velocity (Chapter 2 Section 2.8.3). These investigators found a significance only in 'non circling' sperm trajectories. One research goal of this dissertation was to find a generalizable solution for sperm hyperactivation classification, without restricting the algorithm to specific hyperactivation patterns, such as 'circling' or 'non circling' . This excludes the relative segment angle as viable classifier for this dissertation.

The second element of this algorithm makes use of the segment velocities that is highly significant ($p < 2.2\ 10^{-16}$) between hyperactivated and progressive trajectories in the training data set (Figure 6.14 part II). This does not come as a surprise. The sum of all segment velocities of a trajectory is VCL. An increase in VCL in hyperactivated sperm trajectories has been reported by investigators (Section 4.5.1). But the ambition of the RAVC was to develop an algorithm combining trajectory angles and velocities to capture the erratic motion of hyperactivated sperm trajectories. Descriptive analysis failed to reveal a relationship between segment angles and segment velocities. No further analysis is performed with this algorithm.

	Hyperactivated	Progressive
N	1079	1105
Min.	0.0788112	0.1153500
Max.	178.6204207	175.0013911
Median	102.3892422	75.2966997
Mean	94.0738151	74.0496028

Table 6.5: *Trajectory Angles Training Data Statistics. Angles are in degrees.*

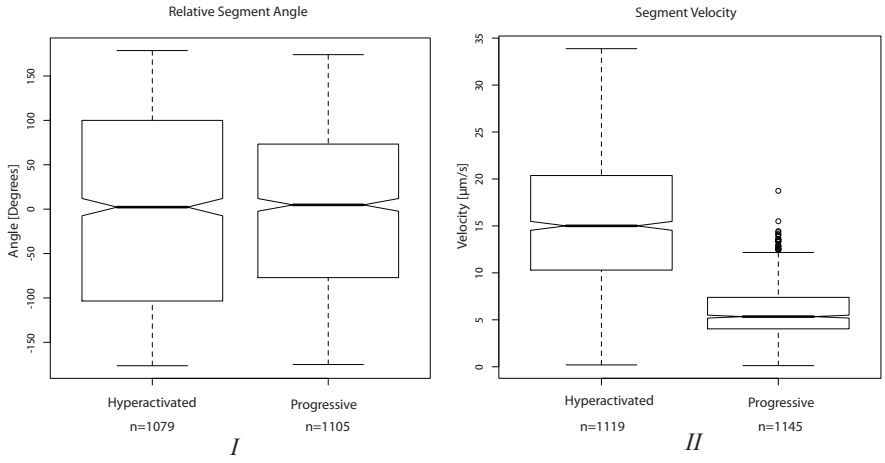

Figure 6.14: *RAVC Training Data Results. I: No significant difference in the relative angle set. Since this algorithm is based on a link between relative angle and segmental velocity, further analysis is not warranted Segment Angles:($p = 0.6412$). II: Segment Velocity: ($p < 2.2\ \dot{1}0^{-16}$)*

6.5 Relative Angle Count RAC

This algorithm is designed to capture a deviation from the symmetry of the flagellum movement of the sperm. This measure cancels two consequent left-right or right-left segmental movements of the sperm and assigns a score otherwise. The result is normalized over the entire sperm trajectory to compensate for the varying number of total data points of the trajectory. RAC is then expressed as a percentage for the entire trajectory. As such, it is another measure of linearity, a feature of progressive sperm trajectories that can be eliminated from the pool of trajectories for hyperactivity classification. As anticipated, this biological phenomenon is reflected in the statistical results of the training data. Hyperactivated sperm ($RAC_{hyper-min} = 3.85\%$ to $RAC_{hyper-max} = 64.28\%$) display a much wider deviation from a symmetrical flagellar beat than progressive sperm ($RAC_{prog.-min} = 0.0\%$ to $RAC_{prog.-max} = 16.02\%$ (Table 6.6). Unfortunately, almost all trajectories of the training data that are classified as progressive lie within the lower half of the data for hyperactivated trajectories.

Threshold Boundaries: The ranges of hyperactive and progressive tracks overlap substantially, making the minimum and maximum whiskers of the box plot unusable for classification (Figure 6.15). As boundaries we chose the first and third quartile of the hy-

	Hyperactivated	Progressive
Min.	3.846154	0.0
Max.	64.285714	35.714286
Median	37.037037	14.285714
Mean	36.361381	16.018586

Table 6.6: *RAC Training Data Statistics. Normalized relative count.*

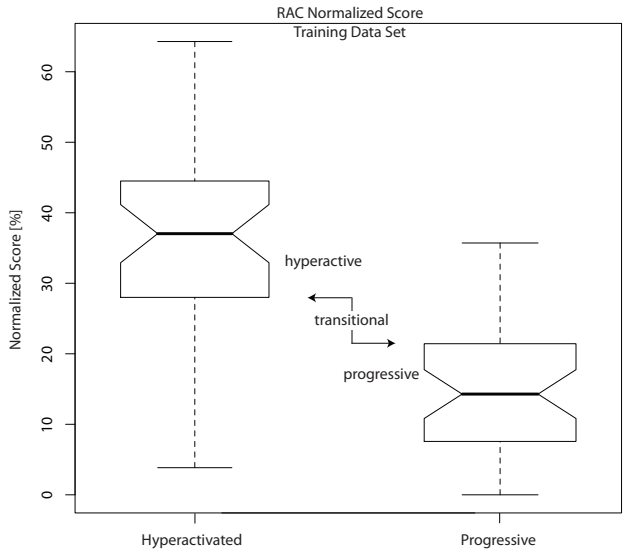

Figure 6.15: *Relative Angles Count Box plot of the training data set.*

peractivated and progressive trajectory set, respectively. The lower boundary for sperm classified as hyperactivated falls at 28.0% and the upper boundary for sperm classified as progressive at 21.43%, defining the classification thresholds for transitional trajectories as $21.43\% < \ transitional \ < 28.0\%$. Considering the overlapping distributions, choosing the quartiles as boundaries is an acceptable solution, since it guarantees a separation of $\frac{3}{4}$ of the hyperactivated and $\frac{3}{4}$ of the progressive trajectories. As in the algorithms before, this assumes that transitional trajectories are falling in between.

Classification Analysis: The classification results for the RAC algorithm can be seen in Figure 6.16. Despite the intriguing theory of translating asymmetrical flagellar movement of the sperm as a score, the all-over classification performance was only 50.81%. In particular, only 12 out of 29 (43.38%) of hyperactivated and only 46 out of 70 (65.71%) of progressive trajectories were correctly classified. The number for correctly classified tran-

sitional trajectories was even lower with 20.0%. Moreover, RAC produced 22 (55.71%) false positives and 17 (58.62%) false negative classifications. With these results, RAC did not dominate any of the three classification categories of hyperactivated, transitional and progressive.

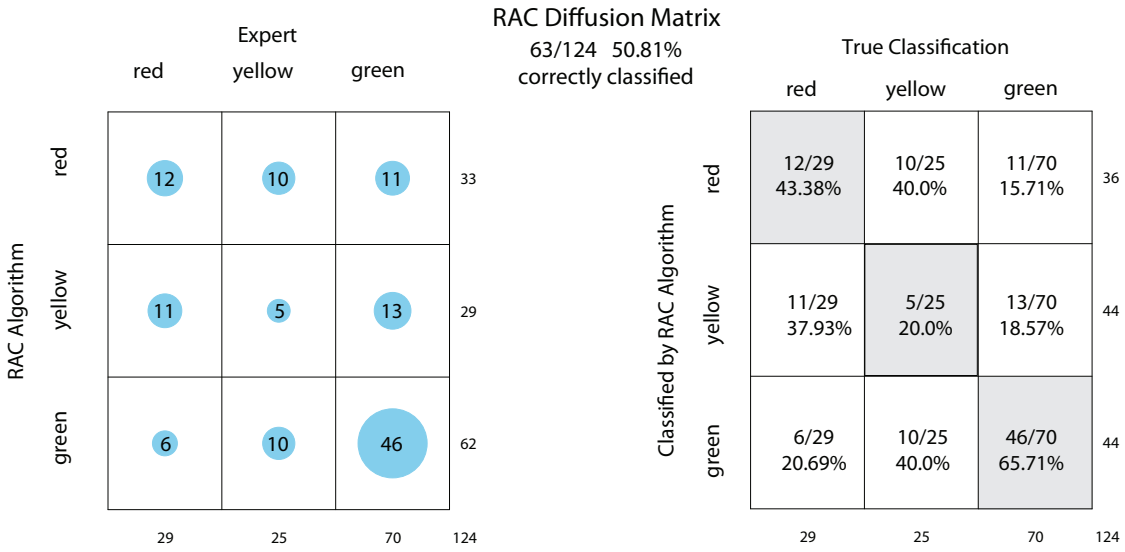

Figure 6.16: *Relative Angles Count Classification Matrix.*

Retrospective Analysis: Contrary to the training data, the test data does not show a $\frac{3}{4}$ separation between the progressive and hyperactive trajectories (Figure 6.17). The maximum of the distribution whiskers of the box plots lie close together ($Hyperactivated_{max} = 48.21\%$, $Transitional_{max} = 43.48\%$, $Progressive_{max} = 42.86\%$). The outlier data point of 65.39% in the hyperactivated group falls more than 1.5 times outside the interquartile range of 16.07% and is not being considered in this analysis. Approximately half of the transitional trajectories of the test data set fall within $\frac{3}{4}$ of the hyperactivated trajectory distribution. Similarly, the other half of the transitional trajectories lie within $\frac{1}{2}$ of the pro-

gressive classification distribution. There is no better placement of the threshold boundaries to improve the classification rate with each classification group without penalizing either one. As with the prior algorithm, RAC classification can be improved without the transitional trajectory group. In this case, the upper and lower boundary could be replaced with a single threshold (23.22%) placed between the lower quartile (21.43%) of the hyperactivated and the upper quartile (25.0%) of the progressive trajectories. In the best case, this would correctly capture approximately three quartiles of the hyperactivated and three quartile of the progressive trajectories as observed in the training data set. But this improvement comes at the expense of classification of the transitional trajectories.

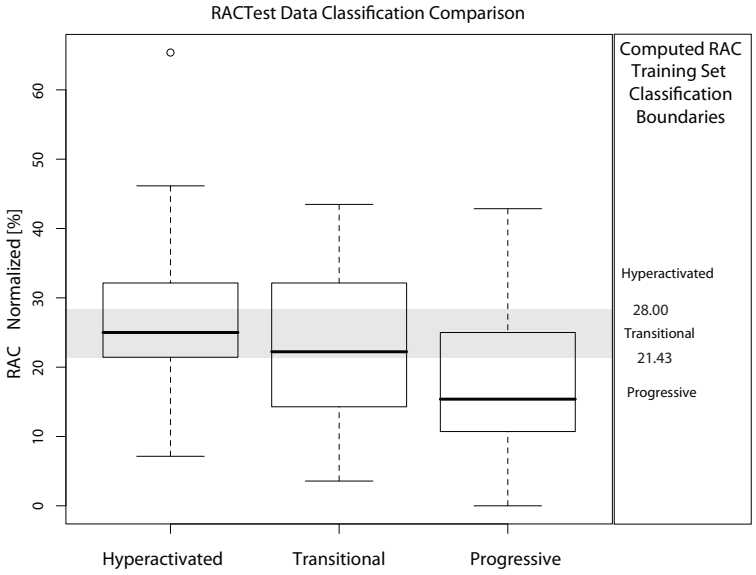

Figure 6.17: *RAC Test and Training Data Outcome Comparison*

6.6 Quadrant Scoring QS

Similar to RAC, the QS algorithm attempts to capture a deviation from a linear movement of the sperm trajectory by counting the occurrence of the sperm location relative to a 2D quadrant Cartesian coordinate system. The standard deviation over these quadrants is used as an indicator for hyperactivation. A higher standard deviation is to be expected for a progressive, more linear, and a lower standard deviation for an erratic moving or circling hyperactivated sperm (Section 4.5.3). Table 6.7 shows the standard deviation of hyperactivated sperm ($QS_{hyper-min} = 0.0\%$ to $QS_{hyper-max} = 5.83\%$) is lower than the standard deviation of progressive sperm ($QS_{prog.-min} = 3.78\%$ to $QS_{prog.-max} = 10.63\%$).

	Hyperactivated	Progressive
Min.	0.000	3.775
Max.	5.852	10.626
Median	2.638	7.089
Mean	2.708	6.980

Table 6.7: *QS Training Data Statistics.*

Threshold Boundaries: The small overlap of the maximum hyperactive (5.86) and the minimum progressive (3.78) whiskers of the box plot training data set are chosen as threshold boundaries (Figure 6.18). Transitional trajectories will fall within $5.86 > \ transitional \ > 3.78$. The maximum value of the hyperactivated (5.83) training data set is close to the value of the first quartile (5.73) of the progressive set and the minimum value of the progressive (3.78) training data set is identical to the value of the third quartile (3.78) of the hyperactivated set. As an alternative to the minimum and maximum, the first hyperactivated and the

third progressive quartile could have been used. These thresholds separate three quartiles of the hyperactivated and three quartiles of the progressive trajectories. A classification detection rate in this range should be expected.

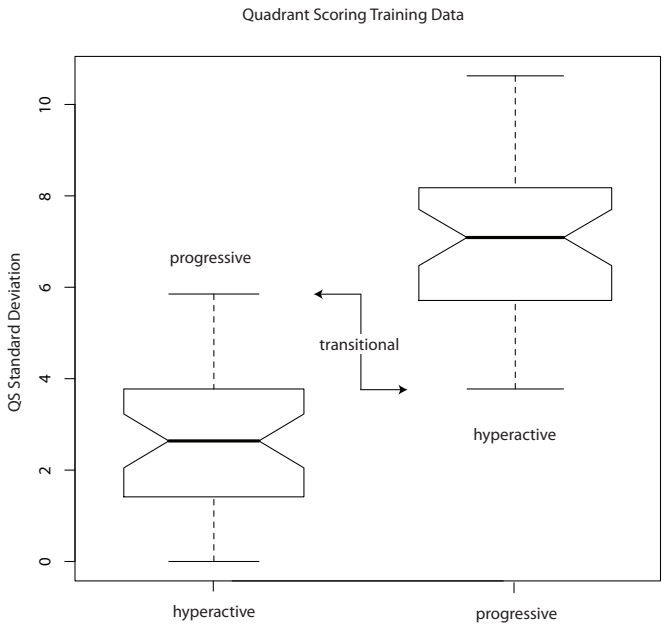

Figure 6.18: *Quadrant Scoring Training Results.*

Classification Analysis: Figure 6.19 displays the classification results of the QS algorithm. Indeed, as the training data threshold suggested, almost three quartiles of the hyperactivated trajectories were correctly classified (72.41%). This rate was lower for progressive (57.14%) and transitional trajectories (48%). But QS produced a high number of false positives ($16/51.14\%$) and false negatives ($8/27.59\%$). The all-over correct classification for the QS algorithm was 58.87%.

Retrospective Analysis: As observed in the training data, the test data is separated by

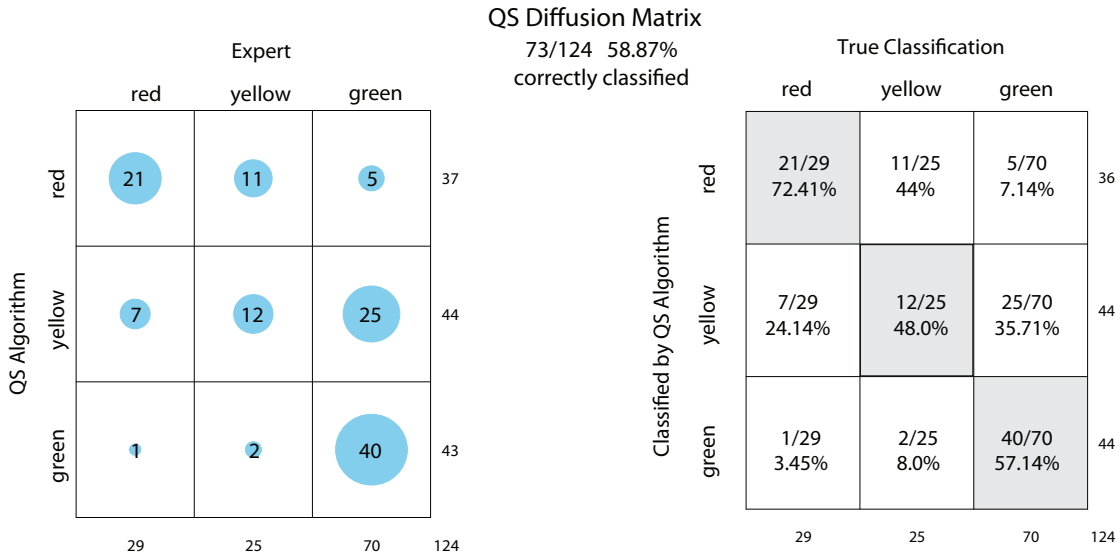

Figure 6.19: *Quadrant Scoring Diffusion Matrix.*

the third quartile (3.86) of the hyperactivated and the first quartile (5.08) of the progressive trajectory classification group (Figure 6.20). Half of the transitional trajectories lie within more than half of the hyperactivated sperm trajectories. But the quartiles of transitional (third quartile 4.83) and progressive (first quartile 5.07) trajectories do not overlap. A slightly better classification result for the hyperactivated and progressive classification group could have been achieved with this test data by raising the lower threshold from 3.78 to the third quartile of the hyperactivated trajectories (3.86) and lowering the upper bound from 5.85 to the first quartile (5.08) of the progressive trajectories. Again, this improvement would come at the expense of the transitional trajectories. In comparison with the previous tested algorithms, QS improved the classification of transitional trajectories, especially vis-a-vis the progressive trajectories, but the overlap with the hyperactivated classification group remains. Also, this algorithm might be best used with a single threshold (for example

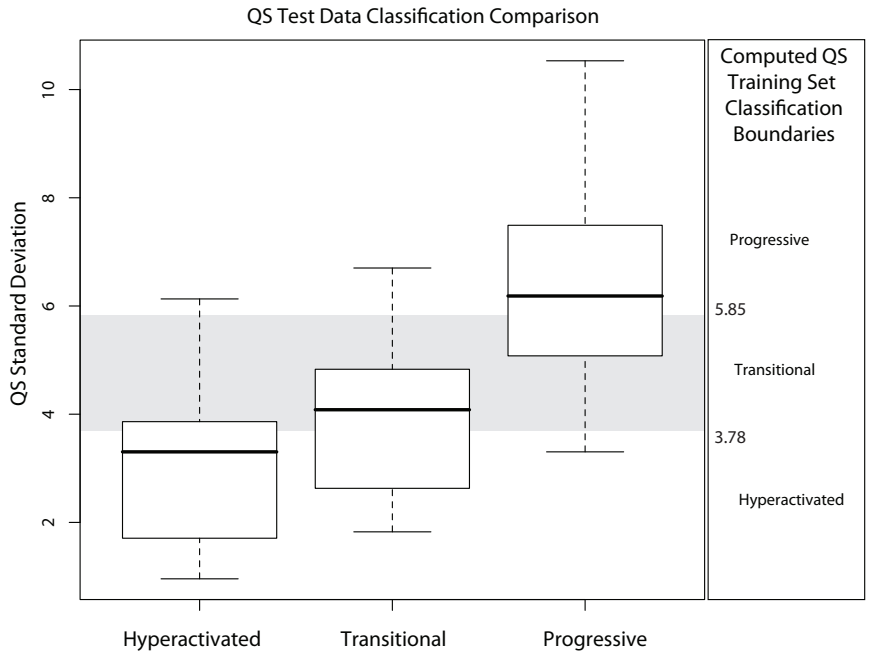

Figure 6.20: *QS Retrospective Analysis*

the median (5.08)) between the first and third quartile of the hyperactivated and progressive classification group.

6.7 Logistic Regression RAC-QS

Logistic regression combines two previously discussed measures (Sections 4.5.3, and 4.5.4) of Quadrant Scoring (QS) and Relative Angle Count (RAC), into one measure. This is an attempt to discover whether an improvement over each individual or both measures can be achieved. We first present the results of the logistic regression together with a classification comparison of logistic regression and its input variables QS and RAC.

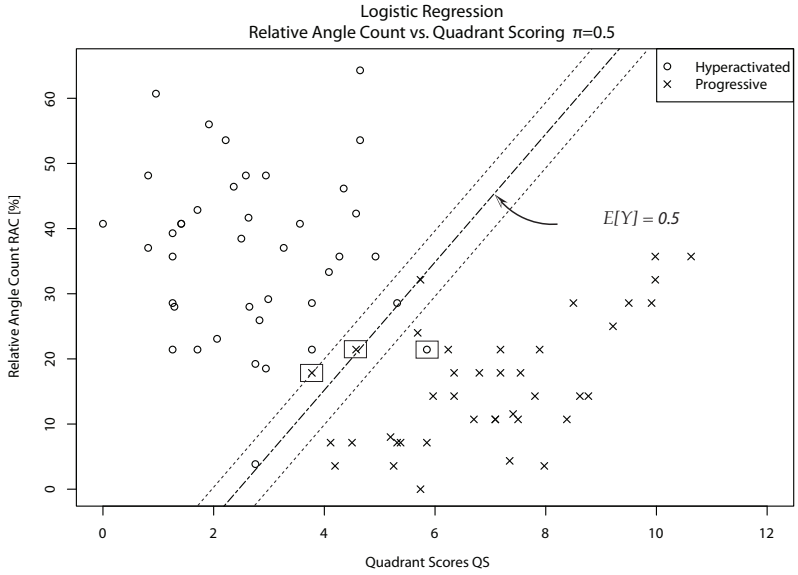

Figure 6.21: *Training data set Linear Logistic Regression Analysis on Quadrant Scoring (QS) and Relative Angle Count (RAC). The regression line has a computed slope of 9.83 and a y-axis intercept of -24.09. The squared markers indicate crossover data points in regard to* $E[Y] = 0.5$.

Threshold Boundaries: The training data set consisted of two classified groups of sperm trajectories, one hyperactivated and one progressive (6.1.1) . This correlates with the response variable of the logistic regression that has also two possible qualitative outcomes.

The 2D logistic regression analysis we used returns a 2D regression line and separates the hyperactivated and progressive training data set with a probability π of 0.5 (Figure 6.21). There are only three crossover data points (squared markers in Figure 6.21). This clear separation is proof that each input measure, QS and RAC, of the logistic regression is capturing a different feature of the sperm trajectory. We propose to use the approximate perpendicular distance to the regression line of these crossover points to define the margins for the transitional sperm trajectories. A range of $\pm$ 5% serves this purpose well, by including all but one crossover point.

Classification Analysis: Using Logistic Regression of QS and RAC, a total of 64.52% of sperm could be correctly classified, an improvement over each individual algorithm tested by itself that scored 58.87% for QS and 50.81% for RAC (Figure 6.22).

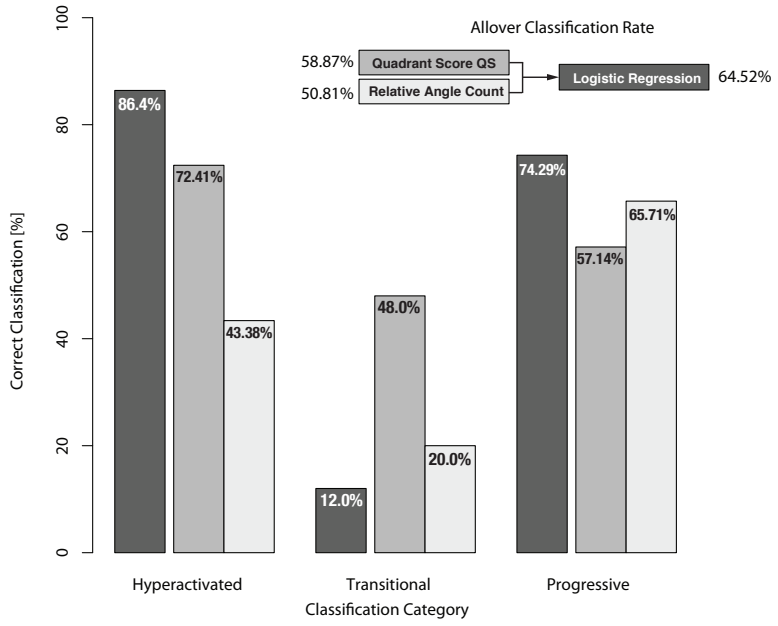

Figure 6.22: *Logistic Regression Comparison Barplot.*

The individual classification performance of logistic regression was 86.21% for hyperactivated and 74.29% for progressive sperm, also higher than QS (72.41%, 57.14%) and RAC (43.38%, 66.71%) for the same classification groups (Figure 6.23). Again, as in the algorithms tested above, transitional sperm detection was low with only 12.0% correctly classified sperm trajectories and lower than RAC in this group with 20.0%. QS, though lower in hyperactivated and progressive sperm trajectory classification, had a with 48.0% a fourfold higher correct classification of transitional sperm than the logistic regression method.

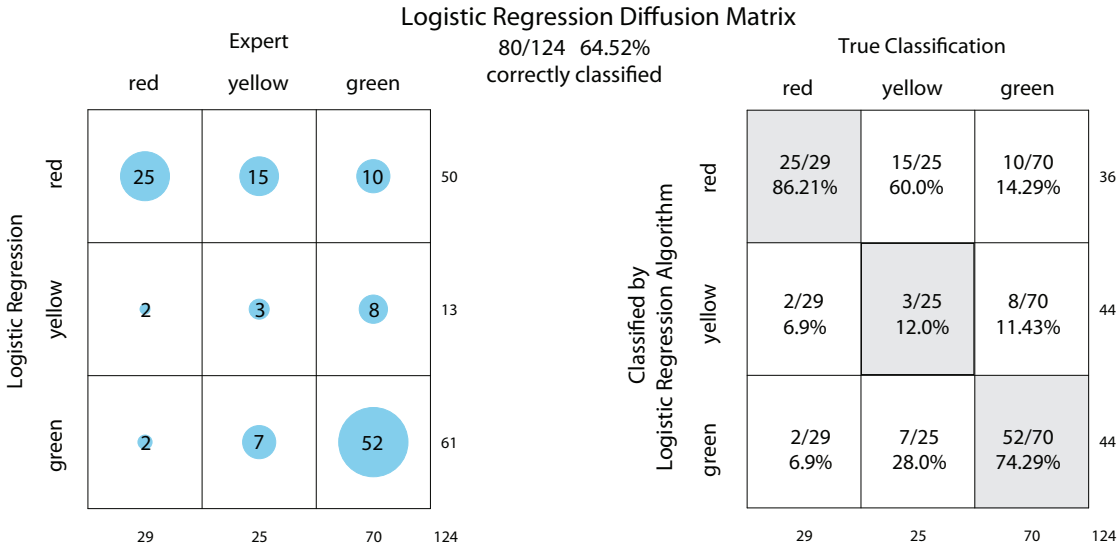

Figure 6.23: *Logistic Regression Diffusion Matrix.*

The improvement of classification with logistic regression came with an increase of 25 false positives, where the logistic regression method wrongly classified a sperm trajectory as hyperactivated, compared to 16 for Qs and 21 for RAC (Figure 6.24). False negatives were reduced to 4 from 8 for QS and 17 for RAC. While logistic regression improved

the classification performance over its input variables QS and RAC, the improvements are not substantial enough and are offset by false positives and lower correct transitional classifications.

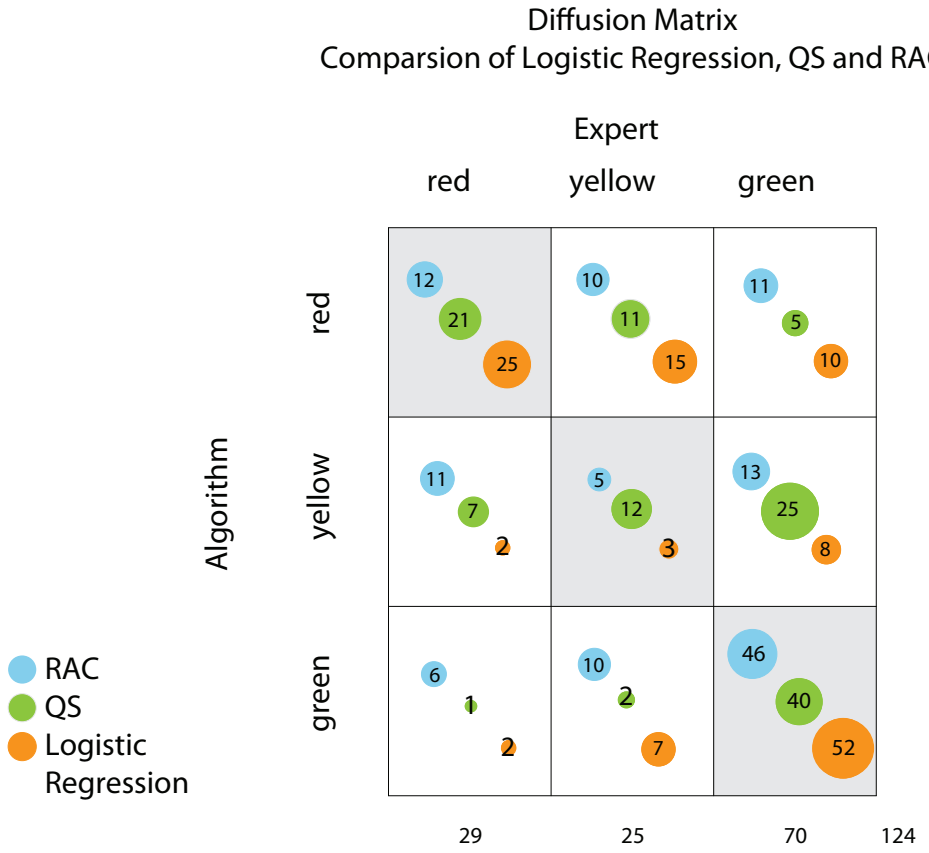

Figure 6.24: *Logistic Regression Comparison overview with its input variables QS and RAC.*

Retrospective Analysis: We overlaid the regression line ($E[Y]_{TrainingData}$) with the $\pm 5\%$ transitional band, computed from the training data on the test data, in order to test how well it matched the test data (Figure 6.25). As opposed to the training data, the test data shows many more crossover points with a much larger perpendicular distance to the

training data regression line. Next, we computed a logistic regression on the test data ($E[Y]_{TestData}$) set and compared it to the training data ($E[Y]_{TrainingData}$) logistic regression line. $E[Y]_{TestData}$ divides the test data with a steeper slope (42.14) than $E[Y]_{TrainingData}$ (9.83), but crosses the x-axis in a in a similar region, 3.39 and 2.44, respectively. This is not overly concerning, since there are many lines that can be drawn separating these two classification groups, considering the clusters of hyperactivated on the lower right and progressive on the upper left of the coordinate system.

The transitional bands computed from the training data cover only 3 transitional sperm trajectories in the test data, with the remaining transitional trajectories (stars in Figure 6.25) spread widely across the graph. This wide spread of transitional trajectories across the chart suggests that a band surrounding the 2D logistic regression line is not suitable for transitional trajectory classification. Whereas the dichotomous 2D logistic regression approach can classify hyperactivated and progressive sperm tracks, it cannot capture the transitional sperm trajectories.

Transitional Band Analysis: We plotted the correct classification rate of hyperactivated, transitional and progressive trajectories as a function of the transitional band width to evaluate the effect of the transitional band on transitional sperm trajectory detection (Figure 6.26). When the transitional band is set at zero percent, which is the 2D logistic regression line itself, approximately 75% progressive and 90% hyperactivated sperm trajectories are correctly classified. Widening the percentage of the band increases the classification rate of transitional trajectories in parallel with a steady decline of hyperactivated and progressive sperm trajectory classification. With a band width of 30% all transitional trajectories are correctly classified, but at the expense of hyperactive and transitional detection of approxi-

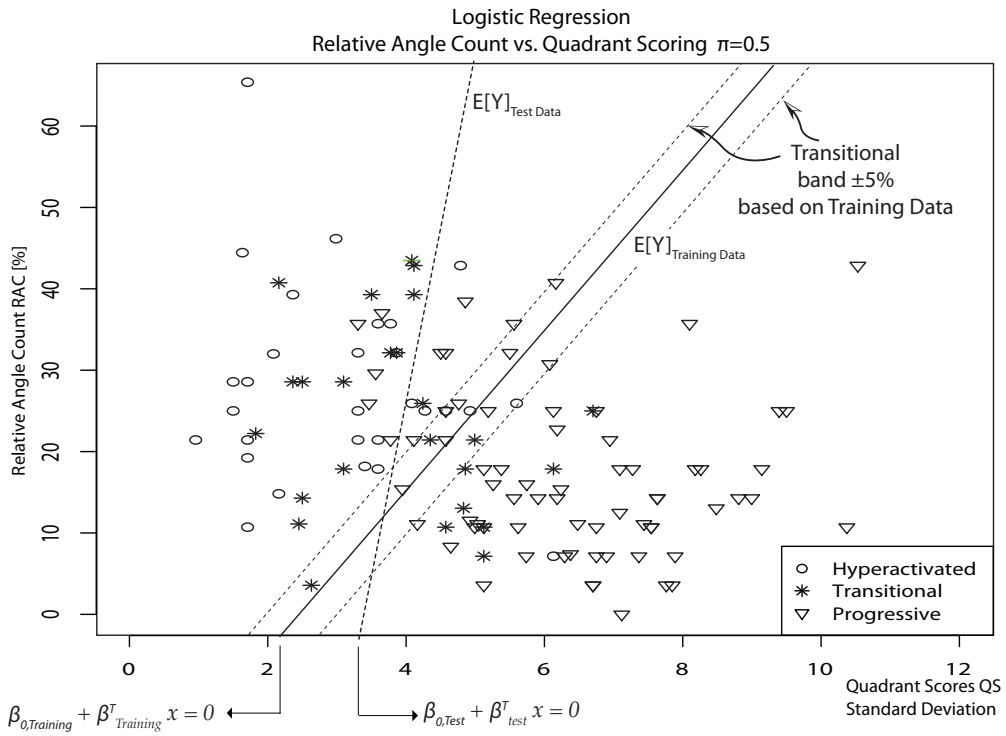

Figure 6.25: *Logistic Regression QS-RAC Test Data Outcome Comparison. The predicted regression from the training data with* ± 5 *margins. Training data coefficients are* -4.9261 *for the intercept,* 2.0098 *for QS and* -0.2045 *for RAC. Test data regression line y-axis intercept is* -142.91 *with a slope of* 42.14*. Training data regression line y-axis intercept is* -24.09 *with a slope of* 9.83*. Note: The training data did not contain transitional trajectories.*

mately 30% and 40%, respectively. There is no effective band width to capture transitional trajectories with a 2D logistic regression approach.

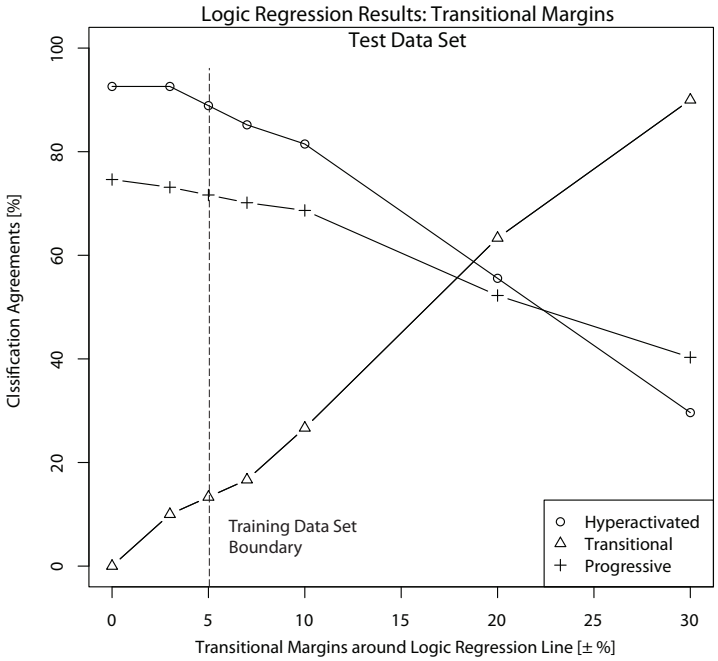

Figure 6.26: *Logistic Regression Transitional Margins. Dotted line: Band width based on the training data.*

6.8 Minimum Bounding Square Ratio, MBSR

The MBSR algorithm reflects the ratio of the trajectory search area over an exploration region of the sperm track (chapter 4 section 4.5.7). The results of the Minimum Bounding Square Ratio algorithm are presented as follows: We first examined the results of its individual components, the trajectory hull A_{hull} and the effect of the number of joint convex hulls forming this trajectory area in section 6.8.1. This is followed by a discussion of expected MBSR values (6.8.2), pursued by the results of threshold boundaries (6.8.3) and classification analysis in a diffusion matrix (6.8.4). We conclude this section with a retrospective analysis of the MBSR algorithm in section 6.8.5.

6.8.1 Trajectory Hull, A_{hull}

The trajectory area A_{hull} is computed as a set of connected convex hulls and is discussed in section 4.5.7.1. Physiologically, a hyperactivated track is performing a wider search pattern than a progressive track and it is therefore desirable to maximize A_{hull}, while minimizing A_{hull} for a progressive trajectory that has not engaged in a search yet. To determine the optimal number of trajectory hulls to reach this goal, we selected two representative sets of $n = 5$ hyperactivated and progressive trajectories, with patterns described in the literature to be challenging to classify [52, 76, 81, 122]. The hyperactivated trajectory pattern is described subjectively as star spin, star shaped or circling (see chapter 2 Table 2.7). The challenge for the algorithm is to correctly represent A_{hull} of a hyperactivated sperm trajectroy, (doughnut shape) without falsely adding the center to the total area. Trajectory H_1 of Figures 6.28 depicts a typical circular hyperactivated sperm trajectory with a single convex hull representing the trajectory area A_{hull}. Increasing the number of joint hulls

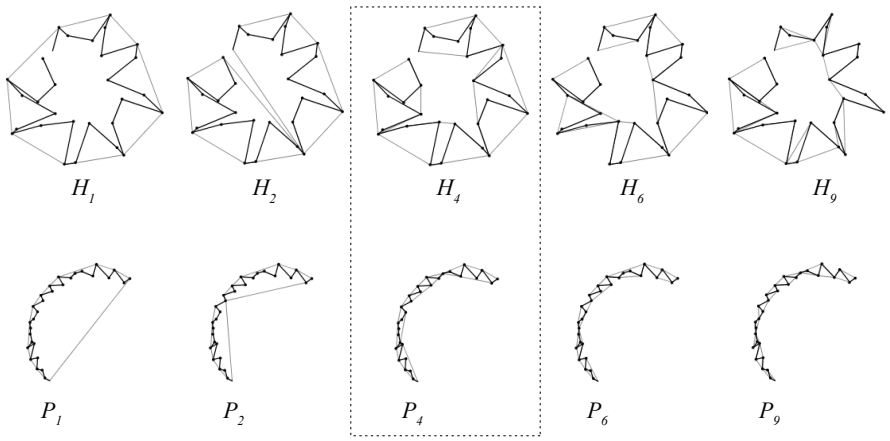

Figure 6.27: *Effect of the number of joint convex hulls on the trajectory regions. A 4-hull trajectory region matches the physiological circumstance best for both hyperactivated and progressive trajectories. Note the overestimation when using* $hull = 1$ *in both, hyperactive and progressive trajectories. Hyperactive (ID 5NL2003):* H_1, H_2, H_4, H_6, H_9. *Progressive (ID 18ML3001):* P_1, P_2, P_4, P_6, P_9.

($H_2,\ H_4$) improves the enveloping contour of the trajectory while the center is no longer falsely added to the trajectory area A_{hull}. Further increasing the number of convex hulls ($H_6,\ H_9$) generates voids in the outside of the trajectory contour. For a data acquisition rate of $60Hz$ over $500\ ms$ (30 data trajectory points) as used in this dissertation (Chapter 4, Section 4.2.5), four joint convex hulls optimally describe the trajectory contour of a hyperactivated sperm, without producing voids or falsely adding center areas, if they exist.

For the progressive trajectories (P_1, P_2, P_4, P_6, P_9 of Figure 6.28), a single convex hull describes a half moon area and does not follow the trajectory contour. As with the hyperactivated trajectory example, the description of the progressive trajectory contour improves with an increase to four hulls (P_4). As the goal for progressive sperm trajectories was to follow the trajectory contour and to minimize the trajectory area, any number of convex hulls

($P_4 - P_9$ or smaller) seems to satisfy these conditions with the constraint for the smallest convex hull being three points. The chart of Figure 6.28 illustrates the average sperm tra-

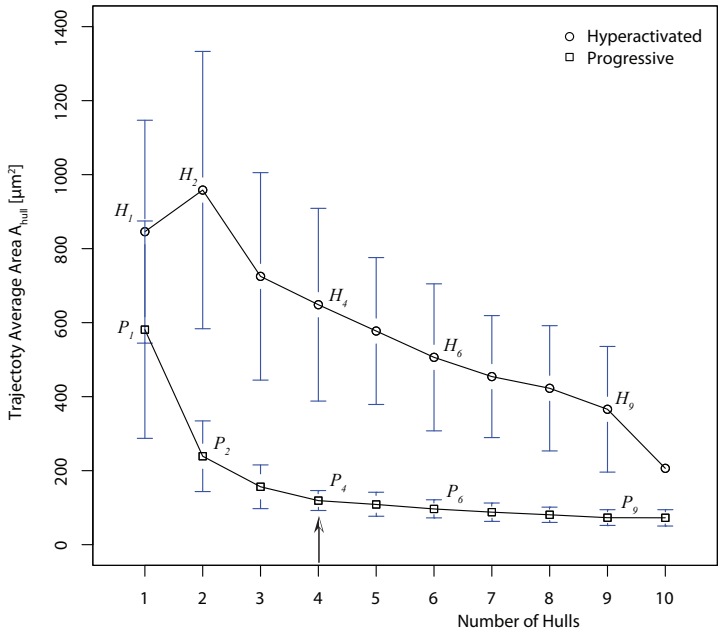

Figure 6.28: *The dependency of the number of convex hulls and resulting trajectory area. Plotted are the average of five typical 'star-shaped' hyperactivated and five progressive trajectories. The arrow depicts the optimal number of joint convex hull for this research. The bars represent the standard deviation.*

jectory area as a function of the number of convex hulls forming this area. The curve of H_1 through H_9 plots the average of the five sperm trajectories representing circling hyperactive sperm. P_1 through P_9 plots the average of five linear moving sperm trajectories. The trajectory area average for the hyperactivated and progressive sperm example decline with an increase of the number of convex hulls. As mentioned in the previous paragraph, the trajectory contour of the hyperactivated sperm trajectory is optimal with four joint convex hulls. Four hulls are also a good choice for the progressive trajectories, considering the

goal of minimizing the A_{hull} and that after P_4 the area decreases only by a little.

6.8.2 Expected MBSR Value

The best theoretical value of MBSR is 100% for a sperm track covering its entire exploration region (4.5.7). This scenario is most unlikely. An inscribed circle representing the area of a circling hyperactivated sperm trajectory A_{hull} within a square, A_{MBS} better reflects the physiological behavior of a sperm trajectory and provides a guideline value for an expected upper bound MBSR (picture I, Figure 6.29). This simulation results in a MBSR of 66.67% and is confirmed with an actual hyperactivated circling sperm trajectory (61.86%) in picture II of Figure 6.29. Picture III shows an example of a trashing hyperactivated tra-

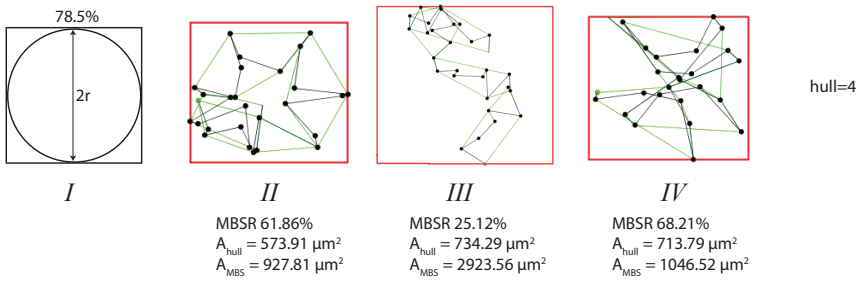

Figure 6.29: *Expected MBSR values for hyperactivated sperm trajectories. I; The square represents the A_{MBS} of a circling hyperactivated trajectory and the inscribed circle its trajectory area A_{hull}. This simulated case will result in a MBSR of 78.5%.. Actual sperm trajectory examples with their MBSR value (II, III, IV).*

jectory, that covers a smaller area and results in a MBSR of 25.12%. The final picture IV is a star-shaped hyperactivated sperm trajectory with a MBSR of 68.21%. The trajectory example IV appears to cover a smaller area of its exploration region square than example II (68.21% vs. 61.86%), but has a higher MBSR . The reason lies in the overlapping convex

hulls, occurring where the trajectory path reverses and crosses itself. Overlapping convex hull areas are then accounted for multiple times in the trajectory area calculation A_{hull}. This amplification of the MBSR is a desirable effect for hyperactivated trajectories, since our goal is to maximize the area covered in this type of sperm trajectory. Contemplating the model and examples from above, a reasonable approximate expected value for MBSR should be in the range of $20\% < MBSR < 70\%$ for hyperactivated sperm trajectories.

Progressive sperm trajectories display more linear behavior and cover a smaller area. The linear extend of the trajectory results in a large exploration region square A_{MBS} adding to a minimizing effect of MBSR. Picture I of Figure 6.30 is an example of a typical pro-

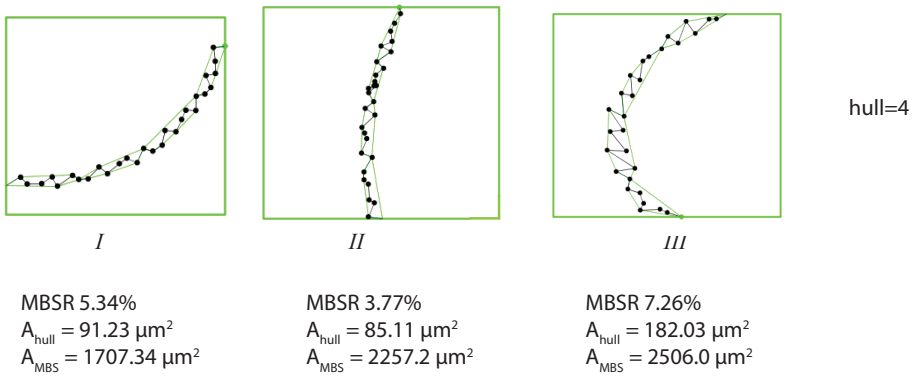

Figure 6.30: *Number of Hulls Effect on the MBSR of Progressive Tracks. A single hull overestimates the track area for sperm with curved progressive tracks. A drastic reduction and better result is reached when moving from a single to quadruple hull. The examples A and$B$ would be falsely classified as hyperactive, if using a single convex hull.*

gressive sperm trajectory resulting in a much lower MBSR of 5.34% in comparison to a hyperactivated MBSR. Other examples (picture II and III) of progressive sperm tracks lie in a similar vicinity of the previous one of 3.77% and 7.26%. Considering these examples,

a $MBSR < 10\%$ is to be expected for progressive sperm trajectories.

6.8.3 MBSR Threshold Boundaries

Threshold values for MBSR were determined by computing two different threshold response curves form the training data. One threshold response curve (TH_{prog} of Figure 6.31) was based on the training data containing only progressive trajectories, by incrementally increasing the MBSR thresholds from $0\ to\ 20\ \%$ while recording the number of detected trajectories. The number of detected trajectories for each threshold were normalized over the total amount (40) of available progressive sperm trajectories. The detection rate of progressive trajectories increased steeply with small increases in MBSR and identified all 40 progressive sperm trajectories at an MBSR of 11%.

We repeated this procedure to acquire a threshold curve (TH_{hyper}) with the hyperactivated trajectories from the training data. Starting at a MBSR of 8% all hyperactivated tracks were recognized until a MBSR threshold of approximately 13.5%, where the detection rate steadily declined and finally dropped to zero with no detected hyperactivated trajectories, at approximately 80% MBSR.

The intersection C of TH_{prog} and TH_{hyper} at approximately 11% was used as the center for a transitional threshold band. As mentioned before, there are few guidelines for characterizing transitional sperm trajectories making the process of finding threshold boundaries for transitional sperm trajectories for the MBSR classification method even more challenging. Both threshold curves of TH_{prog} and TH_{hyper} have a steep incline and decline around their intersection C limiting the threshold band width. Moving the left threshold boundary will quickly result in a $50 - 75\%$ reduction of the detection rate of progressive sperm. We

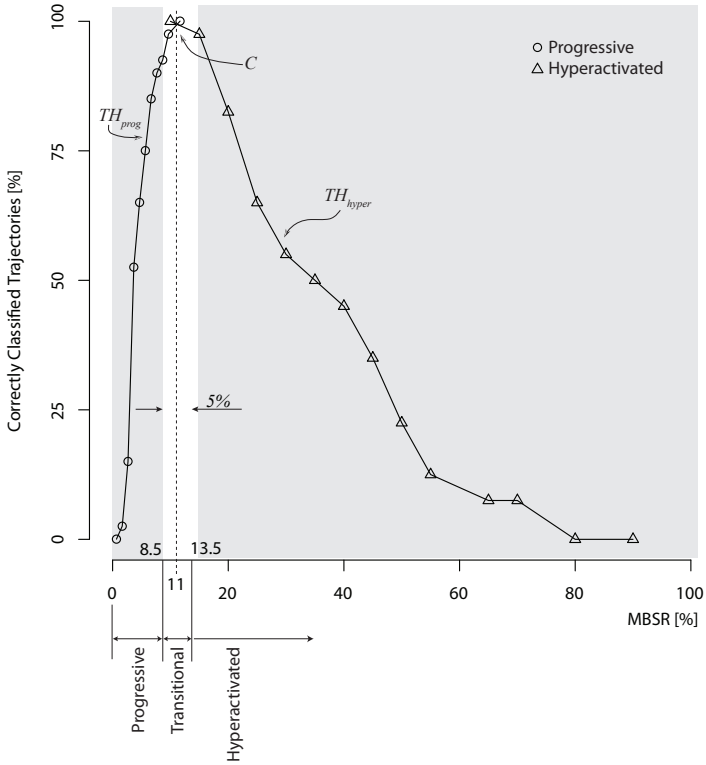

Figure 6.31: *Normalized MBSR Classification Boundaries. Based on a progressive ($n = 40$) and hyperactivated ($n = 40$) training data set. Margins were set to $\pm 2.5\%$ around the curve's intersection at $\sim 11\%$ MBSR. Progressive trajectories: $MBSR_p < 8.5$; Transitional: $8.5 \leq MBSR_t \leq 13.5$, Hyperactive tracks: $MBSR_h > 13.5$;. TH_{prog} : Threshold response curve of progressive trajectories. TH_{hyper} : Threshold response curve of hyperactivated trajectories. C: Intersection of TH_{prog} and TH_{hyper} .*

decided on a $\pm 2.5\%$ (5% width) transitional threshold band to avoid large detection losses. A 5% MBSR transitional band will keep the detection rate well above the 90 percentile for both hyperactivated and progressive sperm trajectories of the training data set, while providing space for potential transitional sperm .

6.8.4 MBSR Classification Results

When applied to the test data containing 138 trajectories, the MBSR algorithm had an all-over classification performance of $111/124$ or 89.52% (Figure 6.32). The individual results were even higher with $27/29$ or 93.1% correctly classified hyperactivated sperm trajectories and $69/70$ or 98.5% progressive trajectories. Transitional sperm tracks were classified correctly with $15/25$ or 60.0%. Although the result is low, it was the highest among all classification algorithms. MBSR produced 8 false positives, where MBSR classified tran-

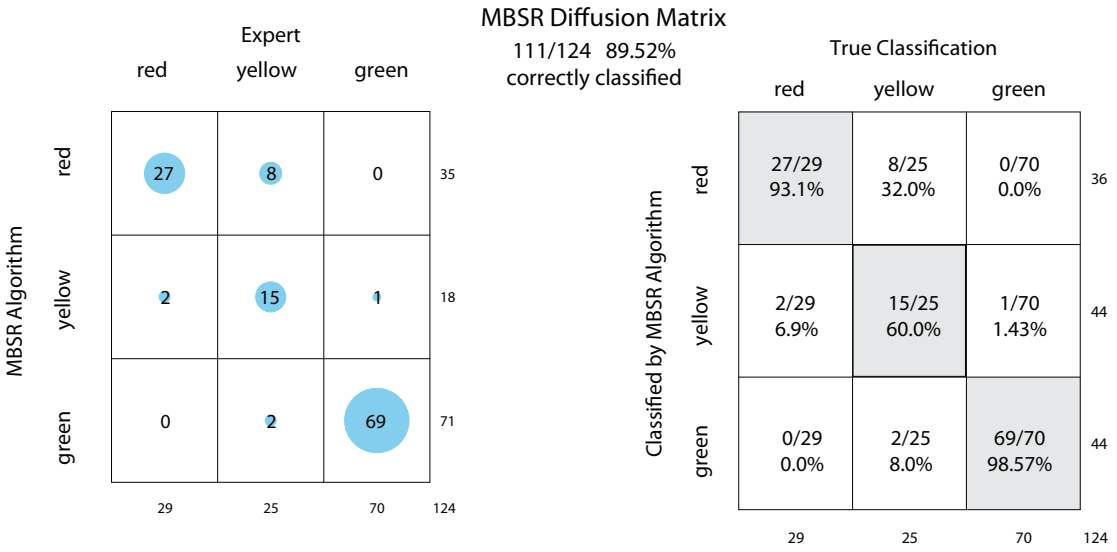

Figure 6.32: *MBSR Diffusion Matrix. x-axis: Human classification as predicted outcome. y-axis: MBSR algorithm as actual outcome. 1, 2 and 3 represent red (hyperactive), yellow (transitional) and green (progressive) classification.*

sitional sperm trajectories as hyperactive, and 2 false positives in the same category. More importantly, no hyperactivated trajectories were classified by the MBSR algorithm as progressive or vice versa. With its high correct classification rate of $> 93\%$, MBSR is an

excellent candidate for classification of hyperactivated and progressive sperm trajectories. Transitional sperm trajectories were also detected with a higher rate than with any other method we tested.

6.8.5 MBSR Retrospective Analysis

Figure 6.33 displays the retrospective analysis of the test data with MBSR training data threshold boundaries of 8.5% and 13.5%. The MBSR algorithm was able to provide a clear separation of the test data distributions of hyperactive to progressive sperm trajectories by a margin of 8% to 13%. MBSR also was capable of narrowing the distribution of

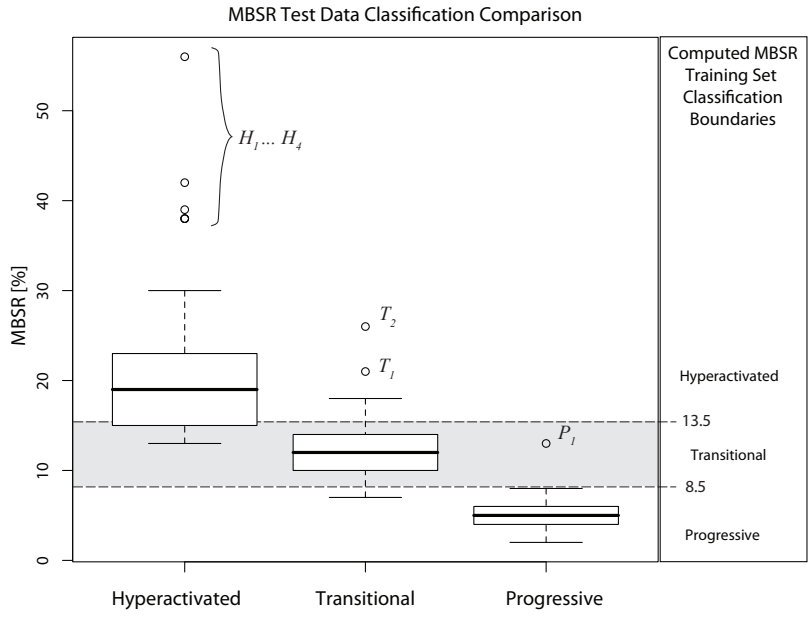

Figure 6.33: *MBSR Retrospective Analysis of the Test Data. P_1: Progressive Trajectory classification outlier. P_1, P_2: Hyperactive Trajectory classification outliers, $H_1, ..., H_4$: Hyperactive Trajectory classification outliers.*

transitional sperm trajectories between 7% and 18%. Less than half of the transitional sperm trajectories lie within approximately one quartile of the hyperactivated classifications group. The upper (13.5%) and lower threshold (8.5%) bounds already correctly classify all but 2 of of the hyperactivated (93.1%) and all but 1 of the progressive (98.57%) sperm trajectories. Elevating the upper threshold boundary from 13.8% to 18% would improve the transitional sperm trajectory classification, but at a substantial decline in detection of hyperactivated trajectories. A lowering of the opposite transitional threshold end from 8.5% down to 7% could slightly improve this classification category, but at the expense to the progressive classification set.

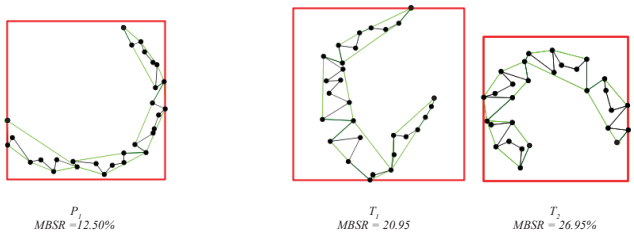

Figure 6.34: *MBSR Test Data Outlier Trajectories. P_1: Progressive Trajectory classification outlier. P_1, P_2: Hyperactive Trajectory classification outliers.*

Outlier Analysis: Figure 6.33 shows one progressive sperm trajectory (P_1) larger than 1.5 times the quartile of this classification distribution. On further analysis with an enlarged view (Figure 6.34) this sperm trajectory with an MBSR of 12.5% has some erratic features and could also have been placed in the transitional group by the experts in the field. Similarly, a closer look at the outliers of the transitional (T_1 and T_2) group revealed some hyperactivated features. This substantiates the inherent difficulty classifying transitional sperm trajectories, lacking consistent definitions by investigators. The trajectory outliers of

the hyperactivated group are of less concern, in view of the fact that any sperm trajectory above the threshold of 13.5% will be correctly classified.

6.9 Summary Results of Classification Algorithms

A comprehensive evaluation of the algorithms takes into account the individual classification performance of hyperactivated, transitional and progressive sperm trajectories. The individual percentages are averaged and presented as the all-over classification success rate. The Minimum Bounding Square Ratio algorithm ranked first with a total correct

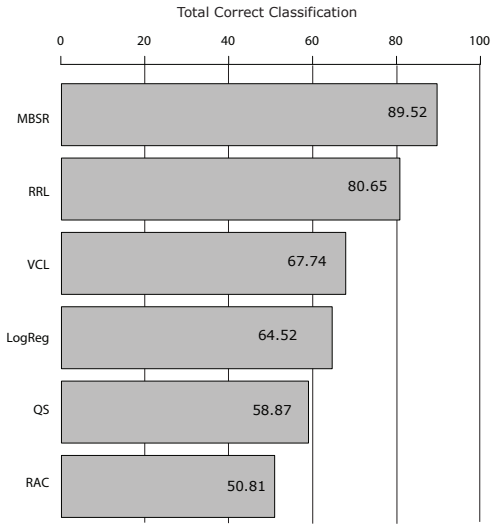

Figure 6.35: *Classification Results. Classification Percentage is based on the total number of classifiable trajectories* $n = 124$.

classification rate of 89.52%. It is followed by RRL with 80.65% and VCL with 67.74%. This is a low performance for VCL, considering that VCL is currently the gold standard by investigators in the field. Logistic regression (64.52%) was able to improve the input classification algorithm of Quadrant Scoring QS (58.87%) and Relative Angle Count RAC

(50.81%). A closer look at the detailed classification performances of hyperactivated, tran-

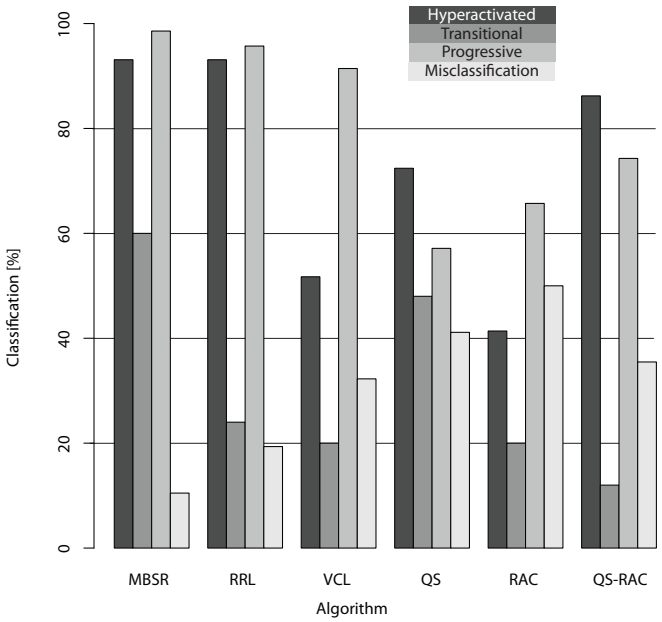

Figure 6.36: *Classification Results Summary. Classification percentages for hyperactivated, transitional and progressive columns are based on the individually available counts in each classification group. Misclassifications percentages are based on the number of incorrectly classified trajectories, divided by the total number of classifiable trajectories.*

sitional, progressive and misclassifications reveals the strengths and weaknesses of each algorithm better than the overall classification chart. The bar chart of Figure 6.36 displays these individual results for the algorithms examined in this dissertation. For better comparison, the same information as in Figure 6.36 is rearranged in Figure 6.37 as ranked groups of hyperactivated, transitional, progressive and misclassification results. MBSR ranked best in all three classification categories (93.10%, 60.0%, 98.57%). It also produced the fewest misclassifications (10.48%). The classification rate of MBSR is at par with the RRL

algorithm for hyperactivated sperm trajectories and slightly below in detecting transitional trajectories, but RRL approximately doubles the misclassified (19.35%) sperm trajectories. In third place for classification of hyperactivated trajectories is the combined measure of logistic regression (86.21%), but it ranks last in the transitional category (12.0%) and in the midfield among the algorithms with respect to the number of misclassifications (35.48%). The logistic regression algorithm is followed by QS with 72.41% correctly classified hyperactivated sperm trajectories. QS ranks second highest in detecting transitional sperm (48%) and last for progressive trajectories(57.14%). With 41.13% misclassified tracks, QS ranks the second highest for this group next to RAC with the most misclassifications of 49.19%. VCL, the current gold standard, had a mediocre hyperactivated sperm trajectory classification rate of 51.72%, followed lastly by RAC with 41.38%. VCL ranked third for progressive trajectories in the ninetieth percentile (91.43), but ranked poorly on place four for transitional (20.0%) sperm tracks and showed 32.26% misclassifications. RAC misclassified the most trajectories (49.19%) and was second to last for detecting progressive sperm (65.71%).

Table 6.37 summarizes the absolute values as well as the percentages of the algorithms classification results.

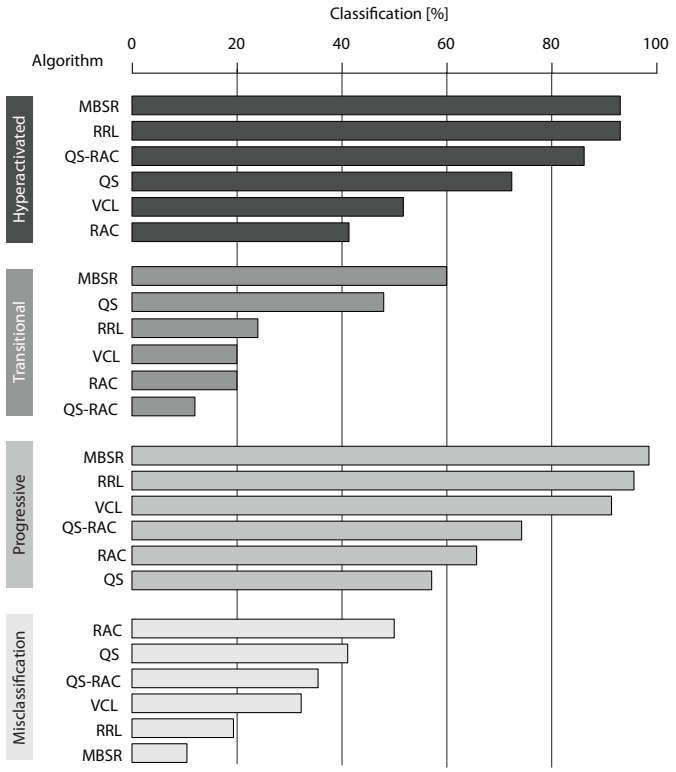

Figure 6.37: *Ranked Classification Results Summary.*

	Test Result Classification						
	Absolute			Percent			
Algorithm	hyperactivated	transitional	progressive	hyperactivated	transitional	progressive	misclassified
MBSR	27	15	70	93.10	60.0	98.57	10.48
RRL	27	6	67	93.10	24.0	95.71	19.35
VCL	15	5	64	51.72	20.0	91.43	32.26
QS	21	12	40	72.41	48.0	57.14	41.13
RAC	12	5	46	41.38	20.0	65.71	49.19
Logistic Regr. RAC-QS	25	3	52	86.21	12.0	74.29	35.48

Table 6.8: *Summary Results.* $n = 124$

Chapter 7

MBSR Hyperactivity Classification Application

In this chapter we present a practical application for spermatozoa hyperactivity classification in a laboratory research study involving the pharmaceuticals Viagra (Sildenafil), Levitra (Vardenafil) and Cialis (Tadalafil). These are popular drugs to treat erectile dysfunction (ED). In addition to effectively treating ED, these pharmaceuticals have been reported to also affect sperm motility parameters, possibly by inducing premature sperm hyperactivation and thus potentially affect fertility [86, 95, 97]. As mentioned earlier in Chapter 2 Section 2.9, there is currently no effective tool to objectively identify and classify hyperactivated spermatozoa. Therefore, previous investigators have relied on the WHO parameters (2.4.1) in their research to describe sperm motility and hyperactivation observations. This laboratory study describes how those drugs influence spermatozoa hyperactivity using the MBSR classification algorithm. We chose MBSR because it ranked best among the algo-

rithms investigated in this dissertation.

7.1 Introduction

Phosphodiesterase inhibitors (PDE) are the main active substances in the popular and effective group of drugs for the treatment of erectile dysfunction. PDEs are in the center of emerging research questions in the field of spermatozoa motility. In recent years, there has been a substantial interest in investigating the non-erectile side effects of PDEs on the spermatozoa cells themselves [7, 34, 39, 85, 95]. Indeed, PDE increase overall intracellular cAMP[1] (cyclic adenosine monophosphate) levels of sperm, part of the process of sperm capacitation, which leads to hyperactive sperm motion. cAMP acts as a second messenger for many cell physiological increases in intracellular cAMP in many biological processes and as a result can dramatically alter cell physiology. It has been reported that the PDE in Viagra and Sildenafil stimulate human sperm motility and capacitation, but do not induce the acrosome reaction [28, 67]. Although investigators have used hyperactivation to express the effect of PDEs on sperm motility, no quantifiable hyperactivity classification was used. Rather, investigators have relied on WHO measures, shown in this dissertation to be an unreliable measure for hyperactivation. The developed algorithms, in particular MBSR, could be used to quantify the drug‘s influence on spermatozoa hyperactivity.

[1] Biological process for the intracellular signal transduction.

7.2 Study Goal

The objective of this study was twofold:

▷ First to show the applicability of one of the hyperactivity algorithms developed in this dissertation in a practical laboratory study.

▷ Second to explore in a quantitative manner the effect of PDE inhibitors on sperm hyperactivity motility.

7.3 Materials and Methods

In this section we cover the specimen used for this study (7.3.1), and preparation of the drugs (7.3.2) followed by the drug-time-response protocol (7.3.3) and data acquisition and data processing (7.3.4). Next, we discuss validity (7.3.5) and lastly we cover hyperactivity classification (7.3.6).

7.3.1 Specimen

Fresh sperm from five different stallions was collected and prepared according to the procedure described in Chapter 4 Section 4.2.4. Prior to diluting the specimen to approximately $20\ 10^6$ sperm/ml, the initial sperm count was obtained. To answer the research questions of 7.2, we present the preliminary results of the analysis of one stallion ejaculate here.

7.3.2 Drug Preparation

Sample tablets of Viagra (50 mg), Levita (10 mg) and Cialis (10 mg) were crushed and dissolved in ethanol (10 mg/ml) at room temperature using a vortex mixer and by fil-

tering the solution through a Sphor© Acrodic© filter (Gelman Sciences, Ann Arbor, MI, USA) having $0.45\mu m$ pores to remove solids and fillers. Mostafa [85, 86] published concentrations used in human studies for Tadalafil $(4.0, 1.0, 0.5\ mg/ml)$ and Sildenafil $(4.0, 2.0, 1.0, 0.5, 0.1\ mg/ml)$. Staying within these published dosage ranges, Viagra and Levitra were added to sperm at 0.125 mg/ml, 0.25 mg/ml, 0.5 mg/ml, 1.0 mg/ml, 1.5 mg/ml and 2.25 mg/ml. But these dosages eliminated most sperm motility in an initial test with Cialis, which contains PDE-5 and PDE-11 inhibitors. To obtain comparable motility responses to the previous groups, Cialis dosages were reduced 50 fold to 0.0025 mg/ml, 0.0625 mg/ml, 0.1 mg/ml, 0.125 mg/ml, 0.25 mg/ml and 0.5 mg/ml.

7.3.3 Drug Time Response Protocol

We developed a protocol (Figure 7.1) to investigate the response of the PDE inhibitors on the sperm samples, according to drug dosage and the length of time of the treatment on the sperm sample. The processed ejaculate was divided into 3 x 6 equal volumes, representing the six dosages (A', A'' and A''') and 3 drugs (Viagra, Levitra and Cialis) used. One volume (A) did not receive any treatment and was used as control to document the natural decay of the sperm specimen. From the three volumes intended for the drug treatment, a $6\ \mu l$ sample was taken immediately (time=0) after the drug was added (Figure 7.1 part I). Another measurement was acquired 30, 60 and 120 minutes after the drug was introduced to the specimen. At each time interval three measurements were taken with the CASA device from the droplet to reduce the error of inhomogeneity. These measurements were repeated for each of the six dosages used and replicated for each of the three drugs, Viagra, Levitra and Cialis. Measurements from the control volume were performed more frequently

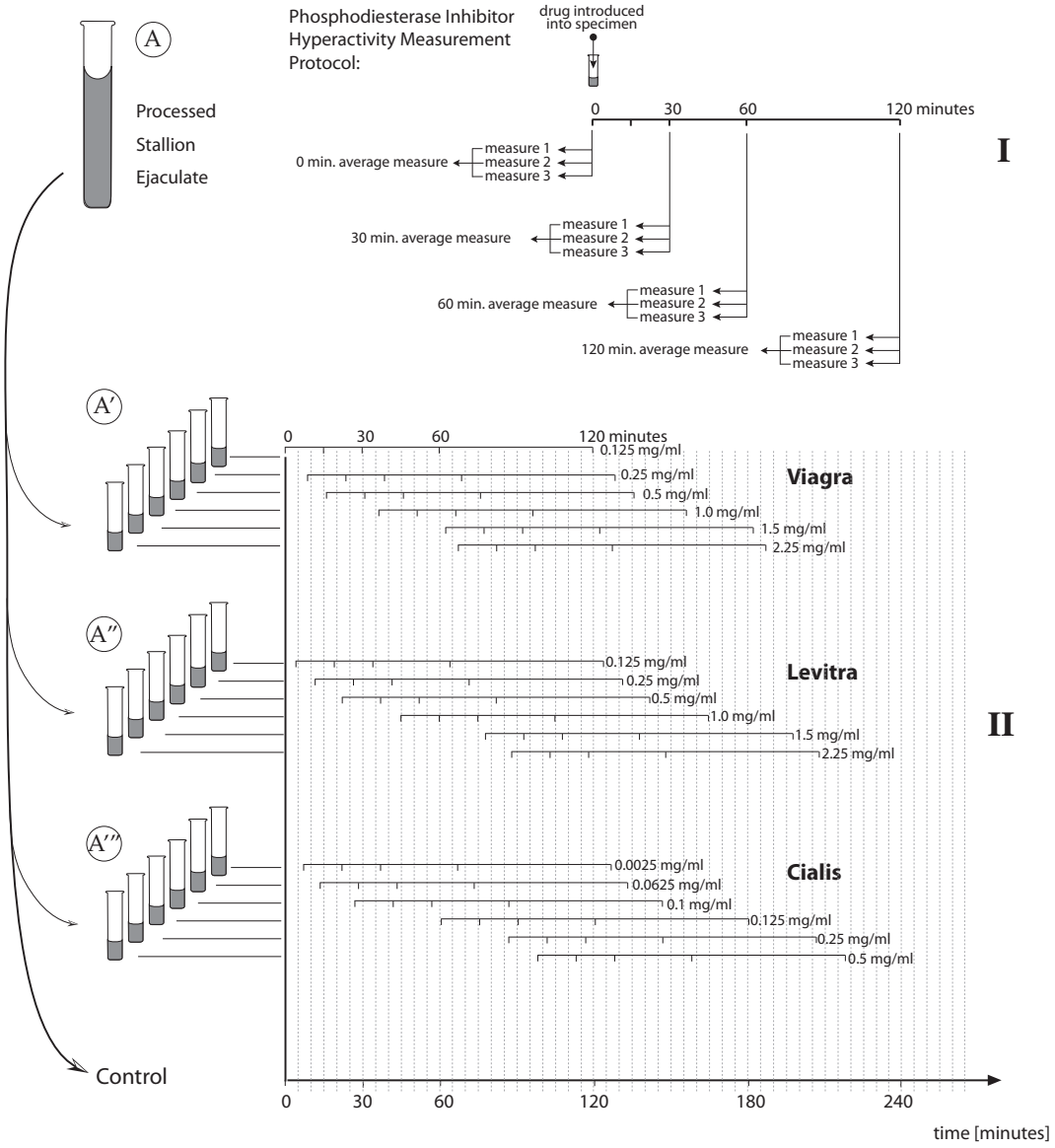

Figure 7.1: *Phosphodiesterase Inhibitor (PED) Treated Specimen Experimental Protocol. The ejaculate (A) is divided into 3 (A', A", A"') groups of 6 dosages. Three measurements (I) were taken at each time marker and droplet. The timer intervals of (I) were staggered to accommodate all dosages and drugs in this protocol (II).*

interleaved between the drug treated samples. A single measurement of a droplet took approximately 1-3 minutes. In order to accommodate all required timed measurements, the initial start time when the drug dosages were added had to be staggered (II).

7.3.4 Data Acquisition and Data Processing

Each droplet was scanned in three different slide locations to compensate for sperm nonhomogeneity on the slide and later added into one single file. We used the standard CASA ASCII output file containing parameters as listed in 4.2.5, although only the x, y trajectory data pairs were required to compute MBSR and classify the sample.

7.3.5 Validity

In this application we have to consider construct validity as a threat to this experiment. There are confounding factors during sperm classification treated with erectile dysfunction drugs, such as phosphodiasterase inhibitors. Since the sperm hyperactivity naturally increases during the elapsed time of the experiment, it could be confused with an effect coming from the drug. We reduce this threat by comparing the drug treated classification with an untreated sample measured over the entire course of the experiment and reversing the test order with another animal at another day.

7.3.6 Classification of Hyperactive, Transitional and Progressive Sperm

The MBSR classification algorithm was implemented in JAVA code on the JAVA JVM 1.5 platform and executed on an off-the-shelf laptop running OS X v10.5.6. First, the MBSR classification algorithm was applied to each measurement from the control sample

(Figure 7.2). For each droplet the resulting number of hyperactivated, transitional and progressive classified trajectories was divided by the total number of sperm trajectories existing in this measurement. Subsequently, this returned the percentage of hyperactivated, transitional and progressive sperm trajectories of this measurement. We plotted the results in an $x - y$ chart, where x is the time the measure was taken and y the percent of classified trajectories in hyperactive, transitional and progressive. A regression line for each of the three classification groups was computed using $R\ Statistical\ Software$ [99]. These regression lines ($f(x)_{hyper}$,$f(x)_{trans}(x)$,$f(x)_{prog}$) were later used to compensate for the natural decay of the specimen over time, such as a natural increase of hyperactive and decrease of progressive sperm trajectories. Figure 7.2 shows this natural decay of the untreated sample in a decline of progressive sperm trajectories ($f(x)_{prog}$) from approximately 18% at the begin of the experiment (time=0) down to approximately 10% after 3 hours. Similarly, the hyperactivity ($f(x)_{prog}$) of the sperm sample naturally increased during the testing period of three hours from approximately 6% to approximately 15%. The transitional ($f(x)_{prog}$) group remained constant throughout the measurement period.

Next, the MBSR classification algorithm was applied to each time measurement and dosage. The computed classification percentages were adjusted according to the regression lines of the control. For example, the MBSR classification algorithm computed 20% hyperactive, 10% transitional and 30% progressive for the '60 minute' time measurement after the drug was added. Note, due to unclassifiable trajectories, the percentages do not add up to 100%. If this '60 minute' measurement actually was taken at 100 minutes after the start of the experiment, the adjusted values for the hyperactivated trajectories would be: $f\left(100\right)_{hyper} = 0.0311 \cdot 100 + 6.371$. The natural hyperactivity percentage at 100 min-

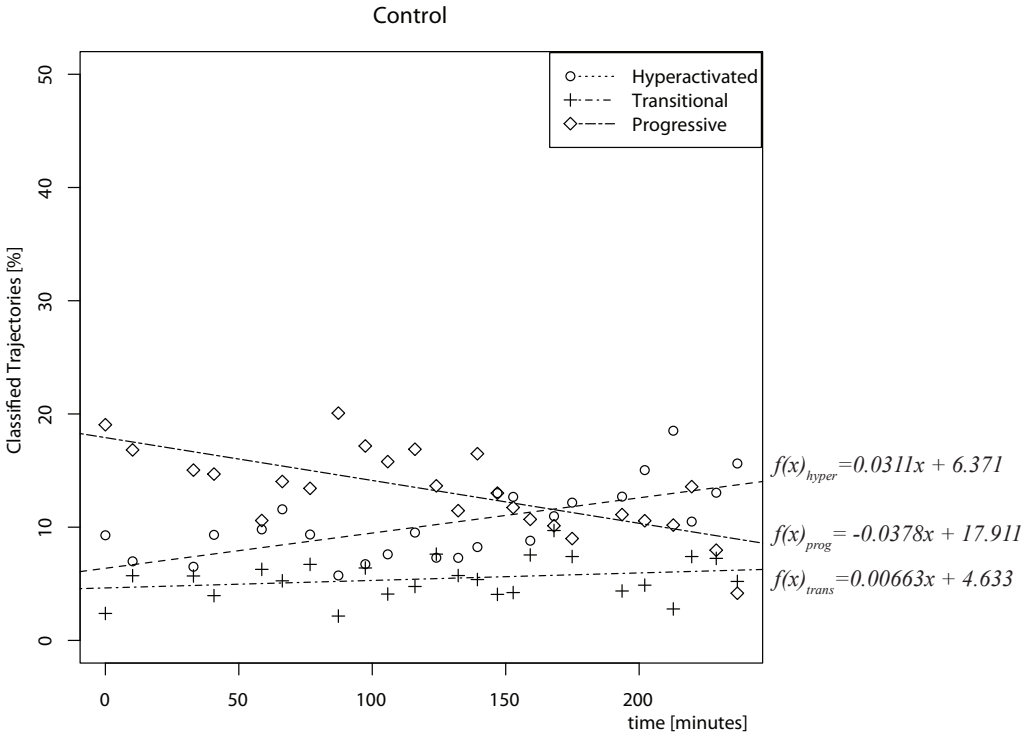

Figure 7.2: *Untreated Specimen Classification. The control showed an increase of hyperactivity over the course of the measurement, while the progressiveness declined. The control is used to adjust for a natural decay of a sperm sample.* $f(x)_{hyper}$*: Hyperactivated trajectories regression line,* $f(x)_{trans}$*: Transitional trajectories regression line,* $f(x)_{prog}$*: Progressive trajectories regression line.*

utes would be 9.48%, making the adjusted hyperactivity result $20\% - 9.48\% = 10.52\%$. Likewise, the natural percentage of transitional trajectories would be $f\left(100\right)_{trans} = 0.00663 \cdot 100 + 4.633$, resulting in 5.3% naturally occurring transitional sperm trajectories, making the adjusted transitional result $10\% - 5.3\% = 4.7\%$. Equally, for the progressive trajectories $f\left(100\right)_{prog} = -0.0378 \cdot 100 + 17.91$, resulting in 14.13% naturally occurring progressive trajectories in this measurement. The adjusted percentage of progressive trajectories would be $30\% - 14.13\% = 15.87$. A positive value from this subtraction denotes

an increase in this particular type (hyperactivated, transitional or progressive) of classified trajectories relative to the control. A negative value from this subtraction denotes a decrease in this particular type of classified trajectories relative to the control.

7.4 Experimental Results

The results are presented as follows: We begin by discussing the percentage of hyperactivated, transitional and progressive sperm trajectories of the control sample (7.4.2). Then, we present the results for progressive (7.4.3) sperm trajectories of the treated sample as the effect of drug, dosage and time, followed by the results for transitional (7.4.3) and lastly for hyperactivation (7.4.4) on the treated sample.

7.4.1 Hyperactivated, Transitional and Progressive Sperm Motility of the Untreated Sample

The spermatozoa of the stallion ejaculate decays naturally over a time period of hours. The sperm cells loose their motility, some enter hyperactivation and ultimately die. This changes the proportion of the specimen over the course of the experiment and needs to be accounted for in the measurement. Figure 7.2 demonstrates the percentage of hyperactivated, transitional and progressive sperm trajectories in the untreated sperm specimen over the course of the experiment of approximately three hours. For each of the three classification groups a regression line is computed ($f(x)_{hyper}$, $f(x)_{trans}$, $f(x)_{prog}$). Initially, the sample consisted of 6.37% hyperactivated, 4.63% transitional and 17.91% progressive sperm trajectories. The specimen started out with a high number of progressive and low number of hyperactive trajectories. As expected, while the experiment progressed, the sample decayed and naturally more progressive sperm trajectories turn into hyperactivated

ones. Interestingly, the proportion of transitional sperm trajectories (transitional regression line slope = 0.00663) remained almost constant. After approximately 3.5 hours (200 minutes) into the experiment, the sample contained an increased number of hyperactivated sperm from 6.37% to 12.59%. The number of progressive trajectories dropped from 17.91% to 10.35% and transitional sperm trajectories slightly increased over the same period with 4.63% versus 5.96%.

7.4.2 Progressive Sperm Motility as Effect of PDE Treatment

Figure 7.3 shows the preliminary results of percent progressive sperm trajectories in relation to the drug (Viagra, Levitra, Cialis), drug dosage, and elapsed time after the drug was added to the sample. A slight increase (5%) in progressive sperm trajectories are produced in the Viagra treated sample with the dosages of $1.0mg/ml$, $1.5mg/ml$ and $2.5mg/ml$ at approximately 30 minutes. The Levitra treated sample shows a drop in progressive sperm trajectories for all dosages after 60 minutes. The Cialis treated sample similarly reduces progressive sperm trajectories throughout all dosages and time. Neither of the treated samples (Viagra, Levitra, Cialis) shows a conclusive link between dosage and response increase or decrease of percent progressive sperm trajectories of the sample.

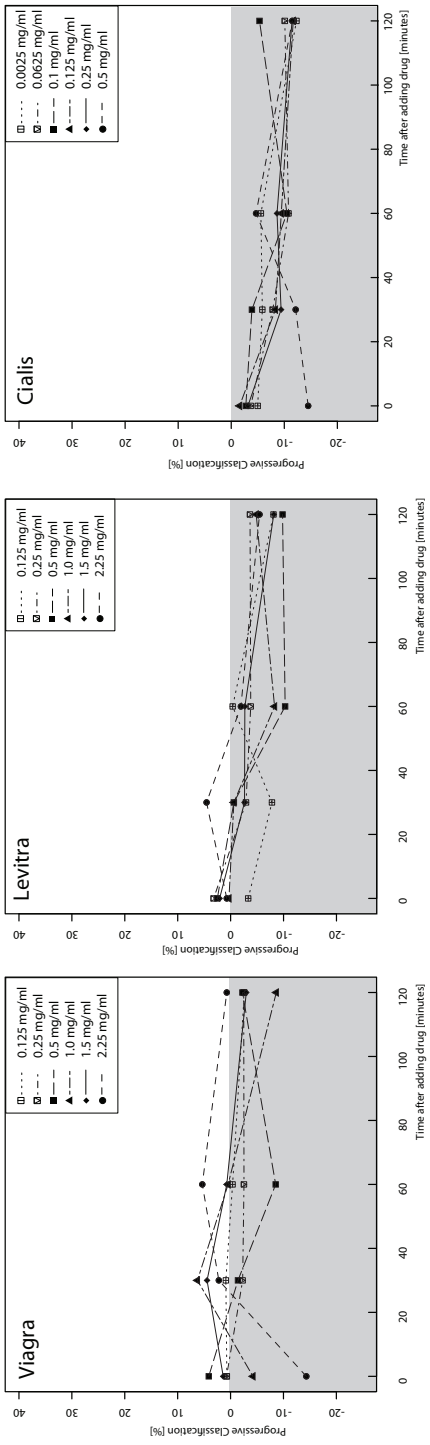

Figure 7.3: *Progressive MBSR Classification of PDE treated Stallion Sperm*

7.4.3 Transitional Sperm Motility as Effect of PDE Treatment

Figure 7.4 displays the preliminary results of percent transitional sperm trajectories as an effect of the drug (Viagra, Levitra, Cialis), drug dosage, and elapsed time after the drug was added to the sample. Little difference between (approximately $< \pm 5\%$) can be observed in transitional sperm trajectories as a result of the drug, dosage and duration the drug acted on the sample.

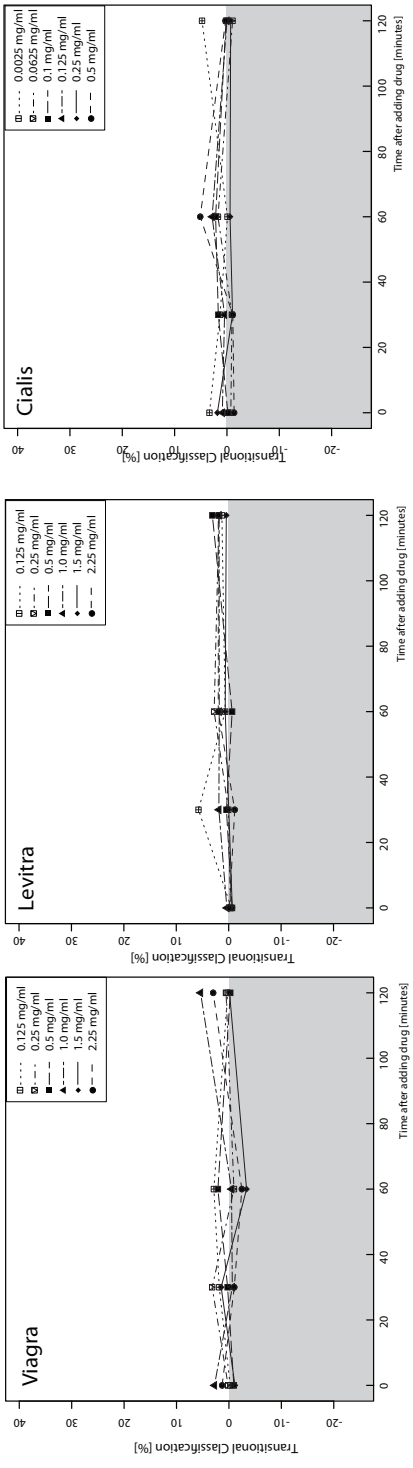

Figure 7.4: *Transitional MBSR Classification of PDE treated Stallion Sperm*

7.4.4 Hyperactivated Sperm Motility as Effect of PDE Treatment

Figure 7.5 shows the preliminary results of percent hyperactivated sperm trajectories in relation to the drug (Viagra, Levitra, Cialis), drug dosage, and elapsed time after the drug was added to the sample. A slight increase ($< 10\%$) in hyperactivated sperm trajectories are produced in the Viagra treated sample with the dosages of $0.5mg/ml$, $0.25mg/ml$ at approximately 60 minutes after adding the drug. The Levitra treated sample also shows a small increase (5%) at a dose of $0.5mg/ml$ at the 60 minutes measurement. All dosages of the Levitra treated sample show small elevated hyperactivation values ($< 5\%$) at the 2 hour measurement. The Cialis treated sample show the highest level of increase in hyperactivated sperm trajectories already at the moment the dose was added (time=0). For example, the dose $0.5mg/ml$ produced a jump of 12% in hyperactivated sperm trajectories that declined to approximately 5% after 2 hours. All dosages produced an increase in hyperactivity after 2 hours between 5% (for $0.0025mg/ml, 0.1mg/ml$) and approximately 10% (for the remaining dosages). As before, neither of the treated samples (Viagra, Levitra, Cialis) shows a conclusive link between dosage and response increase or decrease of percent hyperactivated sperm trajectories of the sample.

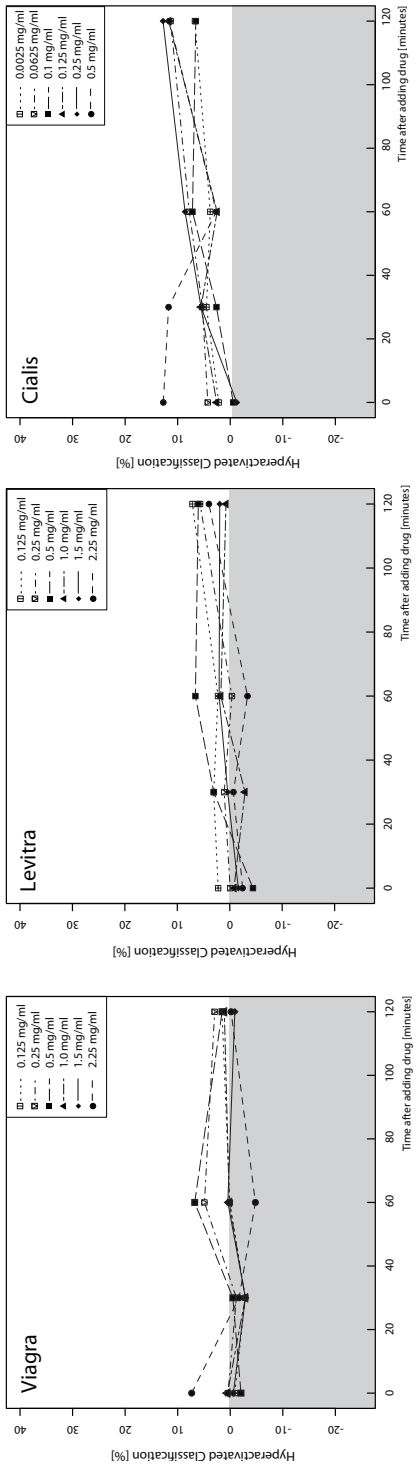

Figure 7.5: *Hyperactivation MBSR Classification of PDE treated Stallion Sperm*

7.5 MBSR Application Conclusion

We performed a laboratory study on stallion sperm to evaluate the effect of erectile dysfunction drugs on hyperactivity at different dosages and exposure times.

To answer the first research question, we successfully demonstrated that the newly developed MBSR algorithm is suitable to be used in a pharmaceutical study. One one protocol of one stallion ejaculate contains 3 measures per droplet, approximately 50 trajectories per droplet, 5 timed measurement, repeated by 6 dosages and 3 drug resulting in $13,500$ measurements, not including the control. Manual review and classification of this many trajectories would be dauntingly tedious.

For the second research question, although the preliminary results are inconclusive, a trend of increased hyperactivity in the Cialis treated sample may emerge.

Future work will include the measurement of several stallions to come up with a more conclusive result.

Chapter 8

Conclusion and Future Work

8.1 Conclusion

We developed five computational algorithms (MBSR, RRL, QS, RAC, Logistic Regression Model) to automatically detect and classify spermatozoa in hyperactivated, transitional and progressive trajectories in comparison to the "gold standard" existing VCL method. Three algorithms (MBSR, QS and RAC) introduced in this dissertation were new developments and one a combination of two (QS and RAC) in a logistic regression model. Another one (RRL) is an improvement over an existing WHO measure LIN.

VCL is the current gold standard used by investigators in hyperactivity classification. In this dissertation, VCL performed inadequately in correctly classifying hyperactivated sperm trajectories (51.72%), but did better with the progressive group (91.43%) and poorly on transitional trajectories (20.0%). VCL also generated a substantial amount of misclassifications (32.26%).

MBSR is an algorithm that interprets the physiological erratic sperm trajectory move-

ment changes observed in hyperactivated sperm as a search pattern to find an oocyte for fertilization. RRL removes an imperfection of the existing LIN and STR measures, by using the largest distance of a minimum bounding rectangle enveloping the sperm trajectory, instead of using the distance between the first and last point of the sperm trajectory. The result is a new robust linearity measure that is unaffected by the shape of the sperm trajectory. QS is a simple linearity measure based on the relative occurrence of two consecutive trajectory points within a Cartesian coordinate system. RAC is an attempt to model the symmetrical flagellar beating of the sperm as an indicator for linear movement. Finally, to improve QS and RAC, we combined both in a 2D logistic regression model.

MBSR performed the best in all three classification categories of hyperactivated (93.10%), transitional (60.0%) and progressive (98.57%), followed by RRL ($93.10\%, 24.0\%, 95.71\%$), respectively. However, RRL performed poorly in classifying transitional sperm trajectories and produced almost twice as many misclassifications as MBSR (19.35% vs. 10.48%). The simple QS algorithm performed adequately in classifying hyperactivated sperm trajectories with 72.41%, detected more transitional sperm (48.0%) than RRL, but fewer progressive trajectories (57.14%). QS (41.13%) also had the second highest misclassification rate after RAC (49.19%). In spite of the promising theory behind RAC, this algorithm performed worst with 41.38% correctly classified hyperactive trajectories, second to last with 65.71% progressive trajectories, and even with VCL (20.0%) with transitional sperm trajectories. Lastly, we showed that a combination of two mediocre algorithms (QS and RAC) can be improved by logistic regression techniques. The logistic regression model correctly classified 86.21% of hyperactivated and 74.29% of progressive sperm trajectories. Transitional trajectory classification was the lowest with only 12.0% and misclassifications were the

third highest among the other algorithms tested.

All algorithms, the best and the lowest scoring, had difficulties classifying transitional sperm,but consistently performed better in classifying hyperactivated or progressive sperm trajectories. The best classification of transitional sperm trajectories was only 60.0% by the MBSR algorithm. This illustrates the need for better descriptions and definitions for transitional sperm trajectories. The difficulty characterizing transitional sperm trajectories is seen throughout this dissertation, from the lack of an agreement among authors about what transitional sperm are, to the omission of transitional sperm from the training data due to the lack of an agreed-upon definition, and to the difficulty experienced by experts in the field in classifying the test data that included transitional sperm. Experts were instructed to classify hyperactive and progressive sperm only, leaving the remaining trajectories as transitional, but other experts could easily arrive at somewhat different classifications.

The current limitations of our algorithms is the availability of a threshold for trajectories for species other than the equines tested. We recommend using the same procedure we used to determine threshold for other sperm trajectories.

Next, we address the research questions *R1* through *R7* from chapter 1 section 1.3:

In chapter 4 we addressed research question *R1* (*Can hyperactivated sperm be identified and classified from 2D trajectory data, obtained from industry standard semen scanners?*), *R2* (*Is it possible to develop computational algorithms to describe sperm hyperactivation?* and research question *R3* (*Can computer algorithms be used to accurately describe movement patterns?*). Chapter 6 and 7 dealt with research question *R4* (*Can such algorithms match or surpass classifications by experts in the field?*) and *R6* (*Are those new measures and algorithms robust enough to be used in daily laboratory testing?*). Research Question

R5 (*Can the existing sperm parameter measures be improved?*) was answered in Chapter 4 Section 4.5.6. Finally, research question *R7* (*Can we automatically detect types of sperm motility using existing laboratory technology with computer science algorithms?*) was addressed in Chapters 4 through 7.

8.2 Future Work

The initial focus of this dissertation was to develop computational algorithms to detect and classify spermatoza hyperactivity automatically, reliably and reproducibly. Overall, this research has developed a detailed understanding of expressing the biological phenomenon of hyperactivity with reasonable computational algorithms. Future work could include aggregates of the developed algorithms assembles according to a variety of statistical methods to further refine the results, especially for the transitional trajectories. Another aspect is understanding and developing better guidelines and definitions for transitional sperm trajectories.

Chapter 9

Appendix

9.1 Training Data Set

Figure 9.1 shows an excerpt of the training data used in this dissertation, Each category, hyperactivated and progressive, consists of 40 trajectories each, selected by experts in the field. To avoid overlapping trajectories an excerpt of 13 progressive and 15 hyperactivated sperm trajectories are shown. The trajectories are rotated to maximize their exploration region A_{MBS} and are displayed with their trajectory area A_{hull} and RRL.

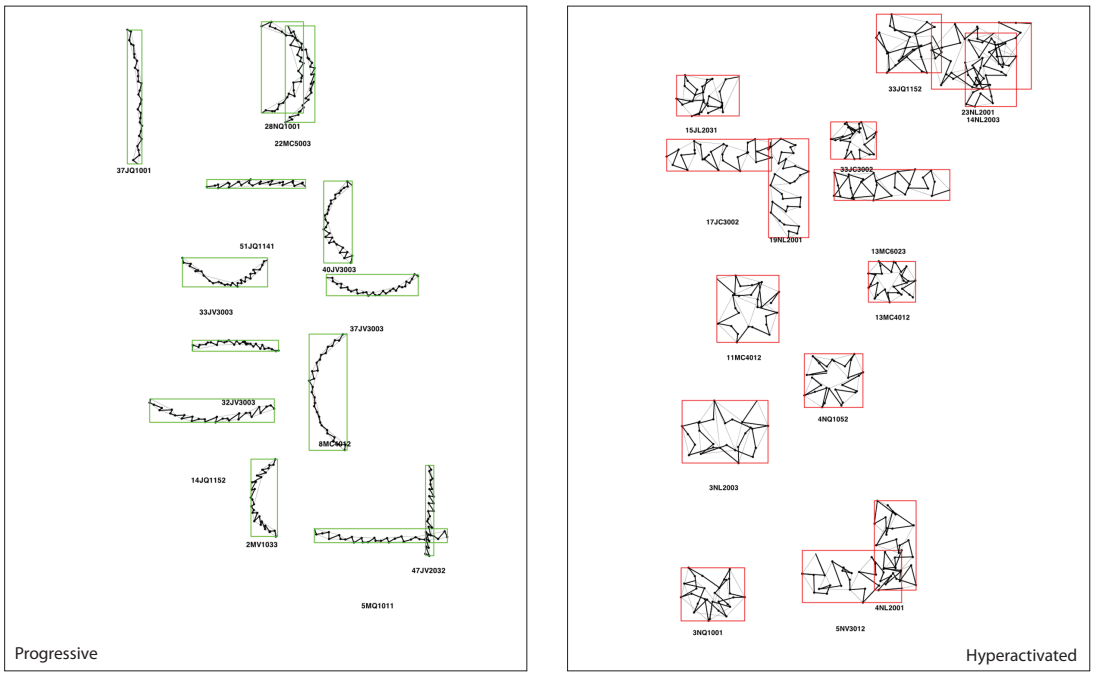

Figure 9.1: *Training Data Excerpt. Excerpt of progressive and hyperactivated training data set with 40 trajectories each. Displayed are the trajectory, trajectory hull and RRL. The largest side of RRL is used for MBSR.*

9.2 Test Data Set

In Figure 9.2 fourteen of 138 sperm trajectories of the test data are displayed. Shown are the trajectories, their trajectory area A_{hull} and their rotated rectangular linearity RRL. The largest side of RRL is used for the trajectory exploration region A_{MBS}.

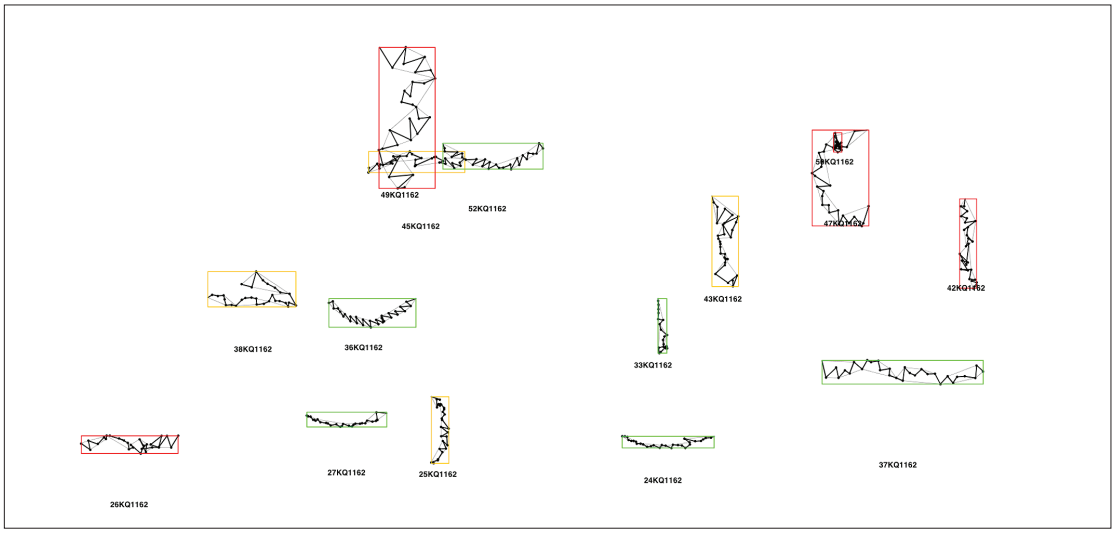

Figure 9.2: *Test Data Set Excerpt. The test data contained 138 trajectories of four random CASA recordings with 18, 21, 52 and 47 trajectories respectively. Displayed are the trajectory, trajectory hull and RRL.*

9.3 Sperm Suspension

The purpose of the solution is to provide nourishment and prolong the life of the sperm and therefore increase the consistency and quality of the experimental data.

Fructose	1.52 g
Glucose	0.1 g
NaPyruvate	0.002 g
NaLactate	0.37 ml
BSA	0.3 g
added to 100 ml Stallion Tyrode's	
NaCl	.216 g
KCL	.075 g
KH_2PO_4	.016 g
$NaHCO_3$	.300 g
$MgSO_4$	.029 g
Hepes	.240 g
$CaCl_2 2H_2O$	.025 g

Table 9.1: *TALP is the acronym for Tyrode's, Albumin, Lactate, Pyruvate. Albumin is a protein (BSA part: Bovine Serum Albumin), Lactate is an energy source and Pyruvate is an acid helping to break down glucose. Tyrode's solution mimics interstitial fluid.*

Bibliography

[1] *Consensus workshop on advanced diagnostic andrology techniques. ESHRE (European Society of Human Reproduction and Embryology) Andrology Special Interest Group.*, 1996 Jul.

[2] *Guidelines on the application of CASA technology in the analysis of spermatozoa. ESHRE Andrology Special Interest Group. European Society for Human Reproduction and Embryology.*, 1998 Jan.

[3] Ashok Agarwal, Rakesh K Sharma, and David R Nelson. New semen quality scores developed by principal component analysis of semen characteristics. *Journal of Andrology*, 24(3):343–352, 2003 May-Jun.

[4] R J Aitken. Sperm function tests and fertility. *International Journal of Andrology*, 29(1):69–75, 2006 Feb.

[5] Rupert P Amann and David F Katz. Reflections on casa after 25 years. *Journal of Andrology*, 25(3):317–325, 2004 May-Jun.

[6] A G Andersen, S Ziebe, N Jorgensen, J H Petersen, N E Skakkebaek, and A Nyboe Andersen. Time to pregnancy in relation to semen quality assessed by casa before and after sperm separation. *Human Reproduction*, 17(1):173–177, 2002 Jan.

[7] J R Andrade, A Traboulsi, A Hussain, and N H Dubin. In vitro effects of sildenafil and phentolamine, drugs used for erectile dysfunction, on human sperm motility. *American Journal of Obstetrics and Gynecology*, 182(5):1093–1095, 2000 May.

[8] C R Austin. Capacitation and its sequelae. *Reproduction, Fertility and Development*, 4(5):459–466, 1992.

[9] C Ayala, E Steinberger, and D P Smith. The influence of semen analysis parameters on the fertility potential of infertile couples. *Journal of Andrology*, 17(6):718–725, 1996 Nov-Dec.

[10] Degan A A Baker, R D. Transport of live and dead boar spermatozoa within the reproductive tract of gilts. *Journal of Reproduction and Fertility*, 28:369–377, 1972.

[11] Barbara Barboni. Methods for the assessment of capacitation. *Zygote*, 2:pp 367–369., Nov. 1994.

[12] C L Barratt. On the accuracy and clinical value of semen laboratory tests. *Human Reproduction*, 10(2):250–252, 1995 Feb.

[13] Julie Baumber and Stuart A Meyers. Hyperactivated motility in rhesus macaque (macaca mulatta) spermatozoa. *Journal of Andrology*, 27(3):459–468, 2006 May-Jun.

[14] D E Boatman and R S Robbins. Bicarbonate: carbon-dioxide regulation of sperm capacitation, hyperactivated motility, and acrosome reactions. *Biology of Reproduction*, 44(5):806–813, 1991 May.

[15] P R Budworth, R P Amann, and P L Chapman. Relationships between computerized measurements of motion of frozen-thawed bull spermatozoa and fertility. *Journal of Andrology*, 9(1):41–54, 1988 Jan-Feb.

[16] L J Burkman. Discrimination between nonhyperactivated and classical hyperactivated motility patterns in human spermatozoa using computerized analysis. *Fertility and Sterility*, 55(2):363–371, 1991 Feb.

[17] A M Cancel, D Lobdell, P Mendola, and S D Perreault. Objective evaluation of hyperactivated motility in rat spermatozoa using computer-assisted sperm analysis. *Human Reproduction*, 15(6):1322–1328, 2000 Jun.

[18] Alan B. M Cantor. Understanding logistic regression. *Evidence-based Oncology*, 3(2):52–53, 2002.

[19] P J Chan, J U Corselli, W C Patton, J D Jacobson, and A King. Heat-induced hyperactivation. *Journal of Assisted Reproduction and Genetics*, 15(1):32–38, 1998 Jan.

[20] M C Chang. In vitro fertilization of mammalian eggs. *Journal of Animal Science*, 27 Suppl 1:15–26, 1968.

[21] M C Chang. The meaning of sperm capacitation. a historical perspective. *Journal of Andrology*, 5(2):45–50, 1984 Mar-Apr.

[22] Eric Chantler, Joanna Abraham-Peskir, and Chris Roberts. Consistent presence of two normally distributed sperm subpopulations within normozoospermic human semen: a kinematic study. *International Journal of Andrology*, 27(6):350–359, 2004 Dec.

[23] B Colenbrander, B M Gadella, and T A E Stout. The predictive value of semen analysis in the evaluation of stallion fertility. *Reproduction in Domestic Animals*, 38(4):305–311, 2003 Aug.

[24] F. Comhaire and A. Mahmoud. Semen analysis and sperm function tests. *Andrology for the Clinician*, pages 381–394, 2006.

[25] F Comhaire and L Vermeulen. Human semen analysis. *Human Reproduction Update*, 1(4):343–362, 1995 Jul.

[26] T G Cooper, L Bjorndahl, J Vreeburg, and E Nieschlag. Semen analysis and external quality control schemes for semen analysis need global standardization. *International Journal of Andrology*, 25(5):306–311, 2002 Oct.

[27] J Cosson, P Huitorel, and C Gagnon. How spermatozoa come to be confined to surfaces. *Cell Motility and the Cytoskeleton*, 54(1):56–63, 2003 Jan.

[28] D L Cuadra, P J Chan, W C Patton, S C Stewart, and A King. Type 5 phosphodiesterase regulation of human sperm motility. *American Journal of Obstetrics and Gynecology*, 182(5):1013–1015, 2000 May.

[29] J. M. Cummins and P. F. Woodall. On mammalian sperm dimensions. *Journal of Reproduction and Fertility*, 75:153–175, 1985.

[30] R O Davis and D F Katz. Standardization and comparability of casa instruments. *Journal of Andrology*, 13(1):81–86, 1992 Jan-Feb.

[31] R O Davis, P W Niswander, and D F Katz. New measures of sperm motion. i. adaptive smoothing and harmonic analysis. *Journal of Andrology*, 13(2):139–152, 1992 Mar-Apr.

[32] R O Davis and R J Siemers. Derivation and reliability of kinematic measures of sperm motion. *Reproduction, Fertility and Development*, 7(4):857–869, 1995.

[33] E de Lamirande, P Leclerc, and C Gagnon. Capacitation as a regulatory event that primes spermatozoa for the acrosome reaction and fertilization. *Molecular Human Reproduction*, 3(3):175–194, 1997 Mar.

[34] Stefan S du Plessis, Paul S de Jongh, and Daniel R Franken. Effect of acute in vivo sildenafil citrate and in vitro 8-bromo-cgmp treatments on semen parameters and sperm function. *Fertility and Sterility*, 81(4):1026–1033, 2004 Apr.

[35] B C Dunphy, R Kay, C L Barratt, and I D Cooke. Quality control during the conventional analysis of semen, an essential exercise. *Journal of Andrology*, 10(5):378–385, 1989 Sep-Oct.

[36] Emelie Engström, Mats Skoglund, and Per Runeson. Empirical evaluations of regression test selection techniques: a systematic review. *ESEM: International Symposium on Empirical Software Engineering and Measurement*, pages 22–31, 2008.

[37] Frank E Harrell Jr. *Design: Design Package*, 2008.

[38] B C Gladen, J Williams, and R E Chapin. Issues in the statistical analysis of sperm motion data derived from computer-assisted systems. *Journal of Andrology*, 12(2):89–97, 1991 Mar-Apr.

[39] David R J Glenn, Carmel M McVicar, Neil McClure, and Sheena E M Lewis. Sildenafil citrate improves sperm motility but causes a premature acrosome reaction in vitro. *Fertility and Sterility*, 87(5):1064–1070, 2007 May.

[40] J K Graham. Department of Physiology, Colorado State University, Fort Collins, CO 80523, USA. jkgraham@colostate.edu.

[41] J K Graham. Assessment of sperm quality: a flow cytometric approach. *Animal Reproduction Science*, 68(3-4):239–247, 2001 Dec 3.

[42] Henry Gray, Peter L Williams, and Henry Gray. *Gray's Anatomy*. C. Livingstone, Edinburgh, 37th ed edition, 1989.

[43] S Green and S Fishel. Morphology comparison of individually selected hyperactivated and non-hyperactivated human spermatozoa. *Human Reproduction*, 14(1):123–130, 1999 Jan.

[44] Hamilton Thorne. Research HTM-IVOS Operation Manual, Dec 1994.

[45] ROY H. HAMMERSTEDT. Tritium release from [2-3h]d-glucose as a monitor of glucose consumption by bovine sperm. *Biology of Reproduction*, 12(5):545–551, 1975.

[46] M Hirai, A Boersma, A Hoeflich, E Wolf, J Foll, T R Aumuller, and J Braun. Objectively measured sperm motility and sperm head morphometry in boars (sus scrofa): relation to fertility and seminal plasma growth factors. *Journal of Andrology*, 22(1):104–110, 2001 Jan-Feb.

[47] Y. Hirano, H.Shibahara, K. Shimada, S. Yamanaka, and T. Suzuki. Accuracy of sperm velocity assessment using the sperm quality analyzer v. *Reproductive Medicine and Biology*, 2(4):151–157(7), Dec. 2003.

[48] C Holt, W V Holt, H D Moore, H C Reed, and R M Curnock. Objectively measured boar sperm motility parameters correlate with the outcomes of on-farm inseminations: results of two fertility trials. *Journal of Andrology*, 18(3):312–323, 1997 May-Jun.

[49] Christopher J. De Jonge. Who manual...who should care? *Human Reproduction*, 14(10):2431–2433(3), Oct. 1999.

[50] N Jorgensen, J Auger, A Giwercman, D S Irvine, T K Jensen, P Jouannet, N Keiding, C Le Bon, E MacDonald, A M Pekuri, T Scheike, M Simonsen, J Suominen, and N E Skakkeboek. Semen analysis performed by different laboratory teams: an intervariation study. *International Journal of Andrology*, 20(4):201–208, 1997 Aug.

[51] K. C. Majumdar 1 S. Shivaji K. Ravinder 1, K. Nasaruddin 1. Computerized analysis of motility, motility patterns and motility parameters of spermatozoa of carp following short-term storage of semen. *Journal of Fish Biology*, 50(6):1309–1328, 1997.

[52] D F Katz and R O Davis. Automatic analysis of human sperm motion. *Journal of Andrology*, 8(3):170–181, 1987 May-Jun.

[53] D F Katz and R Vanagimachi. Movement characteristics of hamster spermatozoa within the oviduct. *Biology of Reproduction*, 22(4):759–764, 1980 May.

[54] Norbert Kaula. Usage of CASA among Clinical Professionals. personal communication, 2007.

[55] V J Kay and L Robertson. Hyperactivated motility of human spermatozoa: a review of physiological function and application in assisted reproduction. *Human Reproduction Update*, 4(6):776–786, 1998 Nov-Dec.

[56] TOMIKO AITA1) NOBUHIRO YOSHIMATSU1) KAZUHIKO HOSHI1), KAORU YANAGIDA1) and AKIRA SATO1). Changes in the motility pattern of human spermatozoa during in vitro incubation. *The Tohoku Journal of Experimental Medicine*, 154(1):47–56, 1988.

[57] Brooks A Keel. How reliable are results from the semen analysis? *Fertility and Sterility*, 82(1):41–44, 2004 Jul.

[58] F. Kime, D. E.; Van Look K. J. W.; McAllister B. G.; Huyskens G. ; Rurangwa E. ; Ollevier. Computer-assisted sperm analysis (casa) as a tool for monitoring sperm quality in fish. *Comparative Biochemistry and Physiology, Part C*, 130(4):425–433(9), December 2001.

[59] L M King, D R Holsberger, and A M Donoghue. Correlation of casa velocity and linearity parameters with sperm mobility phenotype in turkeys. *Journal of Andrology*, 21(1):65–71, 2000 Jan-Feb.

[60] M Kinukawa, M Nagata, and F Aoki. Changes in flagellar bending during the course of hyperactivation in hamster spermatozoa. *Reproduction*, 125(1):43–51, 2003 Jan.

[61] Stefan Kissler, Ernst Siebzehnruebl, Joachim Kohl, Anja Mueller, Nadja Hamscho, Regine Gaetje, Andre Ahr, Achim Rody, and Manfred Kaufmann. Uterine contractility and directed sperm transport assessed by hysterosalpingoscintigraphy (hssg) and intrauterine pressure (iup) measurement. *Acta Obstetricia et Gynecologica Scandinavica*, 83(4):369–374, 2004 Apr.

[62] Peter N Kolettis. Evaluation of the subfertile man. *American Family Physician*, 67(10):2165–2172, 2003 May 15.

[63] W Krause and G Viethen. Quality assessment of computer-assisted semen analysis (casa) in the andrology laboratory. *Andrologia*, 31(3):125–129, 1999 May.

[64] Y L Kuo, W L Tzeng, P C Li, T S Tang, and S T Young. Autostage sperm tracing system for semen evaluation. *Archives of Andrology*, 44(1):29–39, 2000 Jan-Feb.

[65] L Larsen, T Scheike, T K Jensen, J P Bonde, E Ernst, N H Hjollund, Y Zhou, N E Skakkebaek, and A Giwercman. Computer-assisted semen analysis parameters as predictors for fertility of men from the general population. the danish first pregnancy planner study team. *Human Reproduction*, 15(7):1562–1567, 2000 Jul.

[66] Vincent M S Lee, Joycelyn S Y Wong, Sheila K E Loh, and Noel K Y Leong. Sperm motility in the semen analysis affects the outcome of superovulation intrauterine insemination in the treatment of infertile asian couples with male factor infertility. *BJOG : An International Journal of Obstetrics and Gynaecology*, 109(2):115–120, 2002 Feb.

[67] L Lefievre, E De Lamirande, and C Gagnon. The cyclic gmp-specific phosphodiesterase inhibitor, sildenafil, stimulates human sperm motility and capacitation but not acrosome reaction. *Journal of Andrology*, 21(6):929–937, 2000 Nov-Dec.

[68] Sheena E M Lewis. Is sperm evaluation useful in predicting human fertility? *Reproduction*, 134:31–40, 2007.

[69] C. Linneberg, P. Salamon, C. Svarer, L.K. Hansen, and J. Meyrowitsch. Towards semen quality assessment using neural networks. *Neural Networks for Signal Processing [1994] IV. Proceedings of the 1994 IEEE Workshop*, pages 509–517, Sep 1994.

[70] D.Y. Liu, M.L. Liu, G.N. Clarke, and H.W.G. Baker. Hyperactivation of capacitated human sperm correlates with the zona pellucida-induced acrosome reaction of zona pellucida-bound sperm. *Human Reproduction*, 22(10):2632–2638, 2007.

[71] S O Mack, J S Tash, and D P Wolf. Effect of measurement conditions on quantification of hyperactivated human sperm subpopulations by digital image analysis. *Biology of Reproduction*, 40(6):1162–1169, 1989 Jun.

[72] B Marnet, G Vieitez, P Milhet, G Richoilley, F Lesourd, and J Parinaud. Computer-assisted assessment of sperm morphology: comparison with conventional techniques. *International Journal of Andrology*, 23(1):22–28, 2000 Feb.

[73] F Mazzilli, T Rossi, M Delfino, F Dondero, and A Makler. A new objective method for scoring human sperm hyperactivation based on head axis angle deviation. *International Journal of Andrology*, 24(4):189–196, 2001 Aug.

[74] Roelof Menkveld, Wai Yee Wong, Carl J. Lombard, Alex M.M. Wetzels, Chris M.G. Thomas, Hans M.W.M. Merkus, and Regine P.M. Steegers-Theunissen. Semen parameters, including who and strict criteria morphology, in a fertile and subfertile population: an effort towards standardization of in-vivo thresholds. *Human Reproduction*, 16(6):1165–1171, 2001.

[75] S T Mortimer. A critical review of the physiological importance and analysis of sperm movement in mammals. *Human Reproduction Update*, 3(5):403–439, 1997 Sep-Oct.

[76] S T Mortimer. Minimum sperm trajectory length for reliable determination of the fractal dimension. *Reproduction, Fertility and Development*, 10(6):465–469, 1998.

[77] S T Mortimer. Casa–practical aspects. *Journal of Andrology*, 21(4):515–524, 2000 Jul-Aug.

[78] S T Mortimer and W M Maxwell. Kinematic definition of ram sperm hyperactivation. *Reproduction, Fertility and Development*, 11(1):25–30, 1999.

[79] S T Mortimer and D Mortimer. Kinematics of human spermatozoa incubated under capacitating conditions. *Journal of Andrology*, 11(3):195–203, 1990 May-Jun.

[80] S T Mortimer, D Schevaert, M A Swan, and D Mortimer. Quantitative observations of flagellar motility of capacitating human spermatozoa. *Human Reproduction*, 12(5):1006–1012, 1997 May.

[81] S T Mortimer and M A Swan. Kinematics of capacitating human spermatozoa analysed at 60 hz. *Human Reproduction*, 10(4):873–879, 1995 Apr.

[82] S T Mortimer and M A Swan. Variable kinematics of capacitating human spermatozoa. *Human Reproduction*, 10(12):3178–3182, 1995 Dec.

[83] S T Mortimer and M A Swan. The development of smoothing-independent kinematic measures of capacitating human sperm movement. *Human Reproduction*, 14(4):986–996, 1999 Apr.

[84] S T Mortimer, M A Swan, and D Mortimer. Fractal analysis of capacitating human spermatozoa. *Human Reproduction*, 11(5):1049–1054, 1996 May.

[85] T Mostafa. Tadalafil as an in vitro sperm motility stimulant. *Andrologia*, 39(1):12–15, 2007 Feb.

[86] Taymour Mostafa. In vitro sildenafil citrate use as a sperm motility stimulant. *Fertility and Sterility*, 88(4):994–996, 2007 Oct.

[87] E.R. Myers, D.C. McCrory, A.A.Mills, T.M.Price, G.K.Swamy, J.Tantibhedhyangkul, J.M.Wu, and D.B.Matchar. Effectiveness of Assisted Reproductive Technology. Evidence Report/Technology Assessment No. 167

(Prepared by the Duke University Evidence-based Practice Center under Contract No. 290-02-0025). *AHRQ Publication Rockville, MD:Agency for Healthcare Research and Quality*, No. 08-E012, May 2008.

[88] NAFA and ESHRE-SIGA. *Manual on Basic Semen Analysis (2002)*, 2002.

[89] World Health Organization. *WHO laboratory manual for the examination of human semen and sperm-cervical mucus interaction*. Cambridge, UK ; New York, NY : Published on behalf of the World Health Organization [by] Cambridge University Press, c1999, 4th ed. edition, 1999.

[90] Joseph O'Rourke. *Computational geometry in C*. Cambridge University Press, Cambridge, UK,, 2nd ed edition, 1998.

[91] A A Pacey, M B Ladbrook, C L Barratt, and I D Cooke. The potential shortcomings of measuring hyperactivated motility by computer-aided sperm analysis when sperm motion is multiphasic. *Human Reproduction Update*, 3(3):185–193, 1997 May-Jun.

[92] Jean Parinaud, Gerard Vieitez, Helene Moutaffian, Gerard Richoilley, and Pierrette Milhet. Relationships between motility parameters, morphology and acrosomal status of human spermatozoa. *Human Reproduction*, 11(6):1240–1243, 1996.

[93] E B Pasqualotto, J A Daitch, B N Hendin, T Falcone, A J Jr Thomas, D R Nelson, and A Agarwal. Relationship of total motile sperm count and percentage motile sperm to successful pregnancy rates following intrauterine insemination. *Journal of Assisted Reproduction and Genetics*, 16(9):476–482, 1999 Oct.

[94] A M Petrunkina, A-R Gunzel-Apel, and E Topfer-Petersen. Seeking mathematical strategies in sperm function analysis: between scylla and charybdis? *Reproduction in Domestic Animals*, 38(2):125–133, 2003 Apr.

[95] Giorgio Pomara, Girolamo Morelli, Domenico Canale, Paolo Turchi, Carolina Caglieresi, Cecilia Moschini, Giovanni Liguori, Cesare Selli, Enrico Macchia, Enio Martino, and Francesco Francesca. Alterations in sperm motility after acute oral administration of sildenafil or tadalafil in young, infertile men. *Fertility and Sterility*, 88(4):860–865, 2007 Oct.

[96] Stephen Publicover, Claire V Harper, and Christopher Barratt. [ca2+]i signalling in sperm–making the most of what you've got. *Nature Cell Biology*, 9(3):235–242, 2007 Mar.

[97] Ken Purvis, Gary J Muirhead, and Jane A Harness. The effects of sildenafil on human sperm function in healthy volunteers. *British Journal of Clinical Pharmacology*, 53 Suppl 1:53S–60S, 2002.

[98] A Quintero-Moreno, J Miro, A Teresa Rigau, and J E Rodriguez-Gil. Identification of sperm subpopulations with specific motility characteristics in stallion ejaculates. *Theriogenology*, 59(9):1973–1990, 2003 May.

[99] R Development Core Team. *R: A Language and Environment for Statistical Computing*. R Foundation for Statistical Computing, Vienna, Austria, 2008.

[100] R Rathi, B Colenbrander, M M Bevers, and B M Gadella. Evaluation of in vitro capacitation of stallion spermatozoa. *Biology of Reproduction*, 65(2):462–470, 2001 Aug.

[101] Gyu-Jin Rho, Sung-Lim Lee, Yang-Sil Kim, Hyun-Jin Yeo, Sun-A Ock, S Balasubramanian, and Sang-Young Choe. Intracytoplasmic sperm injection of frozen-thawed bovine oocytes and subsequent embryo development. *Molecular Reproduction and Development*, 68(4):449–455, 2004 Aug.

[102] L Robertson, D P Wolf, and J S Tash. Temporal changes in motility parameters related to acrosomal status: identification and characterization of populations of hyperactivated human sperm. *Biology of Reproduction*, 39(4):797–805, 1988 Nov.

[103] Susan A Rothmann and Angela A Reese. Semen analysis: the test techs love to hate. *MLO: Medical Laboratory Observer*, 39(4):18–20, 2007 Apr.

[104] Ruiz, Mariana. Wikimedia Commons. http://en.wikipedia.org/wiki/Spermatozoon, 11 2008.

[105] Harald Schmidt and Gunter Kamp. Induced hyperactivity in boar spermatozoa and its evaluation by computer-assisted sperm analysis. *Reproduction*, 128(2):171–179, 2004 Aug.

[106] Linda Z Shi, Jaclyn M Nascimento, Michael W Berns, and Elliot L Botvinick. Computer-based tracking of single sperm. *Journal of Biomedical Optics*, 11(5):054009, 2006 Sep-Oct.

[107] H Sieme, T Katila, and E Klug. Effect of semen collection practices on sperm characteristics before and after storage and on fertility of stallions. *Theriogenology*, 61(4):769–784, 2004 Feb.

[108] J Spiropoulos. Computerized semen analysis (casa): effect of semen concentration and chamber depth on measurements. *Archives of Andrology*, 46(1):37–42, 2001 Jan-Feb.

[109] B T Storey. Sperm capacitation and the acrosome reaction. *Annals of the New York Academy of Sciences*, 637:459–473, 1991.

[110] S S Suarez and H-C Ho. Hyperactivated motility in sperm. *Reproduction in Domestic Animals*, 38(2):119–124, 2003 Apr.

[111] N Sukcharoen, J Keith, D S Irvine, and R J Aitken. Definition of the optimal criteria for identifying hyperactivated human spermatozoa at 25 hz using in-vitro fertilization as a functional end-point. *Human Reproduction*, 10(11):2928–2937, 1995 Nov.

[112] Regina M Turner. Tales from the tail: what do we really know about sperm motility? *Journal of Andrology*, 24(6):790–803, 2003 Nov-Dec.

[113] Regina M Turner. Moving to the beat: a review of mammalian sperm motility regulation. *Reproduction, Fertility and Development*, 18(1-2):25–38, 2006.

[114] J Verstegen, M Iguer-Ouada, and K Onclin. Computer assisted semen analyzers in andrology research and veterinary practice. *Theriogenology*, 57(1):149–179, 2002 Jan 1.

[115] P Vyt, D Maes, T Rijsselaere, E Dejonckheere, F Castryck, and A Van Soom. Motility assessment of porcine spermatozoa: a comparison of methods. *Reproduction in Domestic Animals*, 39(6):447–453, 2004 Dec.

[116] A M Watkins, P J Chan, T H Kalugdan, W C Patton, J D Jacobson, and A King. Analysis of the flow cytometer stain hoechst 33342 on human spermatozoa. *Molecular Human Reproduction*, 2(9):709–712, 1996 Sep.

[117] R Yanagimachi. In vitro capacitation of hamster spermatozoa by follicular fluid. *Journal of Reproduction and Fertility*, 18(2):275–286, 1969 Mar.

[118] C H Yeung, F Perez-Sanchez, C Soler, D Poser, S Kliesch, and T G Cooper. Maturation of human spermatozoa (from selected epididymides of prostatic carcinoma patients) with respect to their morphology and ability to undergo the acrosome reaction. *Human Reproduction Update*, 3(3):205–213, 1997 May-Jun.

[119] R J Young and B A Bodt. Development of computer-directed methods for the identification of hyperactivated motion using motion patterns developed by rabbit sperm during incubation under capacitation conditions. *Journal of Andrology*, 15(4):362–377, 1994 Jul-Aug.

[120] S.T. Young, W.L. Tzeng, Y.L. Kuo, M.L. Hsiao, and S.R. Chiang. Real-time tracing of spermatozoa. *Engineering in Medicine and Biology Magazine, IEEE*, 15(6):117–120, Nov/Dec 1996.

[121] L J Zaneveld, C J De Jonge, R A Anderson, and S R Mack. Human sperm capacitation and the acrosome reaction. *Human Reproduction*, 6(9):1265–1274, 1991 Oct.

[122] J J Zhu, A A Pacey, C L Barratt, and I D Cooke. Computer-assisted measurement of hyperactivation in human spermatozoa: differences between european and american versions of the hamilton-thorn motility analyser. *Human Reproduction*, 9(3):456–462, 1994 Mar.